Monitoring Electrode Array Tip Fold-over in Cochlear Implantation

Juriaan van der Graaf
MSc thesis – Biomedical Engineering
Delft University of Technology
May 21, 2019

TU Delft

Supervisors
R. K. Kalkman Dr. Ir. R. C. Hendriks

Preface

For the past year I have been working on my MSc (Biomedical Engineering) graduation project, which resulted in this thesis. The project took place at the Leiden University Medical Center (LUMC), in the otorhinolaryngology (Ear, Nose, and Throat) department: a department that specializes in the treatment of diseases and disorders of the head and neck. It is a broad field that ranges from facial surgery (facial paralysis, skull base surgery, tumours, cosmetic surgery) to language, speech and hearing impediments. The otorhinolaryngology department is multidisciplinary and includes ENT-doctors, surgeons, speech therapists, neuroscientists, biologists, clinical physicists and more.

The otorhinolaryngology department of the LUMC is well known for their work on cochlear implantation: a treatment for the deaf and those with profound hearing loss, in which an electrode is inserted into the cochlea in order to artificially stimulate the auditory nerve. Since I developed a hearing disorder myself a few years ago, I have become increasingly interested in this field and this is the reason why I chose to do my graduation project here.

Unsurprisingly, my project is related to cochlear implants. Cochlear implantation is a treatment that has progressed immensely over the past decades, but despite its growth there is still room for improvement. The particular problem I focused on is electrode array tip fold-over. During surgery, an electrode array is slowly inserted into the cochlea by the surgeon. Unfortunately, in some cases the electrode array folds over inside of the cochlea resulting in a shallow insertion and possible trauma to the cochlea. Currently, this can not be detected intra-operatively as there is no way of knowing what is happening inside of the cochlea (visual inspection is not possible as the electrode array is inserted through a small incision in the round window). In this thesis I present the work I've done on this problem.

I would like to thank Yu Dong for his company, help and friendship during the last year. I've learned a lot from you and you made the hours working late at the LUMC tolerable. I would also like to thank Randy Kalkman and Richard Hendriks for their supervision, assistance and patience during my graduation project.

Juriaan van der Graaf

Index

Abstract

In cochlear implantation surgery, the appropriate placement of the electrode array into the cochlea is vital. Suboptimal placement of the electrode array may lead to reduced hearing performance and speech recognition after the surgery. Currently, there are methods to confirm the electrode position post-operatively (e.g. through a CT scan), but it is not possible to monitor the insertion intra-operatively. This, combined with the fact that there is difference in surgical precision and insertion technique between surgeons, leads to great variability in electrode placement and in some cases to electrode malpositioning issues. One of the more problematic issues that may arise is folding of the electrode tip. Folding of the tip causes the electrode array to not reach deep enough into the cochlea, and it is likely to cause trauma due to the increased pressure on cochlear walls and membranes. On top of that, you effectively have "less" contacts to work with because contacts can be positioned very close to eachother due to the folding. Folding of the electrode array also disrupts the tonotopic organization of the cochlear implant (the contacts near the end of the array no longer correspond to the lowest frequencies). The effectivity of the treatment is thus reduced in patients with tip fold-overs.

However, many modern day cochlear implants possess telemetry features. These are primarily used to check the implant's proper functioning, but may also be helpful in monitoring the insertion of the electrode array. The telemetry features of a cochlear implant make it possible to measure the intracochlear electrical potential. The measured current spread is related to the electrode array's shape and position, and thus may provide a way to detect folding of the tip. This can be done post-operatively, but can possibly also be done intra-operatively to monitor the insertion in real time. This application could be a useful tool to aid surgeons and clinicians. When used post-operatively, it may provide a cost-free method to detect tip fold-over. When used intra-operatively, it may provide a way to detect and prevent both fold-over and trauma to the cochlea.

1. Introduction

1.1 History of Cochlear Implants

Around 50 years ago, there was no effective treatment available for hearing loss or deafness. The introduction of the cochlear implant changed that completely, and has revolutionized the field of otology [1]. Cochlear implantation is the only medical procedure that is able to restore partial hearing to a deaf person [2]. The earliest experimentation with electrical stimulation of the auditory nerve goes back to 1790, when Italian scientist Alessandro Volta inserted two battery ends into his own ears. He reported experiencing a shock to the head, which was followed by a noise comparable to the sound of "thick, boiling paste" [3]. Volta believed the experiment to be dangerous, and did not attempt to repeat it. It was not until almost 150 years later that a group of Russian scientists provided the first evidence of electrical stimulation of the auditory nerve. They reported findings of electrical stimulation eliciting hearing sensations in a patient whose middle and inner ears were severely damaged [4]. Not long after, in 1957, the first device purposed for electrical stimulation of the auditory nerve was implanted in Paris, by Djourno and Eyriès [5]. The patient had both cochleae and peripheral sections of the auditory nerve removed during previous surgeries, but was able to hear environmental sounds after being implanted with the device. He could not understand speech, or differentiate between voices, but was able to discriminate large frequency changes below 1,000 Hz [6]. The device failed not long after being implanted. One more patient was implanted by Eyriès, but this device failed within a couple of weeks as well, and Eyriès decided to discontinue the project. The work of Djourno and Eyriès instigated a number of attempts to restore hearing to deafened patients in the United States in the 1960s and 1970s. The early studies done there paved the way to the current state of cochlear implants, as they identified important problems and limitations within the field [2]. Detailed reports of these studies were presented by Bilger in 1977 [7, 8]. Soon after, in 1984, the United States Food and Drug Administration (FDA) approved the first commercial cochlear implant. It was called the House-3M implant and used a single electrode. The device had several hundreds of users [2], and House is regarded by many as the most important pioneer in cochlear implant technology [9]. In the following years the University of Utah, the University of Antwerp in Belgium, and MXM laboratories in France all developed their own cochlear implants (the Ineraid or Symbion, the Laura, and the Digisonic MX20 respectively), mainly for research purposes. These devices are currently no longer available and at this moment there are 3 major manufacturers in cochlear implants: Advanced Bionics (Clarion devices), Cochlear (Nucleus devices), and MED-EL.

Research into cochlear implants has shown exponential growth and progressed immensely over the years. This is confirmed by the increase in scientific publication and patient population. The number of yearly publications on cochlear implants has even surpassed that of conventional hearing aids in the 1990s [2], and the number of cochlear implant users has grown from 60,000 in 2004 [2] to 324,200 in 2012 [10]. The patient population continues to grow and MED-EL states that around 2012, approximately 50,000 implants were sold per year [11]. The qualification requirements for implantation have also been changed drastically and today children as young as 3 months are being implanted, as well as adults with significant residual hearing. Figure 1.1 illustrates the improvement in speech recognition scores for cochlear implant users over the years. The cochlear implant has grown from a single-electrode device that enabled users to pick up environmental sounds and

offered support in lip reading, to a sophisticated multi-electrode prosthesis that allows most of its users to have a conversation on the phone.

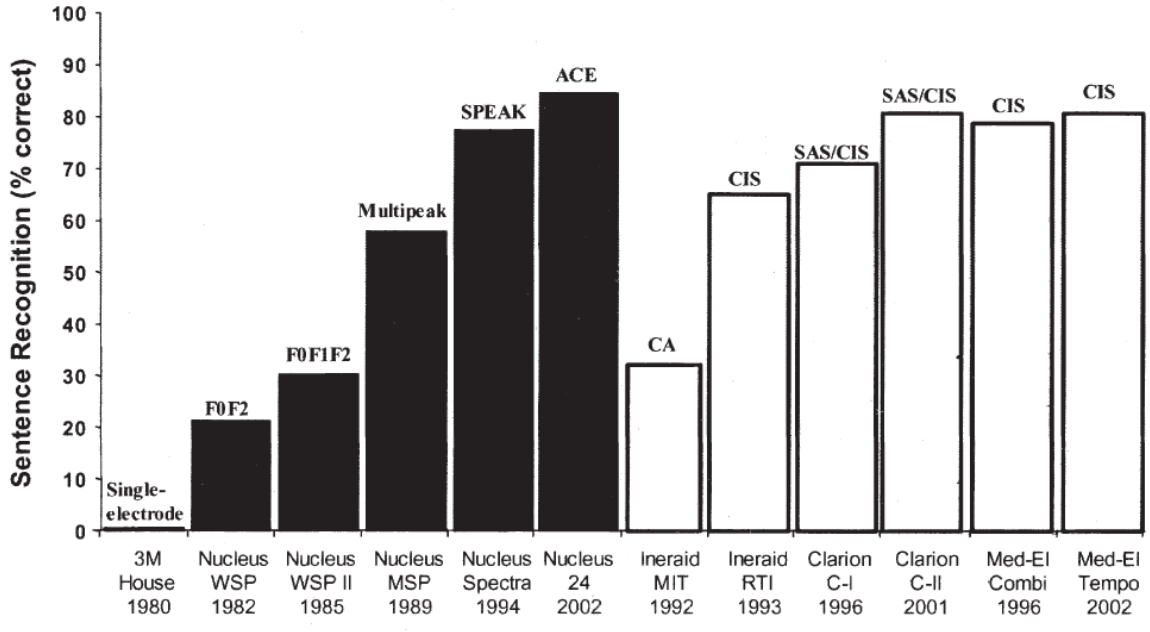

Figure 1.1: Speech recognition scores for different devices over the years **[2]**.

1.2 Working Principle

All state-of-the-art CIs are composed of the same essential components, which are illustrated in Figure 1.2. The components and the basic working principle of the cochlear implant will be discussed briefly. A more comprehensive and in-depth overview of cochlear implant design and components was presented by Wilson in 2004 [12]. A cochlear implant consists of the following:

i. An external microphone
ii. A speech processor
iii. An external transmitter
iv. An implanted receiver/ stimulator
v. An electrode array (implanted into the cochlea)

During surgery, an incision is made behind the ear. A pocket is drilled into the skull, just large enough to fit the receiver/stimulator (iv). Next, a pathway is cleared to the round window, where the electrode array (v) is inserted into a section of the cochlea called the Scala Tympani (ST). The ST extends from the round window to the helicotrema (the tip of the spiral cochlea). The remaining components of the CI are worn externally and are not introduced until after the surgery.
The external microphone (i) is worn on the ear, much similar to the conventional hearing aid. It senses sound in the environment of the user, and the output of the microphone is subsequently converted by a speech processor (ii) into a series of stimuli for the intracochlear electrode array. The transmitter (iii) provides a transcutaneous link to the implanted section of the CI. It provides the receiver/stimulator with power and conveys the stimulus information by producing a radio frequency signal. Next, the receiver/stimulator decodes the information received from the

transmitting coil and generates stimuli. A cable connects the output of the stimulator to the individual electrode contacts within the array. Finally, these electrode contacts stimulate the auditory nerve.

It is important to acknowledge there is large variability in the biological component of the CI procedure. There is difference in anatomical structure of the cochlea between patients, but also difference in residual functioning of the auditory pathways. This may explain why there is diversity in outcomes with patients using the same modern CIs [13, 14]. Surgical precision and technique may also play a role in this [15].

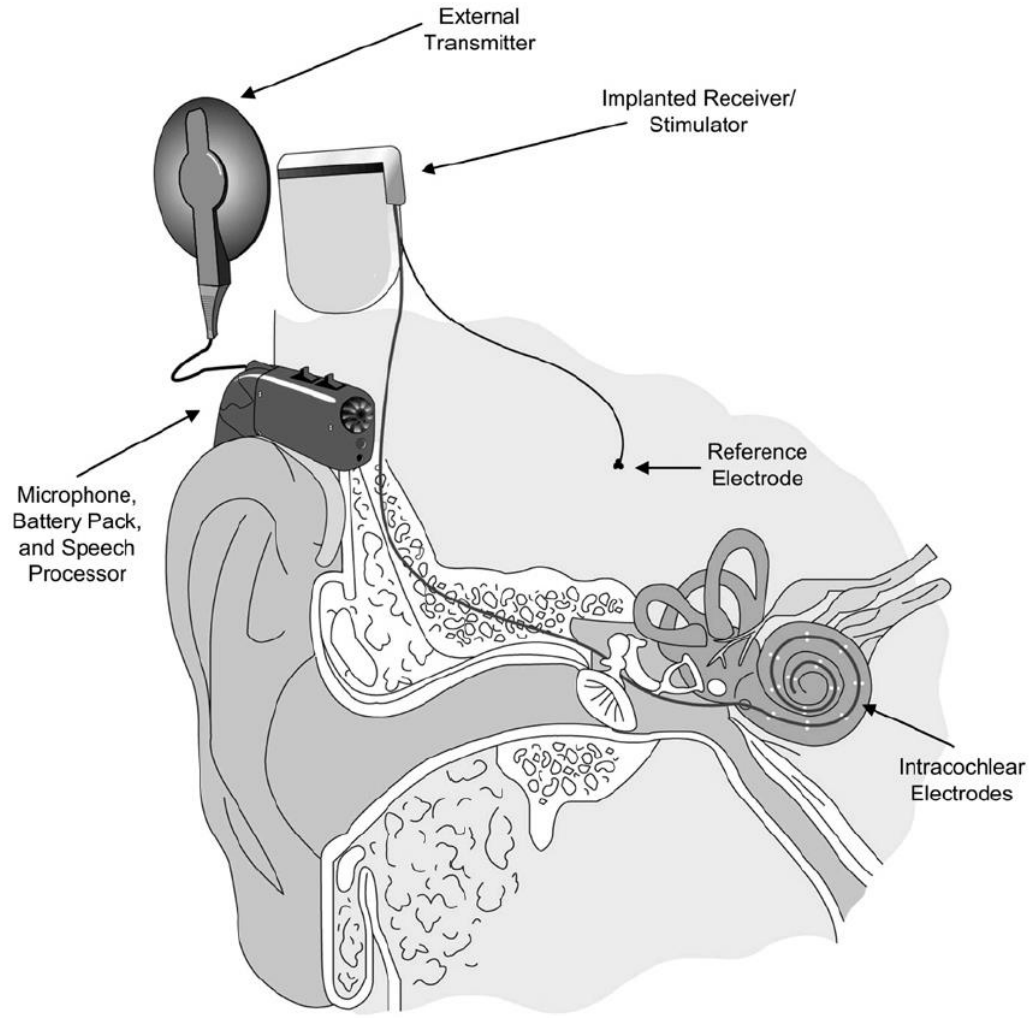

Figure 1.2: The basic components of a state-of-the-art cochlear implant **[16]**.

1.3 Problem Analysis: Insertion Issues

As mentioned earlier, cochlear implantation is now an established and sophisticated treatment for those who suffer from sensorineural hearing loss or deafness. The outcomes of CI surgery are in general successful and the rate of complications is fairly low. For example, in 0.17% to 2.12% of total cases problems occur that are related to the electrode array [17]. Other areas of complication include the insertion of the array into the cochlea, and skin-flap related problems such as inflammation and infection.

One might argue that the actual insertion of the electrode array into the cochlea is the most critical step in cochlear implantation surgery. The electrode position determines how well the CI interfaces with the neural elements within the cochlea and thus affects the final outcome of the treatment [18].

Unfortunately, the insertion is not straight forward, and many factors play a role. These include insertion speed, insertion depth, the type of electrode array used (straight versus perimodiolar), cochlear anatomy, surgical precision, surgical approach (cochleostomy versus round window approach), and the final position within the cochlea (Scala Tympani versus Scala Vestibuli) [19, 20, 21, 22, 23]. Problems that can occur related to the insertion and position of the electrode include lead buckling, migration of the electrode from the Scala Tympani to the Scala Vestibuli, too deep or partial insertion, and folding of the electrode tip [21, 24].
The incidence of electrode malpositioning is rather low (for example, specifically tip fold-over occurred in only 1.98% of total cases in an academic center with experienced surgeons [25]), but the consequences are highly undesirable. Malpositioning may lead to decreased benefit to the hearing performance of the patient and may cause damage to adjacent neurovascular structures in close proximity of the cochlea such as major vessels (carotid artery and jugular vein), the facial nerve, the vestibular system, and neural structures within the internal auditory canal [18].
Specific groups of patients have increased risk of electrode malpositioning. These are patients with congenitally malformed cochlea's [26], patients who suffer from otosclerosis [27], and patients who have suffered from meningitis in the past [28].
Malpositioning occurs in 1,2% to 2% of total insertions [29]. Of all wrongly inserted electrode arrays, 94% needs revision surgery [30, 31], and out of all cochlear implantation revision surgeries performed, 17% to 33% is due to malpositioning of the electrode array [30, 27, 29, 32].
In this project we will focus on electrode tip fold-over, as it is the most problematic insertion issue.

At the time of writing, the placement of the electrode array is often confirmed post-operatively by a combination of telemetry measures (such as measuring the electrical impedance of the electrode contacts, or neural response telemetry) and imaging techniques (e.g. CT). However, there are currently no methods that are widely agreed upon for intra-operative monitoring of the electrode position [18]. Surgeons cannot visually inspect the insertion as sight is limited to the incision site. A way to monitor the insertion in real time, intra-operatively, may be an extremely helpful aid for surgeons to prevent incorrect positioning of the electrode.

The proposed idea is to use the telemetry options of the implant to determine the shape of the electrode array. This way, there is no need for special instrumentation other than the implant itself. If successful, this may provide a way to prevent electrode tip fold-over, and the trauma it can possibly cause, from happening.

Note that other malpositioning issues (too deep or too shallow insertion, and migration of the electrode) will not be resolved, as they are not detectable through the electrode array's shape (but rather through its position relative to the cochlear walls).
Proposed ideas are elaborated upon later on in this report, preceded by an introduction of cochlear implant telemetry.

1.4 Introduction to Cochlear Implant Telemetry

All modern cochlear implant systems feature telemetry options. Telemetry refers to sending information back to the speech processor. It is typically used post-operatively to assess the functioning of both the external and the internal hardware, and is valuable in research relating to the effect of different types of stimulation on the auditory system [33]. However, telemetry might also provide a way to monitor the electrode array's shape during insertion. There are two types of telemetry; telemetry of the Intracochlear Electrical Field, and telemetry of the Compound Action Potential (CAP).

Telemetry of the Intracochlear Electrical Field

Telemetry of the intracochlear electrical field is often referred to as "electrical field imaging" (EFI). This term was introduced by the manufacturer of the Advanced Bionics implant, but is slightly misleading as only the voltage at the exact location of the electrode contacts is observed. Early EFI was performed using the Med-El implant and an experimental hardware platform. Today, all CIs come with stand-alone EFI software provided by their manufacturers [33, 34].

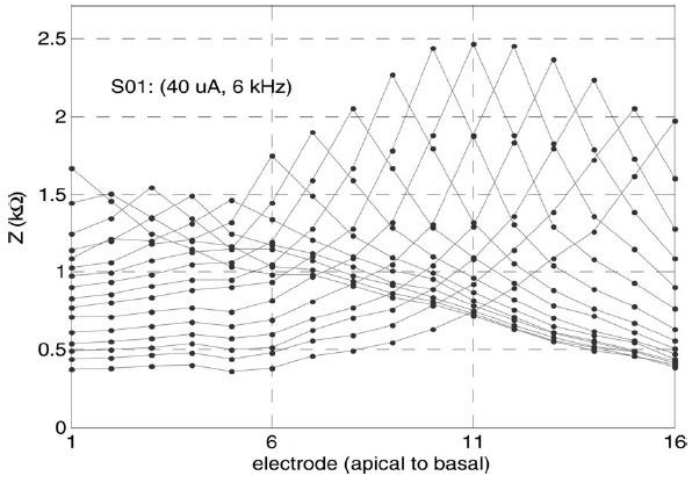

Figure 1.3: Typical EFI measurement recorded with an Advanced Bionics HR90K CI (16 electrode contacts). Each curve represents the intracochlear electrical potential profile recorded along all contacts, when a single contact is stimulated. The intracochlear voltage is divided by the injected current to eliminate influence of stimulation strength and only represent tissue conduction. The contacts are stimulated in monopolar mode; the current flows between the intracochlear contact and an extracochlear reference electrode. This particular EFI was recorded using a 40 µA, 6 kHz stimulus [35].

Modern CI's possess the feature to configure the contacts not only for stimulation, but also for recording. To measure EFI, one contact is stimulated, and subsequently the decay of the electrical potential is recorded on all other contacts. The measured electrical potential is divided by the injected current to eliminate the influence of stimulation strength. This gives us a generalized

impedance value which defines the relation between the injected current at one position, and the electrical potential it induces at another position within the cochlea [36].
CI's are capable of registering the biological response of the auditory nerve (which is in the range of ±0.1 mV), but are configured to record to a larger electrical stimulation field in EFI-mode (±1 V) [33]. In Figure 1.3 a typical EFI measurement is presented. The figure shows 16 intracochlear potential curves, all corresponding to a single stimulating contact. Due to the contact impedance, it is not possible to record and stimulate on the same contact [36]. Therefore, the peak values seen in Figure 1.3 are not actual measurements, but extrapolations based on neighbouring measurements [35]. This is important to keep in mind when attempting real time monitoring through EFI measurements.

CI manufacturers provide software to perform EFI measurements [33, 34]. The user determines the type of stimulus (duration, frequency, pulse or sine), the injected current level, and decides what electrode contacts are to be stimulated. A fixed number of measurements is performed and averaged to produce the intracochlear potential profile. This can take up to 1.5 - 2 minutes when stimulating on all 16 contacts, which is not a problem when using EFI to check the implant's status post-operatively. However, if EFI recordings are to be used for real time monitoring of the electrode insertion, the recording time will need to be brought down drastically. A starting point would be to only stimulate and record the contacts near the tip of the electrode, as this is where folding of the electrode would occur. Furthermore, an optimum needs to be found where the number of measurement repetitions is as low as possible, yet still yielding data reliable enough to detect folding of the electrode tip.

Uses of EFI Telemetry

As mentioned earlier, EFI is typically used to check the status of the implant's electronics. However, there are more potential uses for EFI. EFI measurements provide information about the volume conduction within the cochlea. For example, EFI measurements have shown that in general the voltage gradient towards the base (while stimulating the apex) is roughly three times as large as the voltage gradient towards the apex (while stimulating the base). This indicates current prefers to leave the cochlea through the basal openings (the oval and round windows, the vestibular system, and the internal auditory canal) [33].
Information about the volume conduction within the cochlea can be used to figure out effective stimulation patterns to improve speech recognition in CI users. For example, work has been done on combining the electrical fields of individual electrode contacts by simultaneous multipolar stimulation [37, 38, 39, 40, 41]. This has resulted in new ways to access the auditory nerve (e.g. current focusing and current steering [42, 43]).
The volume conduction within the cochlea also presents information about the relative distance between electrode contacts. When current is injected at the stimulating contact, a recording contact adjacent to the stimulating contact will measure a higher potential than a recording contact further away. Hence, telemetry of the intracochlear electrical field might be a viable option for monitoring the shape of the electrode array.

From EFI measurements, it is also possible to infer the current flow towards the auditory nerve (which lies tangential to the cochlea and the electrode array) using simplified electrical models of the cochlea [44, 45, 46]. In these simplified models, the cochlea is described as longitudinal impedances representing the perilymph between electrode contacts, and transversal impedances representing the resistance between a section of the Scala Tympani and a corresponding spiral ganglion section.

Vanpoucke combined these sections into a ladder network [36]. Aside from the longitudinal and transversal impedances, the model contains one more impedance which represents the volume conduction from the cochlea to the reference electrode (R_{basal}). The model can be seen in Figure 1.4.

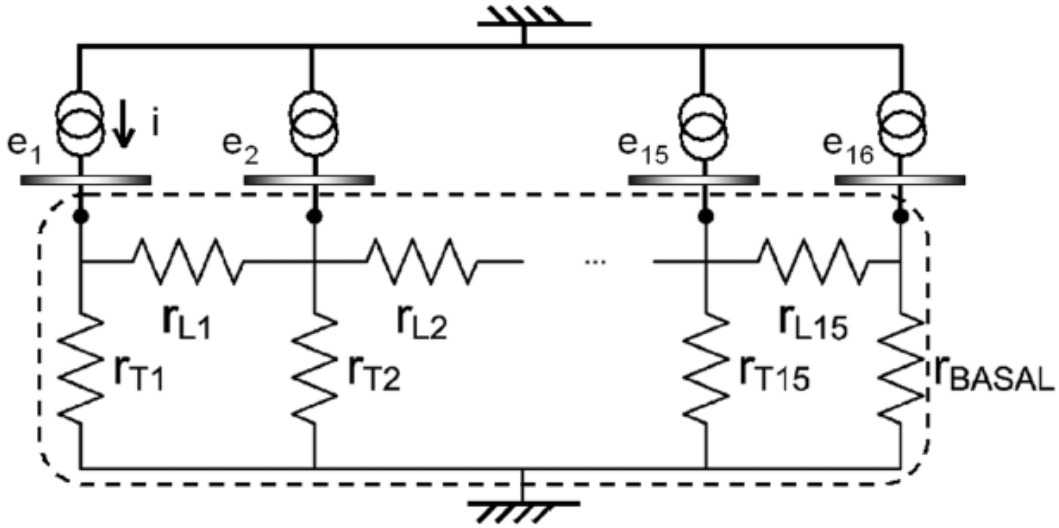

Figure 1.4: Vanpoucke's electrical impedance network describing the cochlea [33, 36]. The lower section, enclosed in dashed lines, is connected to 16 current sources representing the 16 electrode contacts of an Advanced Bionics implant. Longitudinal resistances R_L and transversal resistances R_T represent the impedances created by the tissues in and around the Scala Tympani. The conductance of the base of cochlea to the reference electrode is represented by R_{basal}.

It is important to note that in this model, the cochlea is modelled as a straight semi-insulating tube, as current can only flow from one cochlear compartment to an adjacent one. This seems to be a realistic model as a fit of more than 90% was reported, which is also in line with earlier studies [36]. The impedance values can be adjusted to achieve an optimal fit between the predicted values and the actual field strength values from an individual subject. By applying EFI recordings of a small number of individual subjects to the ladder network, the modelled longitudinal current was found to be two orders of magnitude larger than the transversal current [46]. This is explained by the fact that the conductivity of the bony cochlear walls is low. The perilymph found in between contacts however, is more conductive. This reinforces the idea of modelling the cochlea as a straight semi-insulating tube, and means that if the bony cochlear walls were more conductive, the quality of the model fit would decrease.

Midcochlear Resistance Dip

Using the model, an interesting observation was made by Vanpoucke and his colleagues [46]. In some subjects, a midcochlear impedance tip was observed. At approximately 270° of the basal turn (around electrode contact number 7 and 8), the transversal resistance was found to be 5 to 10 times lower than in other sections. Due to the low resistance, a substantial amount of current will leave the cochlea at this location. The hypothesis is that at 270° of the basal turn, the labyrinthine portion of the facial nerve canal passes close to the cochlea, and the bony wall dividing them is very thin (as seen in Figure 1.5). Electrical current will thus find a less resistive pathway back to the reference electrode here.

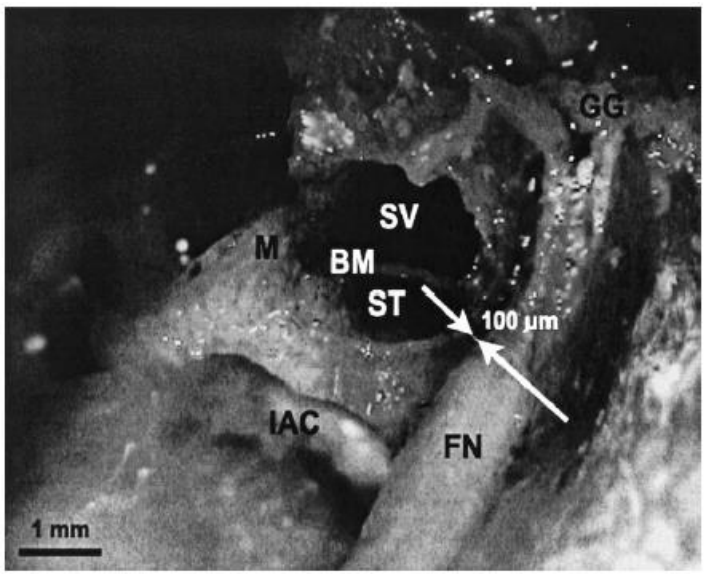

Figure 1.5: Photograph of a human temporal bone specimen [46]. The Scala Tympani (ST), Scala Vestibuli (SV), and the basilar membrane (BM) were cut at 270° of the basal turn of the cochlea. The labyrinthine portion of the facial nerve (FN) can be seen. The thickness of the bony wall dividing the Scala Tympani and the facial nerve is approximately 100µm.

The observations of the midcochlear impedance dip are in line with EFI recordings, where often a change of slope is seen in the voltage curves near electrode contact 7 and 8. In Figure 1.6 it is observed that current flowing from base to apex appears to terminate near these contacts. Furthermore, current flowing from apex to base causes smaller voltage differences at the basal side of contact 7 and 8, compared to the apical side. In future work, this phenomenon should be taken into account when attempting to use EFI recordings for real time monitoring of the electrode array insertion, as it might affect the intracochlear potential profiles around these specific contacts. For this project, we have opted to ignore it due to its complexity and our limited resources. In chapter 6 we very briefly address this issue.

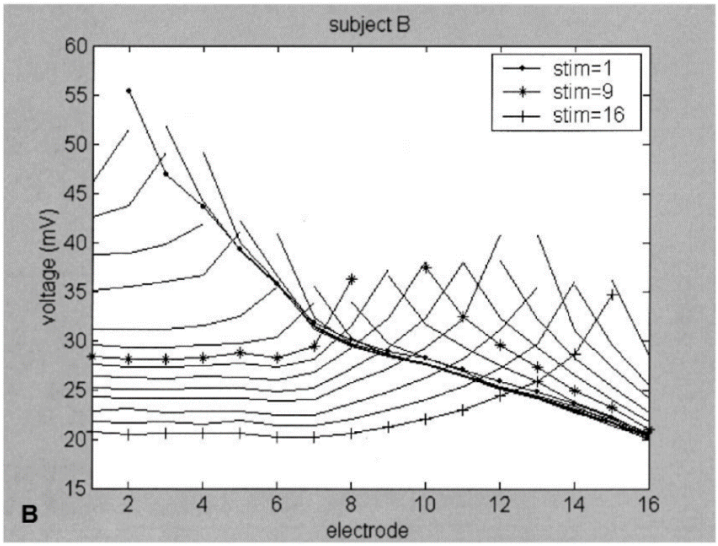

Figure 1.6: EFI measurement showing the effect of the midcochlear dip [46]. The most apical contact is labelled as 1, the most basal contact is labelled as 16. When flowing from base to apex, current terminates at contact number 7. When flowing from apex to base, the slope of the voltage curve decreases past contact number 7.

Telemetry of the Compound Action Potential

Besides telemetry of the intracochlear electrical field,
Recent CI's possess the feature to measure the electrically elicited compound action potential (eCAP) of the auditory nerve. This technique is referred to as either "neural response imaging" (by Advanced Bionics), "neural response telemetry" (by Cochlear Corporation), or "auditory nerve response telemetry" (by MED-EL) [33].

The eCAP is measured by presenting a biphasic pulse on one intracochlear electrode contact and using the implant's casing as the reference electrode. Then, the resulting neural response of the auditory nerve is recorded on a contact close to the stimulating contact. In order to minimize the stimulus artefact present in the recording, contacts directly adjacent to the stimulating contact are not used. By varying the amplitude of the stimulus, the eCAP threshold (the minimum stimulus strength needed to elicit a compound action potential) can be found. Note that the neural response of the auditory nerve is only $\pm 0{,}1\ \mathrm{mV}$ [33]. Due to the small amplitude of this signal, measuring it accurately is not straightforward, and time consuming [35].

Uses of eCAP Telemetry

The eCAP threshold provides valuable objective information used for programming CI speech processors. Objective information on the excitability of the auditory nerve is especially beneficial in paediatric implantation [47, 48]. As a sole means to fit a CI, measuring the eCAP thresholds is not enough, but when combined with other objective measures (such as the electrically evoked stapedial reflex threshold), eCAP measurements can be useful [49, 50, 51].

As the eCAP threshold is a measure of the excitability of the auditory nerve, it provides us with a measure of distance of the electrode array to the auditory nerve (when the auditory nerve is further from the electrode array, the threshold will be higher). Therefore, it might be possible to monitor the electrode array's position and shape relative to the auditory nerve fibers through eCAP measurements. However, the cochlear anatomy is complex and variability between subjects is large. Therefore, in order to detect electrode tip fold-over, knowing the electrode array's shape is more valuable than knowing its position relative to the auditory nerve. In order to eliminate the effect of varying anatomy, information relating to the distance between individual electrode contacts would be preferred over information relating to the distance between electrode contact and auditory nerve.
Furthermore, the amplitude of the electrical stimulation field which is measured in EFI telemetry is much larger than that of the biological response measured in eCAP telemetry. Thus, measuring eCAP accurately is much harder and slower, compared to EFI. In order to detect fold-over during real time monitoring of the electrode array, it is key that measurements can be performed quickly.
Finally, the eCAP threshold is influenced by the number of surviving spiral ganglion cells in the cochlea [33, 52]. This differs greatly in between subjects and is generally an unknown factor.

For these reasons, we assume telemetry of the intracochlear electrical field (as opposed to eCAP telemetry) might be better suited to detect folding of the electrode.

1.5 Previous work

At the time of writing, not much work has been done on monitoring the shape of the electrode array, especially not intra-operatively. The most important work relating to this project will be discussed.

Rotational X-ray imaging

In 2006 Carelsen et al [53]. published an article on insertion monitoring using 3D rotational X-ray imaging. During implantation surgery, a mobile arm was used to acquire 3D X-ray images of the cochlea and electrode array. This allows the surgeon to assess the position of the electrode array with great certainty, as the X-ray images show high bone and implant detail. Using this technique, Carelsen et al. were able to prevent revision surgery in patients by reinserting the electrode directly when scans showed malpositioning [53].

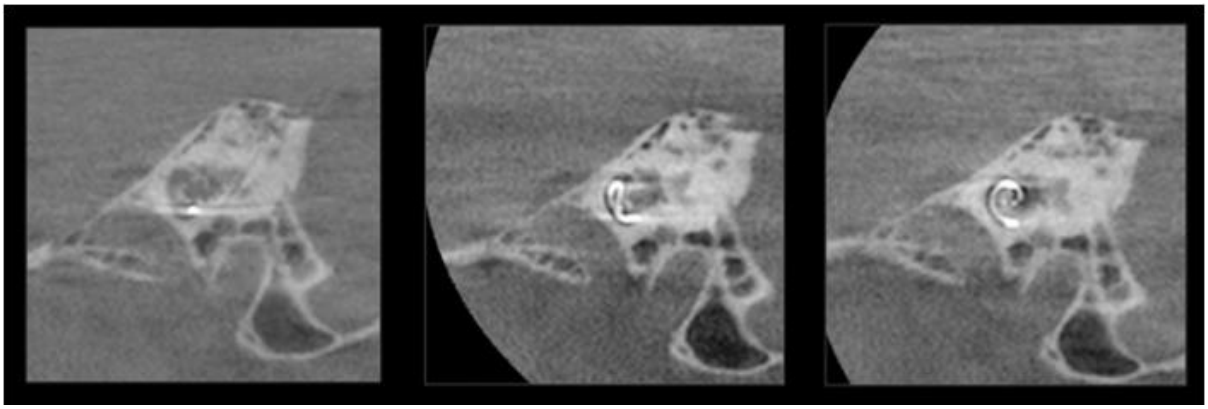

Figure 1.7: 3D X-ray scans of a cochlea during implantation. The left scan shows the start of the electrode insertion, where the electrode array tip is at the opening of the cochlea. The middle scan shows how the electrode array has folded over during insertion. The array was reinserted and the final (correct) array placement is seen in the right scan [53] .

Two scans are performed during surgery. One just before the actual insertion into the cochlea begins, and one after the array is fully inserted into the cochlea and the stylet is removed. This procedure adds 15 minutes to the total surgery time. The method provides accurate images of the implantation intra-operatively, and is a helpful tool for the surgeon to assure optimal electrode placement. As mentioned earlier, specifically patients who suffer from otosclerosis, congenital malformation of the cochlea, or who have suffered from meningitis are at increased risk of electrode misplacement [27, 28, 26]. These patients benefit most from 3D X-ray imaging.

However, the method has a number of limitations. It requires special expensive instrumentation which is not always readily available. Furthermore, the method significantly increases the total surgery time. Most importantly: the X-ray scan is time consuming, and is thus only performed right before and right after the actual insertion into the cochlea. It is useful to detect malpositioning, but only after it has taken place. Due to its nature, it cannot be performed in real-time, and therefore it cannot prevent malpositioning (and the possible trauma to the cochlea it induces) from happening.

Due to the fact that this technique is not suitable for real time monitoring by nature, it will not be considered in this project.

Combining Electrical Field Imaging and Multidimensional Scaling

As we have seen earlier, telemetry of the intracochlear electrical potential provides us with information relating to the relative distance between individual electrode contacts (EFI telemetry). Multidimensional scaling (MDS) is a multivariate analysis technique that has become a common topic in any computer science or data analysis textbook [54]. It is a tool that quantifies estimates of similarity (or dissimilarity) among objects, and presents them in a visually comprehensible way. *Hout* et al. describe MDS as follows: "MDS refers to a set of statistical techniques that are used to reduce the complexity of a data set, permitting visual appreciation of the underlying relational structures contained therein." [55].
When combining EFI and MDS, it is possible to create 2- or 3-dimensional mappings of the relative electrode contact positions, representing the electrode array's shape within the cochlea.

Introductory work on this idea has been done by Vanpoucke [35]. The first step to linking EFI results to physical locations within the cochlea, is constructing an electrical metric, correlating with distance.
When a current source is placed in a homogeneous conducting medium, it is observed that voltage decreases monotonically with increasing distance. This relation is nonlinear and depends on the dimensionality and the material properties of the conducting medium, but it is without exception monotonic [35]. Due to the intricate anatomy of the human cochlea, and the fact that it consists of multiple tissue types, the relation between voltage and distance from the current source is complex and definitely nonlinear, but as stated, it is monotonic nonetheless. Furthermore, studies have shown that, because of the highly resistive cochlear walls, the implanted human cochlea can be modelled by a 1-dimensional curled conductive tube [45].
Therefore, Vanpoucke assumes that the absolute voltage difference between a stimulating and recording contact is an adequate metric for the physical distance between them (the larger the voltage difference, the larger the physical distance between contacts) [35].

This metric can be used to construct a dissimilarity matrix which is used as input for the multidimensional scaling analysis. From the EFI measurements, the absolute voltage difference between contacts is easily derived. Let E be the $n\ x\ n$ matrix of EFI measurement values, where n is the number of electrode contacts. The MDS "input" matrix D is then given by $D(s,r) = |E(r,r) - E(s,r)|$ where s is the stimulating contact and r is the recording contact. Note that MDS requires a symmetric, square matrix as input, and that D is not symmetric due to the varying electrode contact impedances. To solve this, the average of $D(s,r)$ and $D(r,s)$ can be taken. Furthermore, the voltages are divided by the injected current in order to be independent of stimulation strength. Thus, the values in E and D are impedances, and the unit is Ohms.

Performing MDS analysis on matrix D provides us with a possible configuration of points, where the distance between points represent the physical distance between electrode contacts within the cochlea. In this configuration, the shape of the electrode array can be observed. Thus, any abnormalities such as tip-fold over can be detected.

Examples of MDS analysis performed on EFI data can be seen in Figure 1.8 and 1.9 [35]. The left top corner shows the intracochlear voltage profiles (EFI measurements), the right top shows the input matrix D, the left bottom corners shows the MDS solution, and the right bottom corner shows a CT scan for comparison. Figure 1.8 shows EFI data and MDS solution for a patient with a normal,

problem-free insertion. It can be observed that the trajectory of the MDS solution is similar to the CT scan (although rotated by 90°).
In Figure 1.9, the EFI data and MDS solution for a patient with a tip fold-over are presented. The MDS mapping shows an obvious fold over which is confirmed by the CT scan. This indicates that the method is able to detect fold-overs.

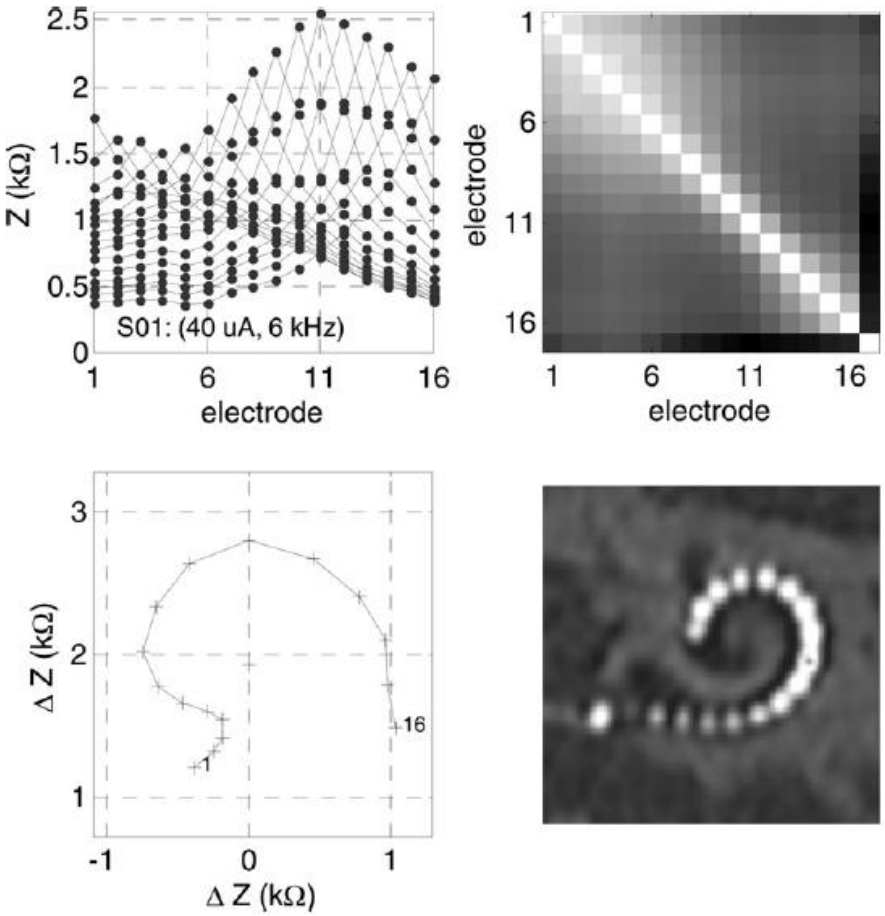

Figure 1.8: Results of MDS on EFI data in a normal insertion [35].

However, there is room for improvement. In Figure 1.8 for example, the apical (electrode contact numbers 1 to 5) end of the array is curled, while in the CT scan it is not. Vanpoucke does not mention possible causes for this. The curling might be explained by a 1-D curled conductive channel not being a perfectly realistic model for the human cochlea.

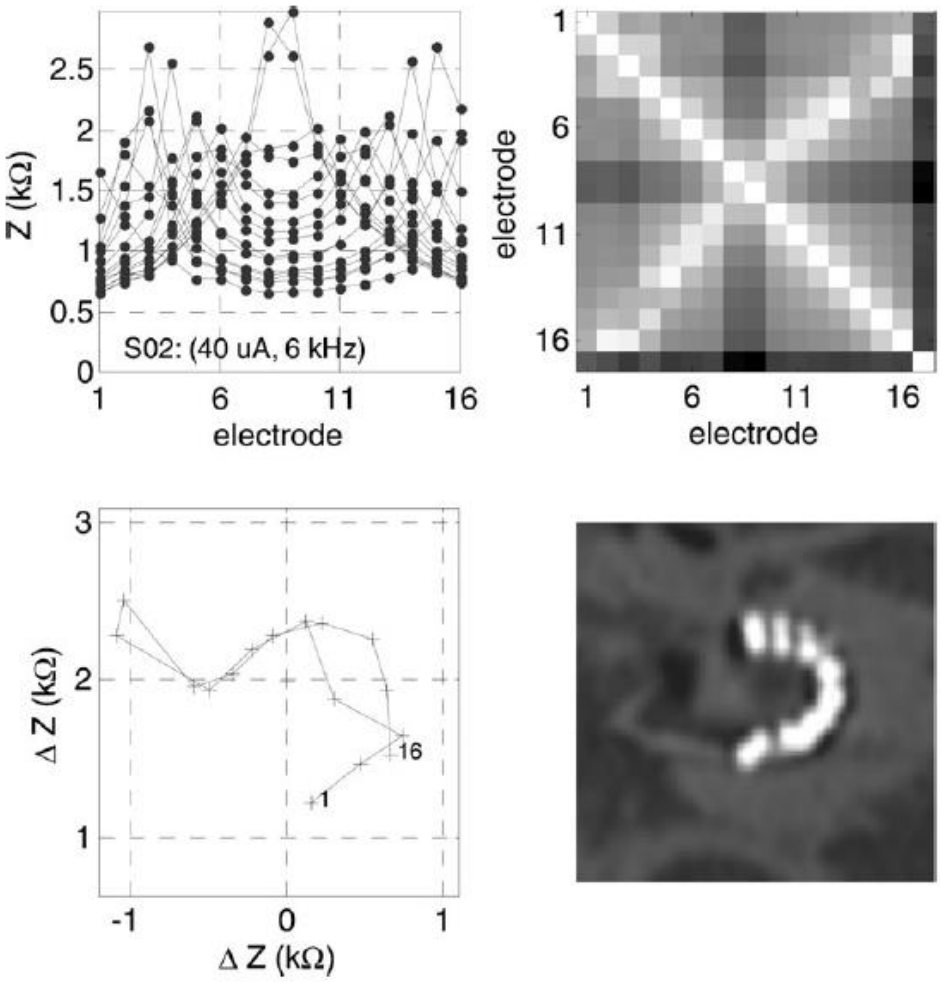

Figure 1.9: Results of MDS on EFI data in a cochlea where fold-over has occurred. In both the MDS map, and the CT scan, a fold-over of the electrode can be seen near the middle of the electrode array (contact number 8) [35].

The EFI measurements used by Vanpoucke were done using Advanced Bionics implants (HiRes90K) and the standard software provided by Advanced Bionics. Using this software, a full EFI measurement takes roughly 1.5-2 minutes. If the EFI measurements can be sped up and subsequent MDS analysis can be performed fast enough, this method could provide means to visualize the electrode array's shape in real time.

1.6 Conclusion

The scientific field has shown immense growth and progress over the years. The population of cochlear implant users continues to grow, and so does the number of publications on cochlear implant research. Due to its effectivity, cochlear implantation has become a common medical procedure.
However, the procedure does not always come without complications. During the insertion of the electrode into the cochlea, there is a number of issues that can occur. The most problematic of these is folding of the electrode tip, which happens in 1 to 2% of cases. Folding of the electrode tip leads to a decreased access to the auditory nerve and thus decreased hearing performance. Furthermore it can potentially cause trauma to neurovascular structures surrounding the cochlea, such as the facial nerve and the vestibular system. Tip fold-over is often reason for revision surgery.

Surgeons would benefit greatly from a tool that allows monitoring of the electrode array's shape during insertion. Such a tool may be able to prevent electrode tip fold-over and possible trauma. Additionally, in an advanced stadium, it might replace the need for a post-operative CT-scan to assess the array's positioning (which is currently common practice).
The goal is to achieve this without using any instrumentation other than the implant itself. External instrumentation (such as a CT scanner) is often expensive, not readily available, and impractical. A quick, reliable method that requires no instrumentation other than the implant itself would be of great value. In this report, two ideas will be researched and discussed.

2. Proposed Method

In this section, two methods are proposed for monitoring the electrode insertion in real time. Both methods require no other instrumentation than the implant itself.

2.1 Method 1: Real-time EFI-MDS

As shown by Vanpoucke [35], combining telemetry of the intracochlear electrical field with multidimensional scaling provides a way to visualize the shape of a cochlear implant electrode array without the use of any special instrumentation. The visualization of the electrode array's shape facilitates the interpretation of abnormal electrical spread data, and it has been used to assess the electrode insertion post-operatively. However, intra-operative use of this technique has not been attempted.
If both the measurement of the intracochlear electrical field and the subsequent multidimensional scaling analysis can be sped up, it may be possible to construct a real-time image of the electrode array's shape during the insertion.

In Vanpoucke's work, EFI measurements were performed using the standard software provided by the implant manufacturer. In this case, all subjects were implanted with an HR90K device with a HiFocus1J electrode, produced by Advanced Bionics. This device features 16 electrode contacts. The software provided by Advanced Bionics is called EFIM (Electrical Field Imaging and Modeling tool).

In EFIM, there is a number of parameters for the user to set. These include the stimulation type (pulse or sine), the pulse duration or sine wave frequency, and what electrode contacts to use. The HiFocus1J electrode features 16 electrode contacts.

A measurement is performed by stimulating the first contact, and the decay of the electrical potential is then measured on all 16 contacts. This is done 1 by 1 (so the first contact is stimulated 16 times). Subsequently, the stimulation contact is moved to number 2, and again the electrical potential is measured on all 16 contacts. This is repeated until every contact has been used as stimulating contact.
Thus, when using all 16 contacts, there is a total of $16x16 = 256$ stimulation/recording cycles. In Vanpoucke's work, EFI measurements were performed post-operatively, and were done using all 16 contacts. Performing such a measurement takes roughly 2 minutes in EFIM. For real-time monitoring, measurements need to be significantly faster.

To realize this, a first step would be to reduce the number of active contacts. When the electrode folds over, the change of shape occurs in the tip of the electrode. Hence, we are only interested in the most apical contacts and their relative positioning. This is illustrated in Figure 2.1. When the number of active contacts is reduced from 16 to 5, the measurement time will be reduced with a factor of $\frac{256}{25} = 10.24$. The downside is that reducing the number of active contacts means there is less current spread data available, and the resulting MDS map will likely be less accurate compared to when all contacts are used. Thus, there is a trade-off between speed and accuracy of the resulting MDS map.

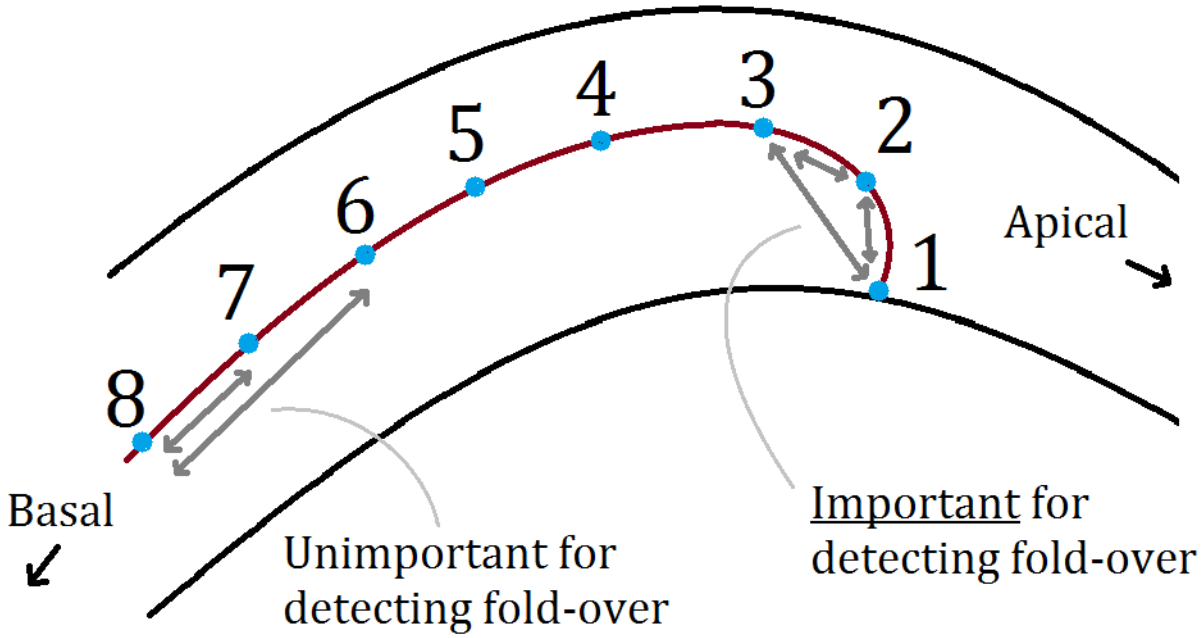

Figure 2.1: Atypical relative distance between apical contacts gives indication for fold-over

A second step is to adjust the stimulation method. In the standard EFIM measurements, only 1 contact is stimulated, and 1 contact is measured in a single cycle. However, cochlear implants are designed to stimulate multiple contacts simultaneously (in order for the user to hear multiple frequencies at the same time). This can for example be used to stimulate 3 contacts using interleaved pulse trains. By recording on a 4th contact, 3 impedances can be measured in one cycle instead of just 1.
To do so, Advanced Bionics provides BEDCS (Bionic Ear Data Collection System), which is software meant for clinical experimentation. In BEDCS, the stimulation can be completely customized (in contrast to the limited options in EFIM).

A third step is to research different types of multidimensional scaling. There are several types of MDS (classic versus distance, metric versus non-metric) and different loss functions (stress, strain, and more). These are addressed in chapter 4. In Vanpoucke's work, classical metric scaling was used, but it is not disclosed why this option was chosen. Other types may potentially be faster, or more effective for this specific application.

By combining these steps, the time needed for an EFI measurement can be drastically reduced, making MDS analysis of EFI data in real time a viable option. It is important to keep in mind that there Is a large trade-off between speed and accuracy, and an optimum will need to be found. To do so, we will compare the relative distance between contacts in the MDS mapping to the relative distance between contacts in a CT scan of the same patient.

2.2 Method 2: Real-time Monitoring of Tip Impedance Values

Another proposed idea is to solely monitor the changes of electrode contact impedances during the insertion. This means that the shape of the electrode array will not be estimated or visualized. Instead, the changes in impedance values over time might indicate when a fold-over is occurring.

This idea is based on the fact that when a current source is placed in a homogeneous medium, the voltage decreases monotonically as a function of distance to the source.
Studies have shown that due to the high resistivity of the surrounding cochlear walls, the cochlea can be approximated by a 1-D curled conductive channel model [45]. This means that when stimulating an electrode contact within the cochlea, the electrical potential measured should be lower, the further away we get from the contact.

However, when a fold-over occurs, the most apical contacts (in the tip) will be brought closer to the basal contacts. Thus, when stimulating a basal contact, an unusually high potential will be measured in the apical contacts. This is illustrated in Figure 2.2.

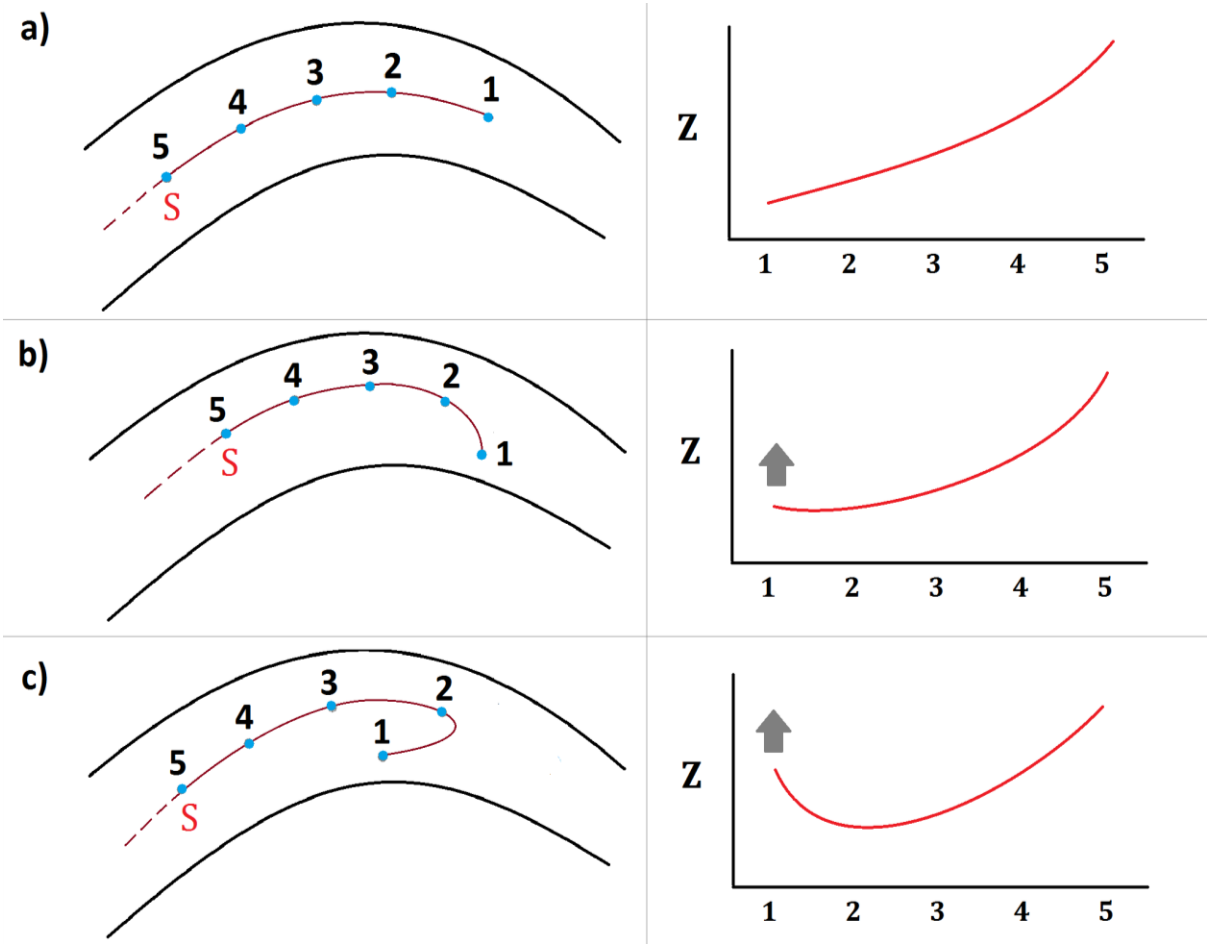

Figure 2.2: Illustration of changes in impedance during a fold-over. The stimulating contact in every case is contact number 5. Note that in the normal case (a), the impedance decreases monotonically as the distance from contact number 5 increases. In case (b), a fold-over starts forming and the impedance in the most apical contacts starts climbing. In case (c) a fold-over has formed, and the impedance measured at contact 1 is higher than that of 2, due to it being physically closer to the current source.

To realize this, one contact will be chosen as recording contact, and a number of contacts will be chosen as stimulating contacts. For example, we will record on contact 3 and stimulate the first 2 contacts shortly after one another, using interleaved pulse trains.
As fold-over occurs, the apical contacts are brought physically closer to the basal contacts, and therefore the absolute difference between the measured impedances will become smaller.
By plotting the absolute difference between these 2 impedance values in real-time, a visual aid is constructed in which fold-over can be detected. In the normal case, the impedance difference should be rather constant. When fold-over occurs, the impedance difference will drop.

It is important to keep in mind that the cochlea is a complex anatomical structure, and a lot of noise is to be expected in the impedance measurements. This can be due to drops of blood on the electrode, or electrode contacts hitting the cochlear wall. Therefore it should be considered to perform this same technique using more contacts (e.g. 4 stimulating contacts). This will reduce the noise and give the surgeon more certainty over whether a fold-over is actually occurring. However, this will also slow down the frame rate of the real-time monitoring, because more impedances need to be measured. Again, there is a trade-off between speed and accuracy which needs to be considered.

3. Electrical Field Imaging and Available Data

As introduced in section 2, Electrical Field Imaging (or EFI) is the term for telemetry of the intracochlear electrical field. Later on in this report, we will attempt to use EFI measurements to monitor the shape of an cochlear implant electrode array. In the following section EFI measurements will be described, and an overview of the available data for this project is given.

3.1 EFI Measurements

EFI measurements are performed by stimulating one of the intracochlear contacts, and subsequently recording the electrical potential along other contacts. The "standard" EFI measurement stimulates all contacts (16 in the case of an Advanced Bionics implant [56]) and also records the decay on all contacts (so, this provides $16x16 = 144$ values). This is exactly the type of measurement that was performed in Vanpoucke's work [57].

In Figure 3.1 a standard EFI measurement for a problem-free insertion is presented. Note that there are 16 curves, one for each stimulating contact. The peaks indicate the stimulating contact, and as we move away from the stimulating contact (either in apical or basal direction) the voltage decreases monotonically. This makes sense, as the electrical potential should decrease as we move along the scala tympani, away from the current source. It is important to note that in some cases, the potential can slightly rise at the apical end of the cochlea. The reason for this is that the current might traverse the cochlear walls (in a straight line) instead of flowing through the actual curved scala tympani. The y-axis shows the impedance $Z(\Omega)$, which is equal to the measured electrical potential (V) divided by the injected current (A). This is done to eliminate the influence of stimulation strength and provide a generalized impedance value which defines the relation between the injected current at one position within the cochlea, and the electrical potential it induces at another position. Note that recording and stimulating on the same contact produces an unrealistically high voltage due to the interface impedance, hence the large peaks.

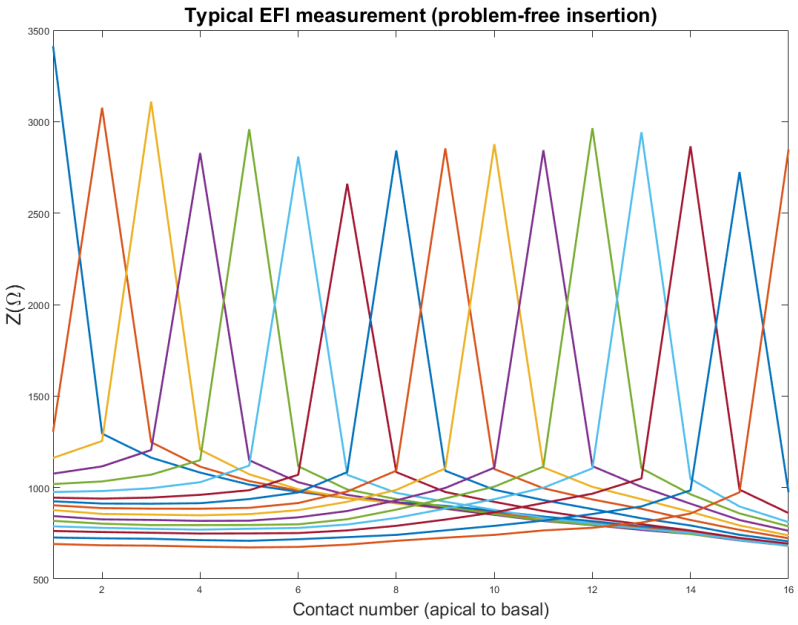

Figure 3.1: A typical EFI measurement for a problem-free insertion. This was recorded with the Advanced Bionics HiRes 90k HiFocus implant, using all 16 contacts. The most apical contact is labeled "1", the most basal contact is labeled "16".

All patients that were included in this research used Advanced Bionics implants. These implants come with stand-alone software provided by Advanced Bionics [58, 59]. The clinician using the software has the option to set a number of parameters such as the stimulus type (pulse, sine), the injected current level, and what contacts to stimulate or record on. After setting these parameters, a fixed number of measurement cycles is performed and averaged to produce the intracochlear potential profile.

3.2 Available data

In the Leiden University Medical Center, where this project was conducted, most patients are implanted with 'HiRes 90K Advantage 1J' or 'HiRes 90K Advantage MS' devices by Advanced Bionics. For patients with an Advanced Bionics implant, it has been standard procedure since 2003 to measure EFI in the operating theatre directly after the implantation. This measurement is done using the software provided by Advanced Bionics called 'EFIM' (short for Electrical Field Imaging Measurement tool).
For patients that are implanted with CI's from different manufacturers (MED-EL, or Cochlear) it has not been common procedure to measure EFI.

For this project, we have chosen to only include EFI data of patients with an 'HiRes 90K Advantage' or 'HiRes 90K 1J' implant by Advanced Bionics. Other than this criteria, there is no preselection. Thus the patient group spans all ages, sexes, medical conditions, etc. The final number of patients included in this research is 267, of which 3 patients have an electrode fold-over. These 3 patients will be addressed later on in this section.

On each of the patients, a standard measurement was performed using EFIM. This means the measurements are done directly after surgery, in the operating theatre. The intracochlear electrical potential profile is measured 4 times, each time with a different stimulus. The 4 different stimuli are:

1. "Sine wave 1": A sine wave with frequency of 6000Hz & amplitude of 40µA
2. "Sine wave 2": A sine wave with frequency of 1000Hz & amplitude of 40µA
3. "Pulse 1": A biphasic pulse with frequency of 15000Hz & amplitude of 40µA
4. "Pulse 2": A biphasic pulse with frequency of 15000Hz & amplitude of 120µA

Inherently, there are 4 impedance matrices (such as the one shown in Figure 3.1) for each patient representing the intracochlear potential profile. Later on we will determine which of the 4 stimuli produces the most suitable results for our application.

In Figure 3.2 an overview of the available data is given.

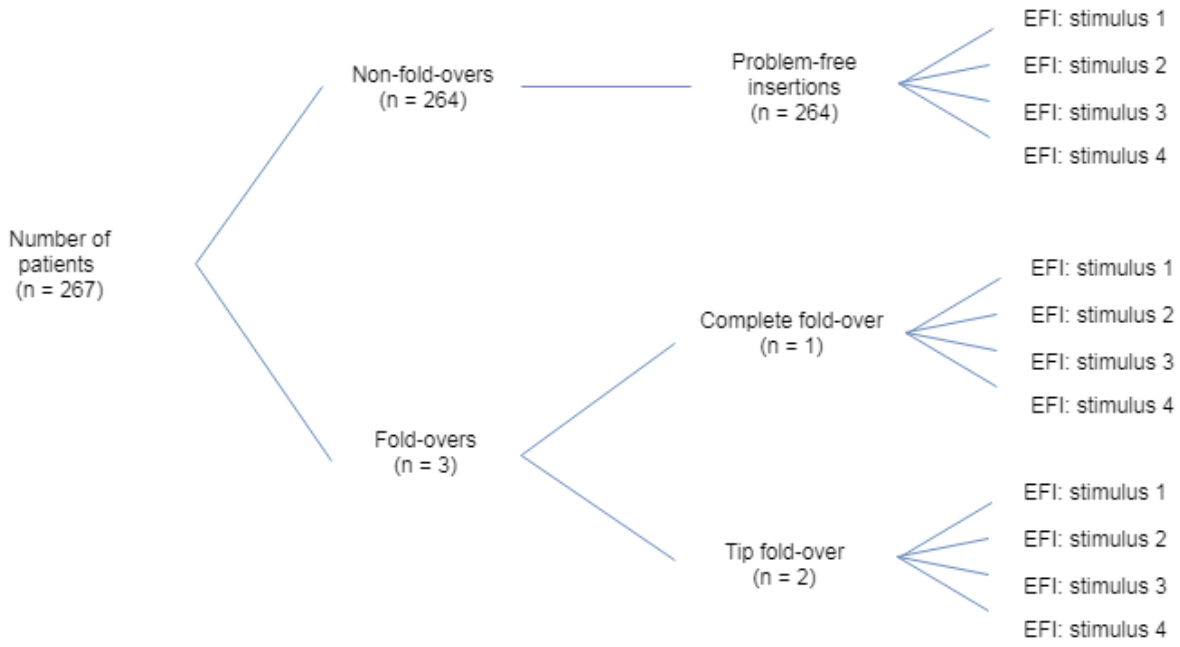

Figure 3.2: An overview of the data available for this project. All 267 patients are implanted with HiRes 90k HiFocus devices. Of the three fold-overs, one is a complete fold-over (where the electrode is folded in half). The other two are tip fold-overs, where only the first few contacts are folded.

3.3 Fold-over EFI data

As seen above, there are only 3 patients with electrode fold-overs in the LUMC. It is important to realize that this is an extremely small sample size compared to the group of patients with problem-free insertions (n = 264). There are more patients with electrode fold-overs in other medical centers, but unfortunately it was not possible to access this data for this project. However, the data does exist and could possibly be gathered for future work in this area. The lack of data needs to be taken into account for the statistic tests performed in this project. It will be addressed in the associated sections of the report.

Furthermore, the 3 patients with electrode fold-overs are not all similar. Two of the patients suffer from an electrode tip fold-over, where only the first one or two contacts are folded. The last patient suffers from a complete fold-over, where the first eight contacts have folded over (in other words, the first and the last contact are "on top" of each other). This is important, because these patients have dissimilar intracochlear electrical potential profiles. Thus, for example comparing $\frac{Z_{r3,s1}}{Z_{r5,s1}}$ will give different results for the tip fold-over patients, and the complete fold-over patients (where $Z_{r3,s1}$ is the impedance measured at contact 3 when stimulating contact 1, and $Z_{r5,s1}$ is the impedance measured at contact 5 when stimulating contact 1). This is another significant fact to keep in mind when analyzing the data. In Figure 3.3 the CT-scans for one of the patients with a tip fold-over (A) and for the patient with a complete fold-over (C) are presented. The CT-scans for all 3 fold-over patients can be found in Appendix A.

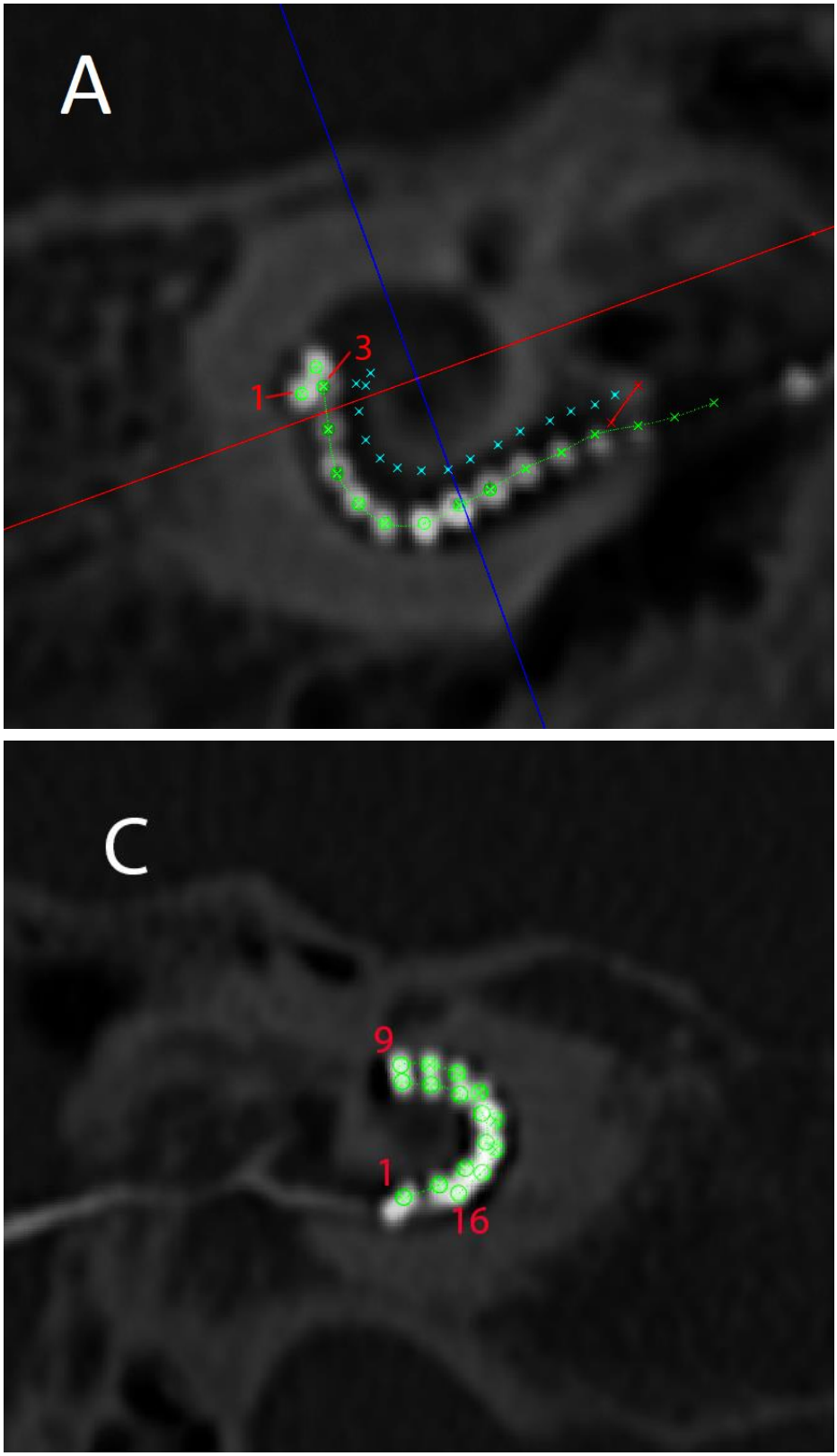

Figure 3.3: Computed tomography scans for two patients with a fold-over. Patient A suffers from a tip fold-over, where only the first contact is folded over. Patient C suffers from a complete fold-over (note that contact 16 is very close to contact 1). Both images were constructed by layering several CT scan slices on top of eachother, in order to make all contacts visible.

4. Introduction to Multidimensional Scaling

Telemetry gives us a means of checking the implant's status, and also provides us with the possibility to measure intracochlear electrical potentials. The intracochlear electrical potential profile can in turn provide us with information relating to the distance between electrode contacts (EFI). Multidimensional scaling offers a way to construct a 2D or 3D visualization of the electrode array's shape, using the data produced by telemetry.
In this section, multidimensional scaling will be introduced.

In section 1.5 we have seen that multidimensional scaling (MDS) is a multivariate analysis technique that is widely applied. It is a method that presents estimates of similarity or dissimilarity among objects in a visually comprehensible way. As input, MDS takes dissimilarity measurements among pairs of objects. If only the similarity information is known, this can be converted to dissimilarity information through a monotone decreasing transformation (high similarity means low dissimilarity). The output is usually a two- or three-dimensional map in which the objects are presented as points. In this map, objects that are similar are located proximal to each other, and objects that are dissimilar are located further apart. The distance between two points in the map therefore represent the (dis)similarity between these objects [54, 55, 60, 61, 62, 63]. To illustrate this: applying MDS to a set of pairwise similarity ratings among different color samples ("On a scale of 1 to 10, how much are these two colors alike?") would result in a map resembling Newton's color wheel. Red would be located close to orange, but far away from green and blue [55].
MDS is a valuable tool because it has the potential to reduce complex data to a visually comprehensible map. Furthermore it provides us with a quantitative measurement (the distance between two objects on the map) of the perceived (dis)similarity of objects. It is widely applicable and utilized in many fields [55], including marketing [64], ecology [65], political science [66], psychophysics [67], sociology [68] and neuroscience [69]. It is also a commonly used tool in many forms of psychology such as social [70], cognitive [71], clinical [72], and developmental psychology. [73]

Proximity Data and Loss Functions

As stated earlier, MDS uses dissimilarity information for *pairs* of objects as input. This is referred to as "proximity data". Note that this is not the same as multivariate data, as multivariate data describes information for *individual* objects.
Let's now assume we have a number of objects labelled $i = 1, \dots, N$. The proximity data is then presented in square matrix form ("distance matrix", or "dissimilarity matrix") given by dissimilarity values D_{ij}. MDS aims to map the objects $i = 1, \dots, N$ to points $\boldsymbol{x}_1, \dots, \boldsymbol{x}_n$ in a k-dimensional space, so that the distances $\|\boldsymbol{x}_i - \boldsymbol{x}_j\|$ approximate the dissimilarity values D_{ij}. The value of k can be chosen freely, but in practice $k = 3$ or lower is used, so that the mapping can be easily visualized.

In Figure 4.1, two trivial examples of dissimilarity matrices are given, which both have zero-error MDS solutions. The corresponding MDS solutions are also presented. In reality, a much larger number of objects is usually considered, and there is usually no error-free solution. It is important to note that the solutions are not unique, but can be rotated and translated freely.

$$D = \begin{array}{c} \\ a \\ b \\ c \\ d \\ e \end{array} \begin{array}{c} \begin{array}{ccccc} a & b & c & d & e \end{array} \\ \begin{bmatrix} 0 & 1 & 2 & 3 & 4 \\ 1 & 0 & 1 & 2 & 3 \\ 2 & 1 & 0 & 1 & 2 \\ 3 & 2 & 1 & 0 & 1 \\ 4 & 3 & 2 & 1 & 0 \end{bmatrix} \end{array} \qquad D = \begin{array}{c} \\ a \\ b \\ c \end{array} \begin{array}{c} \begin{array}{ccc} a & b & c \end{array} \\ \begin{bmatrix} 0 & 3 & 4 \\ 3 & 0 & 5 \\ 4 & 5 & 0 \end{bmatrix} \end{array}$$

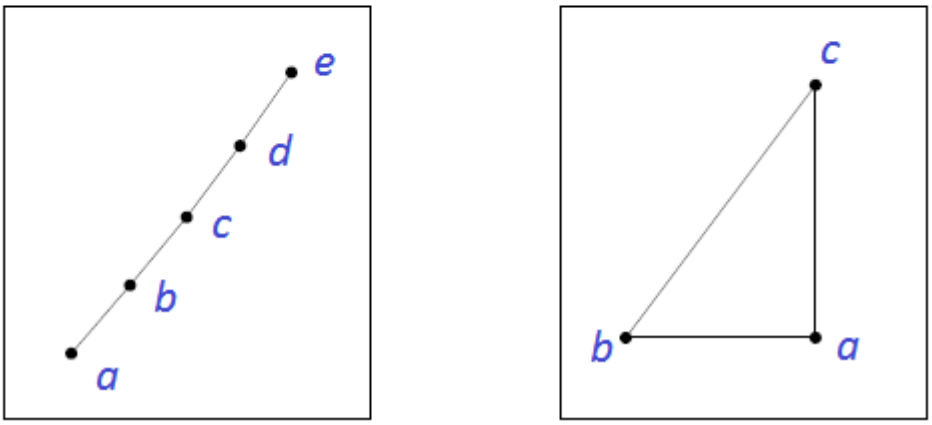

Figure 4.1: Two trivial examples of distances matrices and their optimal, error-free MDS solutions [74]

The original version of MDS, often referred to as "classical MDS", or "Togerson Scaling" was introduced by Togerson in 1952 [75]. A classical MDS algorithm follows the following steps to find the coordinate matrix X [54, 76]:

1. Construct the squared proximity matrix D^2
2. Use the centering matrix $J = I - \frac{1}{n}11'$ (where n is the number of objects) to apply double centering to the squared proximity matrix: $B = -\frac{1}{2}JD^2J$
3. Determine the eigenvalues $\lambda_1, \dots, \lambda_n$ and eigenvectors $e_1, \dots, e_n$ of B.
4. The coordinate matrix X is now given by $X = E_k\Lambda_k^{\frac{1}{2}}$, where Λ_k is the diagonal matrix of the k largest eigenvalues of B and E_k is the matrix of corresponding k eigenvectors. Here, k is the number of dimensions desired in the MDS map.

It can be proven this classical MDS algorithm minimizes a loss function called *Strain* [54]. Strain is defined by [77]:

$$Strain_D(\boldsymbol{x}_1, \dots, \boldsymbol{x}_N) = \left(\frac{\sum_{i,j} \left(b_{ij} - (\boldsymbol{x}_i, \boldsymbol{x}_j) \right)^2}{\sum_{i,j} b_{ij}^2} \right)^{\frac{1}{2}}$$

In which b_{ij} are terms of the matrix B, which was introduced in step 2 of the algorithm above. The coordinates $\boldsymbol{x}_i, \boldsymbol{x}_j$ that result in the smallest *Strain* are found in step 4 of the algorithm (coordinate matrix *X*).

However, 12 years after the introduction of classical MDS by Togerson, it was Kruskal [78, 79] who introduced a loss function named *Stress* to MDS, and it is his version of MDS that has become the most commonly used [74]. It is referred to as "distance MDS" as opposed to "classical MDS". Kruskal characterized MDS in terms of minimization of the loss function Stress. Stress is a measure that indicates the "badness" of fit between the fitted distances $\|\boldsymbol{x}_i - \boldsymbol{x}_j\|$ and the dissimilarity values D_{ij}. A stress of 0 indicates a perfect fit (such as in Figure 4.1) and if the stress increases, the fit decreases. Stress in defined as the square root of the residual sum of squares [74]:

$$Stress_D(\boldsymbol{x}_1, \dots, \boldsymbol{x}_N) = \left(\sum_{i \neq j = 1 \dots N} \left(D_{ij} - \|\boldsymbol{x}_i - \boldsymbol{x}_j\| \right)^2 \right)^{\frac{1}{2}}$$

Distance MDS uses gradient-based minimization applied to the Stress, in order to find the optimal configuration of points [74].

Types of Multidimensional scaling

There are a number of different types of multidimensional scaling, all best suited for slightly different purposes. It is possible to make the following general subdivisions:

- **Classical** multidimensional scaling (Togerson)
- **Distance** multidimensional scaling (Kruskal)
    - **Metric distance** multidimensional scaling versus **nonmetric distance** multidimensional scaling

Distance Scaling versus Classical Scaling

In classical scaling, the dissimilarity data D_{ij} is fitted by inner products $\langle \boldsymbol{x}_i, \boldsymbol{x}_j \rangle$ by transforming the dissimilarity data D_{ij} to "inner-product" data B_{ij}. Whereas in distance scaling, the dissimilarity data D_{ij} is fitted by the distances $\|\boldsymbol{x}_i - x_j\|$.
An important difference between the two is that inner products rely on an origin, while distances do not. This can be interpreted as follows: a set of inner products determines a unique set of distances, but a set of distances does not determine one unique set of inner products. It determines a set of inner products, with an unknown origin. For this reason, classical scaling is used for mean-centered configurations [74].
Furthermore, distance MDS requires iterative minimization in order to be solved, whereas classical MDS can be solved using simple and fast eigendecompositions.
Classical MDS can also be solved by applying iterative gradient descent on a loss function named strain, which is parallel to a gradient descent on the loss function stress in distance MDS. The advantage of this is that it is possible to introduce missing values or add weights to values, which is not possible when using eigendecompositions.

Metric distance Scaling versus Nonmetric distance Scaling

Within distance scaling, we can make a subdivision in metric and nonmetric scaling.
Metric scaling aims to produce a set of points whose inter-point distances approximate the given dissimilarities. In some cases however, this requirement can be too strict.
Non-metric scaling is designed to relax this requirement and aims to approximate a non-linear monotonic transformation of the dissimilarities (instead of the original dissimilarities).

In other words, metric scaling is applicable when the available data is in the form of observed quantities, measured in terms of coordinates, where distances are meaningful (such as in the examples presented earlier).
However, it is also possible to perform MDS on ordinal data which is observed on a scale where only "ranking" is important, and not the actual differences [62, 63]. For example, if $p_{12} = 3$ and $p_{34} = 7$, an ordinal model would read this only as $p_{34} > p_{12}$, and ignore the actual values of p_{12} and p_{34}. This is called nonmetric MDS.
Just like in metric scaling, a loss function is used. The difference being, in nonmetric MDS, a non-linear monotonic transformation is first performed on the dissimilarities.
Due to the monotonicity, larger distances on the plot will correspond to larger dissimilarities. However, the nonlinearity implies that only the ordering of dissimilarities is attempted to be preserved.

Because time is of the essence in our application, classical MDS is desirable as it is faster than distance MDS (distance MDS is solved iteratively, while classical MDS is solved by fast eigendecomposition). However, experimentation with all types of MDS should be conducted.
If we were to opt for distance MDS as opposed to classical MDS it would be straight forward to choose metric scaling over nonmetric, as the actual voltages at the electrode contacts are known. We want to find the best approximation of the dissimilarities possible, and it is not necessary to work with a monotonic transformation of the dissimilarities.

5. Method 1: EFI-MDS

In the previous chapters EFI measurements and Multidimension Scaling were introduced. In this chapter we will be combining the two to produce a visual representation of the electrode array's shape. This might possibly provide a useful tool for surgeons and clinicians to detect and perhaps even prevent electrode tip fold-overs.

Very little scientific research has been conducted in this area. In fact, only one paper has been published on this specific topic (combining EFI and MDS), by *Vanpoucke* [57]. Although Vanpoucke's work is introductory, they did manage to distinguish a number of problem-free insertions from problematic insertions. The EFI measurements were performed post-operatively and analyzed through MDS to produce a 2D visual representation of the array's shape.

In section 6.1 we determine what combination of MDS type and EFI stimulus type provides the most reliable results (in other words, the MDS solution that is closest to the CT-scan coordinates).
In section 6.2 we will try to find an objective measure based on EFI-MDS to distinguish fold-overs from non fold-overs.
Finally, in section 6.3, we will assess the viability of performing EFI-MDS in real time.

5.1 Comparing MDS types

As we've seen in chapter 5, there are a number of different types of MDS. In the work done by Vanpoucke [57] only one of these types is explored (metric distance scaling using the "stress" criterion), and it is not disclosed why this specific type was chosen.

In this section we will determine what type of MDS is most suitable for the application of monitoring cochlear electrode array shapes. To do so we will be using the EFI data of 264 cochlear implant patients who have clean, problem-free insertions. The following types of MDS are included in the research:

- Classical MDS (Togerson) (1)
- Nonmetric Distance MDS:
  - Stress (2)
  - Squared Stress (3)
- Metric Distance MDS:
  - Stress (4)
  - Squared Stress (5)
  - Sammon (6)

All patients are implanted with Advanced Bionics Hi-Res 90k devices, and EFI was measured post-operatively (i.e. still in the operating theatre, but after the array has been fully inserted) using standard software (EFIM) provided by Advanced Bionics. This standard software performs 4 measurements, each using a different stimulus. The 4 stimuli are:

1. "Sine wave 1": A sine wave with frequency of 6000Hz & amplitude of 40µA
2. "Sine wave 2": A sine wave with frequency of 1000Hz & amplitude of 40µA
3. "Pulse 1": A biphasic pulse with frequency of 15000Hz & amplitude of 40µA
4. "Pulse 2": A biphasic pulse with frequency of 15000Hz & amplitude of 120µA

To determine what type of MDS is most suited for our application, the following main steps will be taken:

1. **EFI-MDS Analysis**
   The EFI data of every patient (for all 4 stimulation types) is analyzed through all 6 types of MDS. This provides us with 24 MDS solutions per patient.
2. **Computing MSE between MDS solution and CT-scan**
   Each MDS solution consists of 16 sets of xyz-coordinates. These are compared to the 16 sets of xyz-coordinates derived from CT-scans of the same patients through the mean squared error. This is comparison is not straightforward and is addressed later on in this section.
3. **Results and discussion**
   The combination of stimulation type and MDS type that provides the smallest mean squared error will be deemed most suitable for our application, as this combination gives the best approximation of the true inter-contact distances (derived from CT-scans). Also, the time needed to perform the analysis is taken into account.

5.1.1 EFI-MDS Analysis

In order to analyze the EFI data through MDS, we first need to transform the transform the $n\ x\ n$ EFI matrix (n is the number of contacts. In case of an AB implant, 16) to a new metric that relates to the physical distance between contacts.

From EFI to physical distance metric

When we place a current source in a homogeneous conducting medium, the voltage decreases monotonically when moving away from the source. This relationship is nonlinear and it depends on the dimensionality and the material properties of the conducting medium, but it is always monotonic. Due to the intricate anatomy of the human cochlea, and the fact that it consists of multiple tissue types, the relation between voltage and distance from the current source is complex and definitely nonlinear, but still monotonic in most cases (in some cases, it is not completely monotonic due to the minor effect of current crossing over through the cochlear walls). Therefore, we make the assumption that the absolute voltage difference between a stimulating and a recording contact is an adequate metric for the physical distance between them (the larger the voltage difference, the larger the physical distance between the contacts).

From the EFI measurements, the absolute voltage difference between contacts is easily derived. First, we adjust the peak values in the EFI measurement (as stated in chapter 4, they are unrealistically high) by fitting exponential curves through the other 15 measured points. Now, let E be the $n\ x\ n$ matrix of EFI measurement values, where n is the number of electrode contacts. The absolute voltage differences then given by $D(s,r) = |E(r,r) - E(s,r)|$ where s is the stimulating contact and r is the recording contact.
Note that MDS requires a symmetric, square matrix as input, and that D is not symmetric due to the varying electrode contact impedances and noise.
To solve this, the average of $D(s,r)$ and $D(r,s)$ can be taken: $D_{av} = \frac{D(s,r)+D(r,s)}{2}$. Note that the matrix D is nearly symmetric, thus, taking the average as described above does not have a dramatic effect. Furthermore, the measured voltages are divided by the injected current in order to be

independent of stimulation strength. Thus, the values in E and D are impedances, and the unit is Ohms.

Performing MDS

We now have the input matrix D_{av} and are ready to perform MDS. The MDS analysis was performed in MATLAB 2016a, using the functions *cmdscale* (for classic MDS) and *mdscale* (for all other types of MDS). This produces a set of *n* points in a *k*-dimensional space, where n is the number of contacts (16) and *k* is chosen to be 3 because we would like to easily visualize the points. The time taken for each analysis was recorded and will be addressed later on.

The procedure was done for all 268 patients, and for all possible combinations of EFI stimulus type and MDS type per patient. With 4 EFI stimulus types, and 6 MDS types, this leads to 24 MDS solutions per patient.

In Figure 5.1 a MDS solution for a patient with a problem-free insertion is presented. All other patients with problem-free insertions show similar results. This specific solution was produced by Metric Squared Stress scaling, using the “sine wave 1” EFI data.

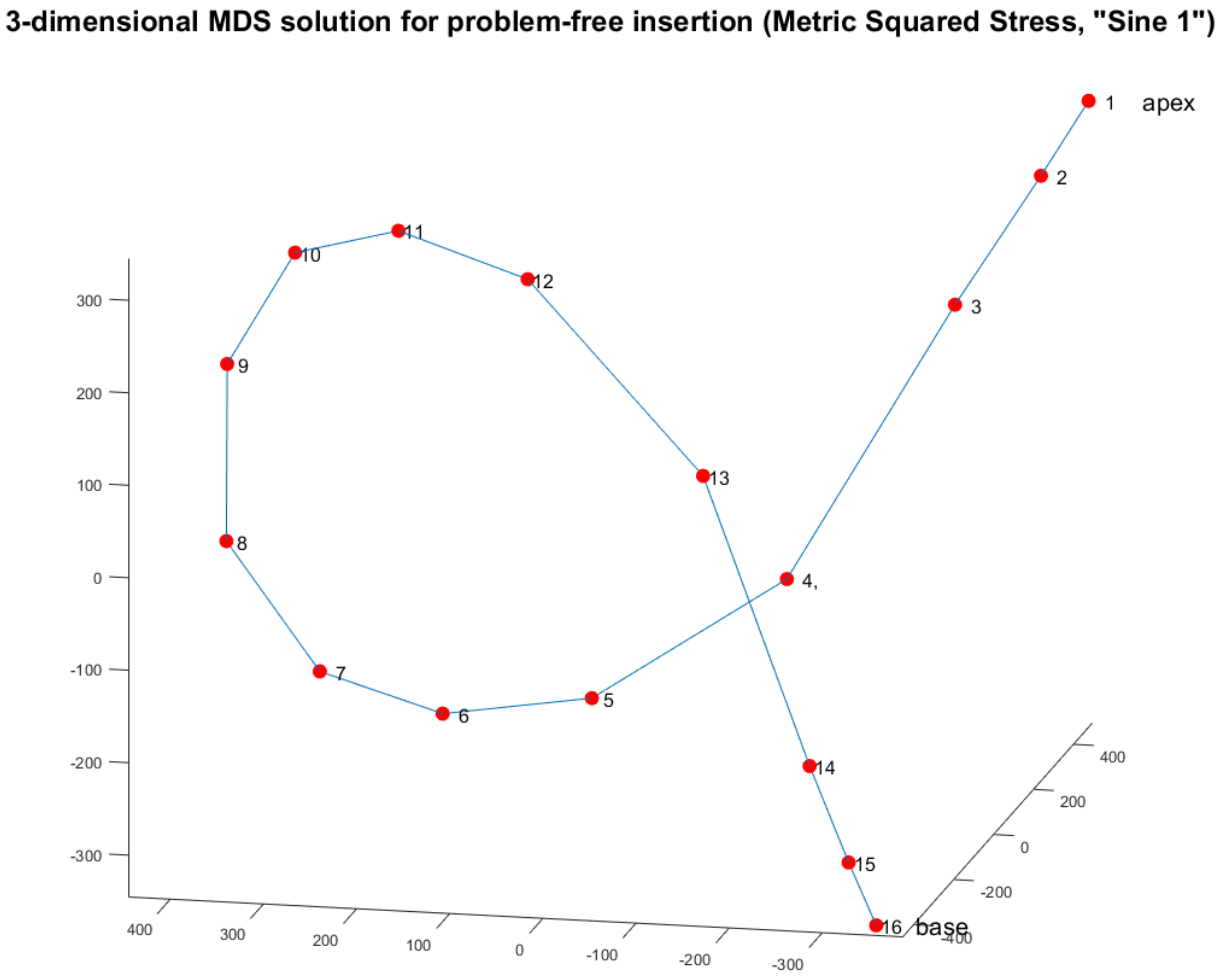

Figure 5.1: 3-dimensional MDS solution for a problem-free insertion. This specific solution was produced by Metric Squared Stress scaling, using the “Sine 1” EFI data.

Note that the electrode shape is smooth. There are no jagged corners or fold-overs. For comparison, in Figure 5.2 the MDS solution for patient "C" (see Appendix A), who suffers from a complete fold-over is given (also Metric Squared Stress scaling, using "sine wave 1" EFI data).

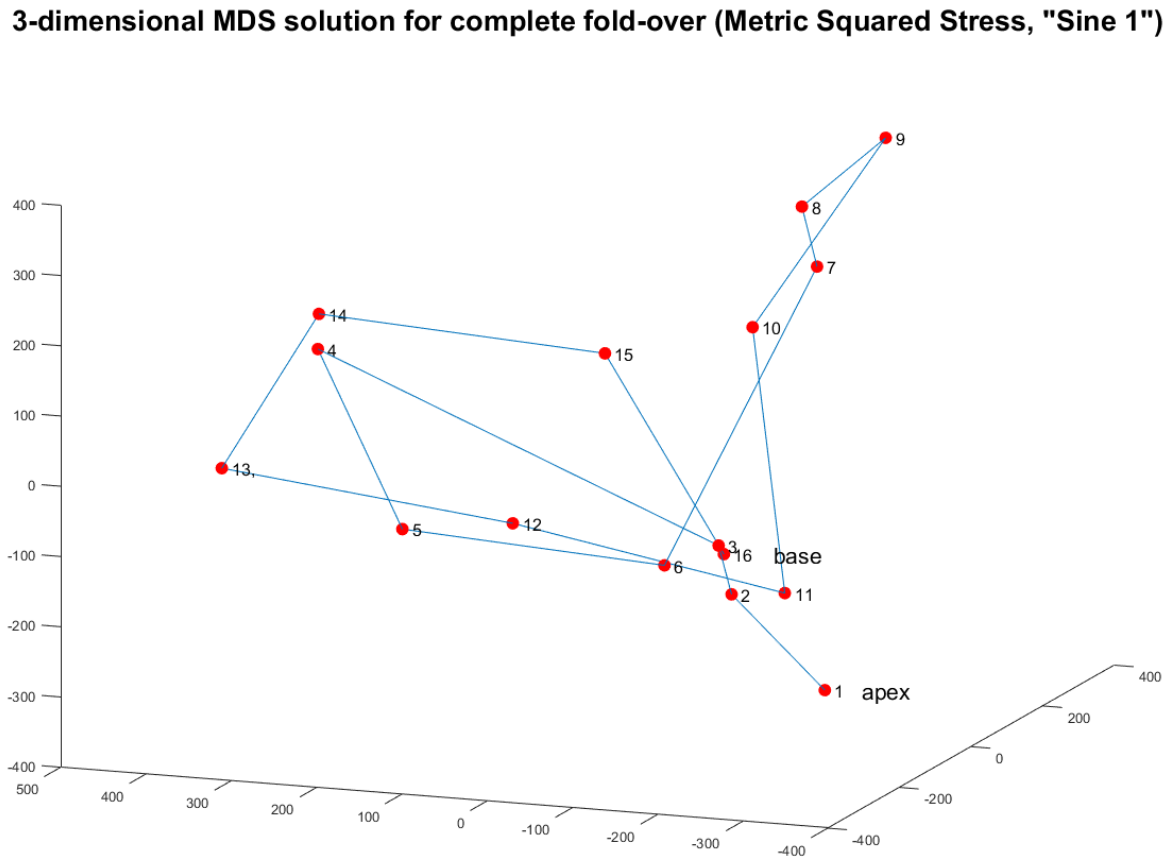

Figure 5.2: 3-dimensional MDS solution for patient "C", who suffers from a complete electrode array fold-over. Again, this MDS solution was produced using Metric Squared Stress scaling and the "Sine 1" EFI data.

Here, it can be observed that the electrode folds over near contact 8 and 9. Hence, the most apical contacts of the electrode (number 1 and 2) are actually in the basal part of the cochlea, near contact 16. Considering these two solutions, it is clear that it is possible to visually distinguish a fold-over from a problem-free insertion.

5.1.2 Computing MSE between MDS solution and CT-scan

In order to determine what combination of MDS type and EFI stimulus type yields the best results, we will compare the MDS results to coordinates derived from CT-scans.

In the LUMC, it is standard procedure to perform a CT-scan after insertion of the electrode. In these CT-scans, the electrode contacts can be identified. An origin is chosen based on anatomical landmarks (the modiolus and the round window), and coordinates for each of the contacts are determined.
However, the following limitation needs to be taken into account. There is a fixed distance between CT-scan slices (0.5mm) and thus there are discrete steps in between z-coordinates. To combat this, an algorithm is used that interpolates z-coordinates based on how bright they appear on adjacent slices. This is no problem for regular insertions, but for fold-overs the algorithm can not always distinguish the electrode contacts because they are so close to each other. Therefore, the z-

coordinates for the fold-over patients have been determined manually and are set in discrete steps of 0.5mm. Hence, the CT coordinates for fold-over and non-fold-over patients can not easily be compared, as the z-coordinates for fold-over patients are continuous and those for non-fold-over patients are discrete.

There are a number of other problems when comparing the CT-scans to the MDS solutions:

- **Rotation**
  The MDS solution is contains the relative distances between contacts. However, the constellation of points is arbitrarily rotated. The orientation is most likely not the same as the orientation of the CT coordinate set. The solution can also be mirrored.
- **Translation**
  The origin is chosen arbitrarily in MDS. Thus, constellation of points might not only be rotated, but also translated compared to the CT coordinate set.
- **Scaling**
  The axes in the CT coordinates are in millimeters. The axes in the MDS solution are based on the values in the input matrix (matrix D_av which contains averaged impedances differences in Ohms). Hence, these axes are in a completely different range.

In order to compare the MDS solutions to the CT-scans, we want to compute the mean squared error (MSE) between them. However, we first need to handle the problems listed above.

The first step is to take both the MDS solution and the CT coordinates and transform them to inter-point distance matrices $\boldsymbol{R}_{mds}$ and $\boldsymbol{R}_{\boldsymbol{ct}}$, instead of coordinate sets. In other words:

$$\boldsymbol{R}_{mds}(m,n) = \sqrt{\left(x_{m_{mds}} - x_{n_{mds}}\right)^2 + \left(y_{m_{mds}} - y_{n_{mds}}\right)^2 + \left(z_{m_{mds}} - z_{n_{mds}}\right)^2}$$

Where $\boldsymbol{X}_{mds} = \begin{bmatrix} x_{1_{mds}} & y_{1_{mds}} & z_{1_{mds}} \\ & \vdots & \\ x_{16_{mds}} & y_{16_{mds}} & z_{16_{mds}} \end{bmatrix}$ and *m* and *n* are the contact indices.

In which *m* and *n* are the contact indices, and x_{mds}, y_{mds} and z_{mds} are the coordinates of the 16 contacts (produced by the MDS analysis).
$\boldsymbol{R}_{mds}$ is a square matrix of size *16 x* 16 (as there are 16 contacts) and along the diagonal of $\boldsymbol{R}_{mds}$ are zero's (as the distance between contact *v* and contact *v* is zero). The same steps are taken for the CT coordinates, to produce $\boldsymbol{R}_{ct}$.

By looking solely at the inter-point distances, the translation and rotation problem are resolved (rotating or translating a constellation of points will never affect the relative distances between the individual points).

To take care of the scaling problem, we compute the eigenvalues $\boldsymbol{L}_{\boldsymbol{mds}} = [\boldsymbol{\lambda}_1 \ldots \boldsymbol{\lambda}_{16}]$ of $\boldsymbol{R}_{mds}$ and $\boldsymbol{L}_{ct} = [\lambda_1 \ldots \lambda_{16}]$ of $\boldsymbol{R}_{ct}$. We then find the ratio of the largest eigenvalues and scale $\boldsymbol{R}_{mds}$ by that factor.

$$\boldsymbol{R}_{mds_{scaled}} = \frac{\max(\boldsymbol{L}_{ct})}{\max(\boldsymbol{L}_{mds})} \cdot \boldsymbol{R}_{mds}$$

$\boldsymbol{R}_{mds_{scaled}}$ and $\boldsymbol{R}_{ct}$ are in the same range, and we can now compute the MSE.

This procedure was done for all 267 patients, and all combinations of EFI stimulus type and MDS type. The lower the MSE, the closer to MDS solution is to the CT-scan coordinates. In the next section the results will be presented.

5.1.3 Results and discussion

The steps described in the previous sections were performed for all 267 patients, and all combinations of EFI stimulus type and MDS type. Here, the results will be presented. Since the z-coordinates derived from the CT-scans for patients with a fold-over are in discrete steps (see section 6.1.2), these patients will be left out. It is not problematic that these patients are not included, as we are only comparing EFI stimulus types and MDS types (and not fold-over versus non-fold-over). The 264 patients with problem-free insertions are all included.

In Figure 5.3 the MSE between $\boldsymbol{R}_{mds_{scaled}}$ and $\boldsymbol{R}_{ct}$ is presented for every possible combination of EFI stimulus type and MDS type.

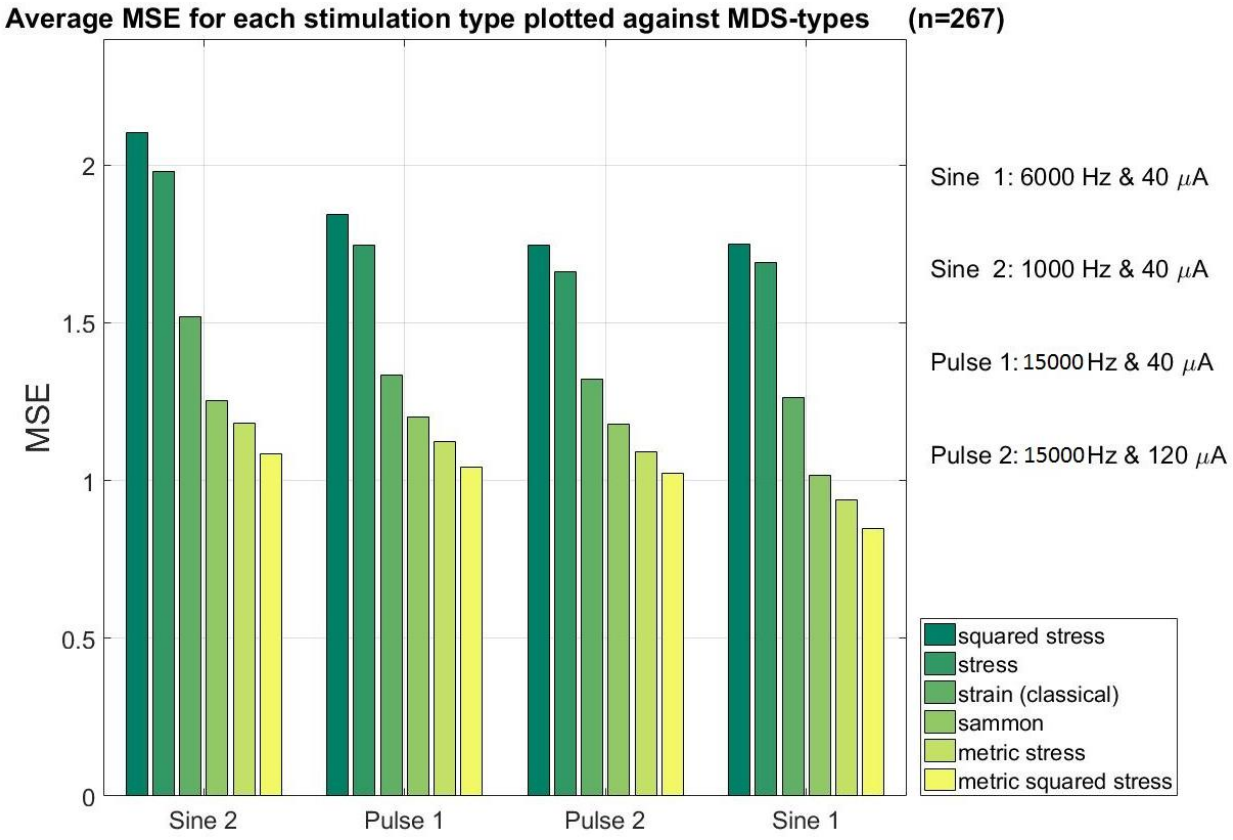

Figure 5.3: Average MSE for each stimulation type and MDS type. Note that the trend is the same for each stimulation type: The non-metric MDS types always have the highest MSE, and metric squared stress always has the lowest MSE. The combination of metric squared stress & "sine 1" lead to the overall lowest MSE.

As expected, the non-metric types of MDS show the worst results. This is because in non-metric MDS, the dissimilarity data is first transformed to ordinal data by a non-linear monotonic transformation. Hence, information is lost. We see that metric MDS using the squared stress

criterion performs best for every stimulus type. Furthermore, the stimulus type “Sine 1” performs better than the other stimulus types.

Next, let us take a look at the time taken to perform the MDS analysis. In Figure 5.4 we see the average MSE’s for stimulus type “Sine 1”, and the average analysis time (in seconds) for each MDS type.
As expected, classical MDS is much faster than the other types (~1.5ms, 37 times faster than the second best option), as it is the only type that does not use iteration. Metric MDS using the squared stress criterion scores second best with an average of 54.9ms.

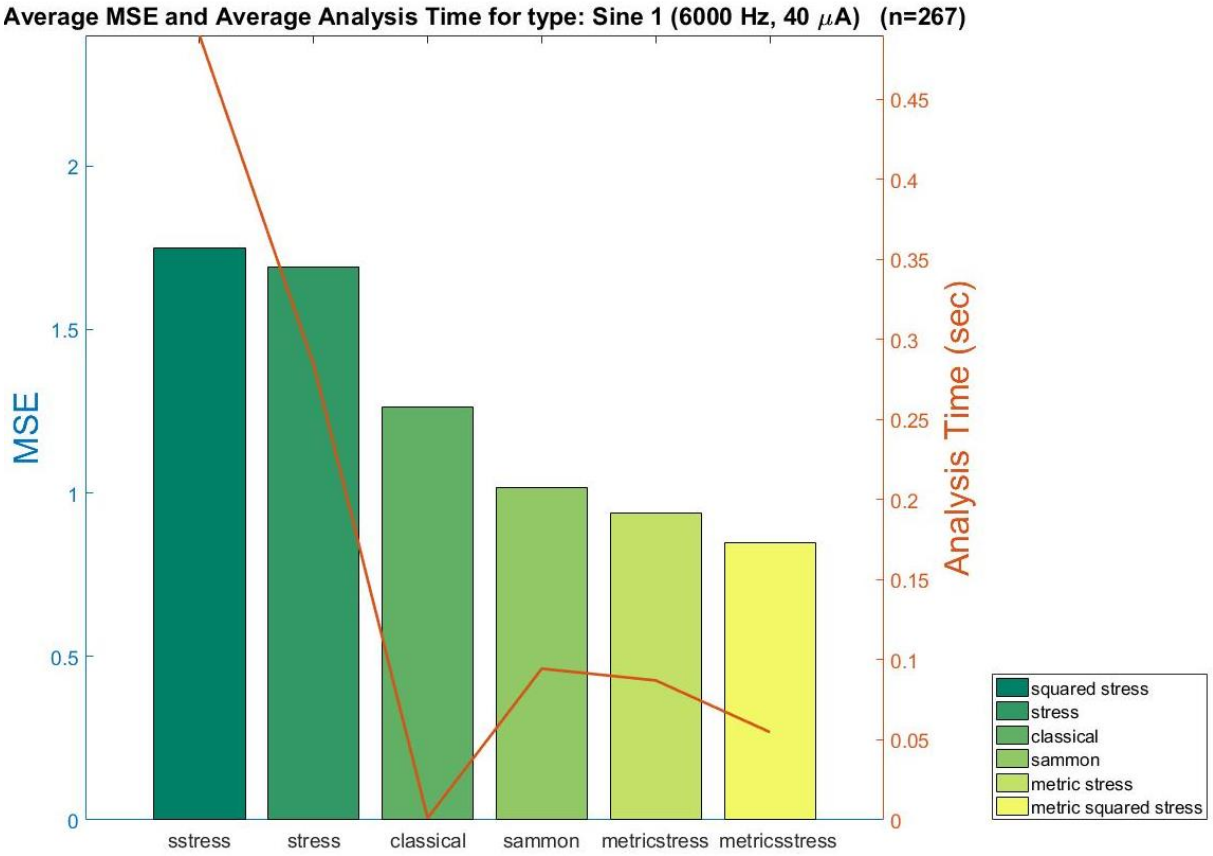

Figure 5.4: Average MSE and analysis time for “Sine 1” EFI data. The bars relate to the left vertical axis (MSE), the red line relates to the right vertical axis (time). As expected, classical MDS is a lot faster than the other types, as this is the only type that does not use iteration.

Note that here we are only considering the time needed for the actual MDS analysis, and the time needed for the EFI measurement is not included. A “common” EFI measurement using 16 electrodes as performed in EFIM can take up to 2 minutes. Ofcourse, this can be brought down by using only the contacts in the tip, and reducing the number of measurement cycles that are averaged. For example, switching to 4 contacts instead of 16 and reducing the number of measurement cycles by 50% will result in $\frac{16^2}{4^2} \cdot \frac{1}{2} \cdot 120 = 3.75$ second EFI measurements. Still, relative to this number, the difference of ~53ms between classical MDS analysis time and metric squared stress MDS analysis time is insignificant. Therefore, we conclude that metric squared stress MDS combined with EFI stimulus type “Sine 1” is the most suitable for this project. From here on, we will stick to this combination.

5.2 Finding an objective measure to detect fold-overs

In section 5.1.1 we have seen that it is possible to distinguish fold-overs from non fold-overs, purely by visually judging the 3D plot of the MDS solution. However, it would be ideal to find an objective measure that indicates whether we are dealing with a fold-over or not.

To do so we will focus on the distance between two apical contacts (1 and 3) in the MDS solution. This distance is expected to decrease when a fold-over is induced, as the most apical contact (1) will move past the more basal contacts as the fold-over progresses. In case of a fold-over, the distance between the two contacts should be smaller than in the case of a problem-free insertion. See Figure 5.5

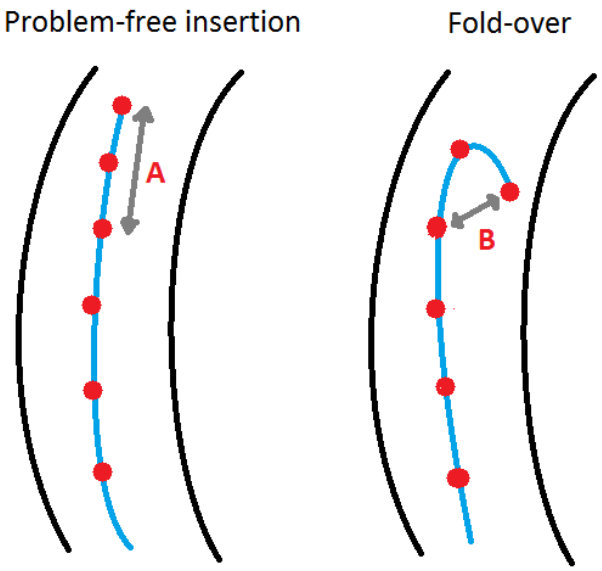

Figure 5.5: Illustration of electrode array tip fold-over. When a fold-over occurs, the most apical contact (1) will move closer to a more basal contact. When the physical distance between two contacts decreases, the measured impedance in these contacts is expected to converge.

Of course, it is also possible to focus on the distance between any other pair of 2 contacts located in the tip. For example, the distance between contact 1 and 4, 2 and 5, or a composite of multiple contact pairs. However, we currently lack the means to compare the effectivity of these options, as the sample size of the fold-over population is extremely small. For now, we decide to stick to the distance between contact 1 and 3, as this is first contact pair that should show changes when a fold-over starts occurring.
Take note that experimentation with different contact pairs or composites of contact pairs should be conducted when more fold-over data is available.

We will attempt to find an objective measure by looking at the distribution of the distance between contact 1 and 3 in the MDS solution, for both the population of problem-free insertions and the population of fold-overs. Although the sample size for the fold-over group is extremely small (n = 2, note that the complete fold-over is left out as its intracochlear potential profile is not comparable to the tip fold-overs), we assume that both populations are normally distributed.
Through a Minimum Probability of Error Test, we will attempt to find a decision boundary which we can use to decide to what population a measurement belongs.

It is important to realize that the due to the sample size, the decision boundary we find is unreliable. However, this section aims to present the method that can be used in future work when more fold-over EFI data is available.

Minimum Probability of Error test

In Figure 5.6 the distributions of the distance between contact 1 and 3 in the MDS solution is presented for both populations.

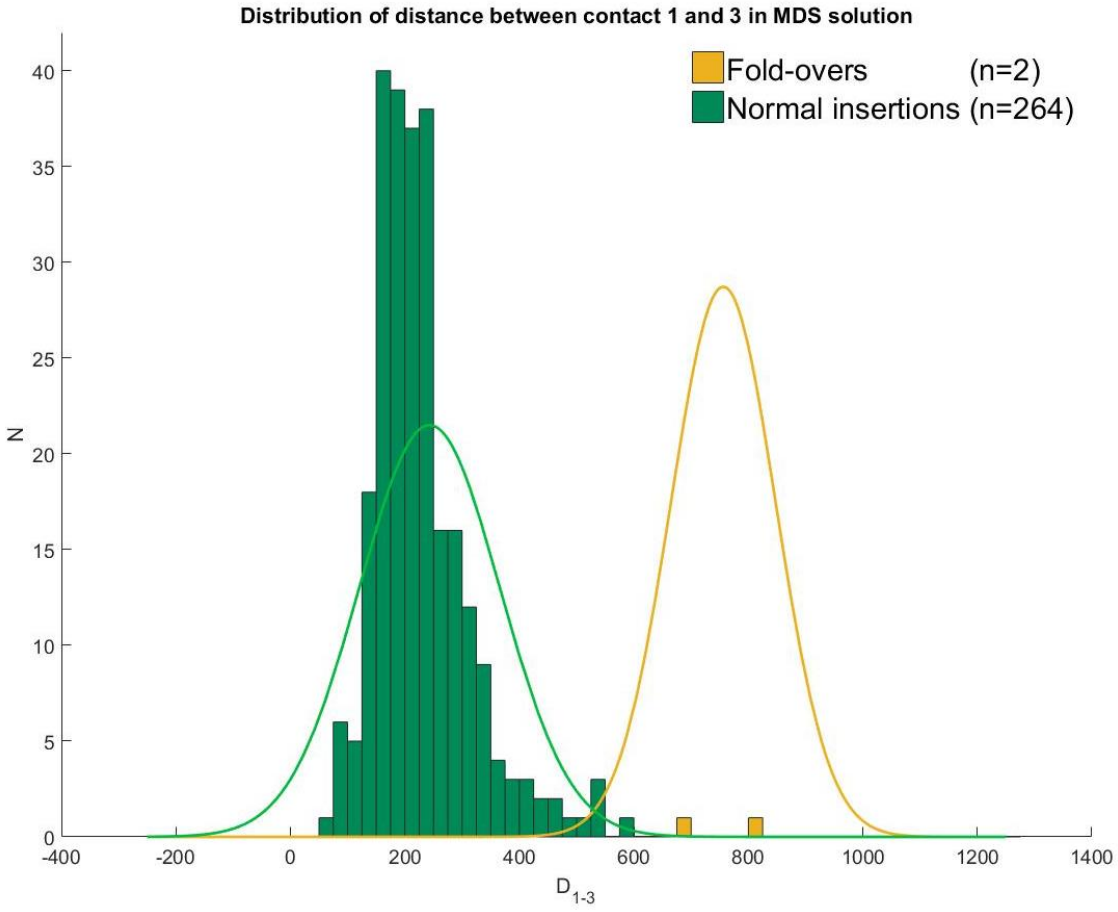

Figure 5.6: Distribution of distance between contact 1 and 3 in the Metric Squared Stress / "Sine 1" MDS solutions. The patient with a complete fold-over is excluded as this situation is not comparable to the two tip fold-overs. Note the extremely small sample size of the fold-over population.

Contrary to what we expected, we see that the pairwise distances in normal insertions are actually smaller than in fold-over situations. This may be explained by the fact that coordinates in the MDS solution are arbitrarily scaled but the range is dependent on the input values.
We expect the distance between contact 1 and 3 to be smaller in case of a fold-over, but when a fold-over occurs, the input values (measured impedances) will be different and hence the coordinates in the MDS solution are in a different range.
This is not necessarily a problem, as we just want to find a measure which is significantly different for both populations. The distributions shown in Figure 5.6 barely overlap, which suggests that it is possible to distinguish fold-overs from normal insertions using this measure. But again, we have to take into account that the sample size for the fold-over population is extremely small and that this is a very rough, extremely unreliable representation of the actual fold-over population. For now, we will work with the distributions as shown above.

Assume we measure EFI during the insertion of a cochlear implant. MDS analysis is performed on the EFI data and the distance between contact 1 and 3 is computed. Let this distance be $\boldsymbol{x}$.
We present 2 hypotheses:

$$H_0 = Measured\ value\ of\ \boldsymbol{x}\ does\ \boldsymbol{not}\ belong\ to\ a\ foldover$$

$$H_1 = Measured\ value\ of\ \boldsymbol{x}\ \boldsymbol{does}\ belong\ to\ a\ foldover$$

To decide what hypothesis is more likely, we perform a Minimum Probability of Error test and compute

$$\textbf{(1)}\quad \frac{p(x \mid H_1)}{p(x \mid H_0)} > \frac{p(H_0)}{p(H_1)}$$

Where

$$p(x \mid H_0) = \frac{1}{\sqrt{2\pi\sigma_0^2}}\, e^{-\frac{1}{2\sigma_0^2}(x-\mu_0)^2}$$

And

$$p(x \mid H_1) = \frac{1}{\sqrt{2\pi\sigma_1^2}}\, e^{-\frac{1}{2\sigma_1^2}(x-\mu_1)^2}$$

And $p(H_0)$ and $p(H_1)$ are the prior probabilities ($p(H_0) = \frac{264}{266}$ and $p(H_1) = \frac{2}{266}$). Here μ_0 and σ_0 are the mean and standard deviation of the problem-free insertion population, and μ_1 and σ_1 are the mean and standard deviation of the fold-over population.

Substituting the equations for $p(x \mid H_0)$ and $p(x \mid H_1)$ in **(1)** and rearranging gives us

$$\frac{\sigma_0}{\sigma_1} \cdot e^{-\frac{1}{2\sigma_1^2}(x-\mu_1)^2 + \frac{1}{2\sigma_0^2}(x-\mu_0)^2} > \frac{p(H_0)}{p(H_1)}$$

Taking the natural logarithm on both sides and rearranging leads to

$$x^2(2\sigma_0^2 - 2\sigma_1^2) + x(4\mu_0\sigma_1^2 - 4\mu_1\sigma_0^2) + 4 \cdot \ln\left(\frac{p(H_0)\cdot\sigma_1}{p(H_1)\cdot\sigma_0}\right) + 2\sigma_0^2\mu_1^2 - 2\sigma_1^2\mu_0^2 > 0$$

And solving for $\boldsymbol{x}$ gives us the decision boundary

$$x_{1,2} = \frac{-(4\mu_0\sigma_1^2 - 4\mu_1\sigma_0^2) \pm \sqrt{(4\mu_0\sigma_1^2 - 4\mu_1\sigma_0^2)^2 - 4\cdot(2\sigma_0^2 - 2\sigma_1^2)\cdot 4\cdot \ln\left(\frac{p(H_0)\cdot\sigma_1}{p(H_1)\cdot\sigma_0}\right) + 2\sigma_0^2\mu_1^2 - 2\sigma_1^2\mu_0^2}}{4\sigma_0^2 - 4\sigma_1^2}$$

In which μ_1 and σ_1 are currently unreliable due to the small sample size of the fold-over population.

For the full step-by-step proof, see Appendix B.

In Figure 5.7 the distribution are presented once more, including the decision boundary.

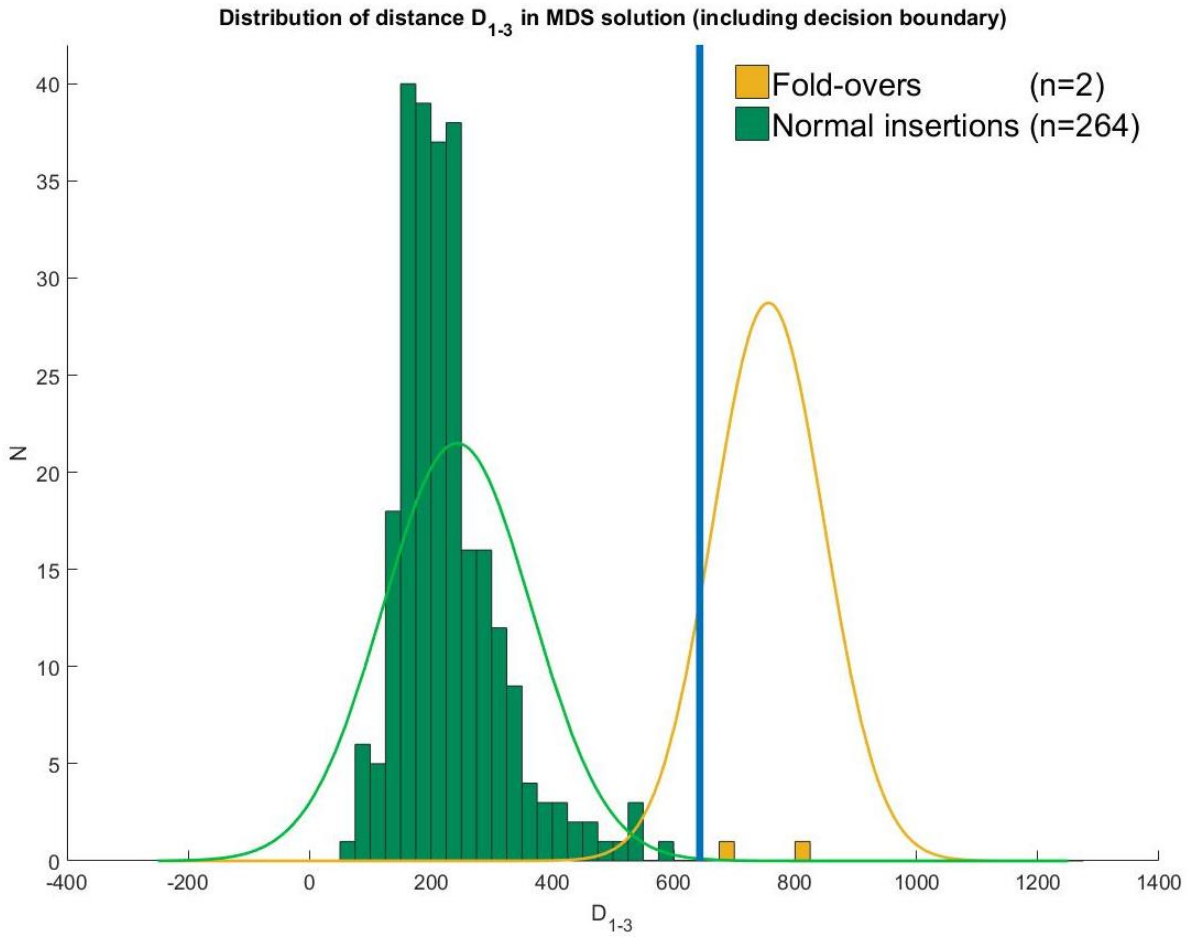

Figure 5.7: The same distributions presented in Figure 5.6, but including the decision boundary. In this case, all insertions are classified correctly.

Here it can be observed that with the current data the decision boundary is able to classify all cases correctly. All the normal insertions are classified as normal insertions and all fold-overs are classified as fold-overs. Further experimentation (with a larger sample size for the fold-over population, and with other electrode pairs or composites of electrode pairs) is to be conducted. However, the above suggests that the method might be effective.

5.3 Performing EFI-MDS in real-time

We have now seen that MDS analysis of EFI data enables us to distinguish fold-overs from normal insertions. This can be done visually by plotting the MDS solution (as seen in section 5.1), but can possibly also be done through an objective measure (as seen in section 5.2). This can already be a useful tool by itself. The method can be used to check the electrode's positioning post-operatively and could possibly replace the need for the standard post-operative CT scan.

However, our goal was to construct a tool that is able to detect tip fold-over in real-time, intra-operatively. This means we want to achieve a certain speed at which we can perform the EFI-MDS analysis. According to Rajan [80], the insertion speed for a cochlear implant electrode array insertion is between 0.25 – 1 mm/s and the electrode array is inserted approximately 20-23mm into the cochlea In the LUMC operating theatre, a complete electrode array insertion is said to take between

60-120 seconds, which is in line with the findings by Rajan [80]. Due to the insertion speed being so low, it is not necessary to achieve a very high framerate. For now, we will assume that 1 EFI-MDS cycle per second is sufficient to detect when the electrode array tip starts folding. This presents a problem, as the EFI measurements that we have previously used take approximately 2 minutes to record (using the standard Advanced Bionics software: EFIM).
In this section we will present ideas on how to deal with this issue.

Speeding up EFI-MDS cycles

The EFI-MDS cycle consists of 2 parts: measuring the EFI, and the subsequent MDS analysis.
In section 5.1 we have seen that the type of MDS we are using (metric squared stress) takes an average of 55.7ms for an input matrix of 16 x 16. This is negligible when compared to the time consumed by measuring the EFI (120 seconds). If preferred, there is the option to use classical MDS which takes 1.5ms on average for a 16 x 16 matrix, but the MSE between the MDS solution and CT-scan will be larger.

The reason a common EFI measurement takes 120 seconds is that it consists of a very large number of recording/stimulation cycles. Every contact is recorded, and for each recording contact, every contact is subsequently stimulated 10 times and then averaged. This adds up to a total of $16 \cdot 16 \cdot 10 = 2560$ recording/stimulation cycles. On top of that, switching recording contact is time consuming due to design of the hardware.

To reduce the EFI measurement time there are several options which will be discussed briefly.

Reducing the number of contacts measured

By reducing the number of contacts measured the measurement time will go down drastically. By using just the 4 most apical contacts, the number of recording/stimulation cycles is reduced by a factor of $\frac{4^2}{16^2} = 0.0625$. This would bring the 120 seconds down to 7.5 seconds. However, it is not clear what effect this has on the EFI-MDS analysis. With a “less informative” input, we expect a “less informative output” and perhaps it is not possible to detect fold-overs using only 4 contacts.
As we still lack regular fold-over data, and possess no data at all in which EFI was measured using only 4 contacts, this is not straightforward to investigate.

In an attempt to do so, we “crop” a 4 x 4 EFI matrix out of the 16 x 16 EFI matrices we have used before, pretending that only the 4 most apical contacts were measured. Using these downsized matrices, we repeat all the steps discussed in section 5.1 and 5.2.
We find 2 new distributions of the distance between contact 1 and 3 in the MDS solution in both fold-over cases and normal insertion cases, and also a new decision boundary. These are presented in Appendix C. This time the decision boundary is not able to distinguish fold-overs from normal insertions (both of the fold-overs are classified as normal insertions), and that the distributions largely overlap. This suggests that using 4 contacts is less effective than using 16. Again, this is based on an extremely small sample size and should be repeated once more data is available. Unfortunately, this data could not be produced during this project in the LUMC.

Reducing the number of recording cycles

Another option is to reduce the number of recording cycles per contact pair. Currently, in the software provided by Advanced Bionics, the standard is to perform 10 cycles and subsequently take the average of these 10 measurements to find the actual voltage. Bringing this number down will lead to faster EFI measurements, but also decreased accuracy. This means there is an optimum number of cycles; where the voltage readings are still accurate enough to detect tip fold-over, but the number is as low as possible to minimize the time needed for the measurement. During this project it was not possible to experiment with this, as the software provided by Advanced Bionics does not allow this parameter to be changed. However, this topic will be addressed shortly later on in section 6.

Using interleaved pulse trains instead of sine waves

As shown in chapter 3, all the available EFI data was measured using 4 different types of stimuli: 2 sine waves, and 2 pulses. In Figure 5.4, we see that the "Sine 1" stimulus provides the best results, but "Pulse 2" comes in at a close second with an average MSE that is only slightly larger. Hence, we suggest using pulse stimuli in order to reduce the EFI measurement time.

Cochlear implants are designed to stimulate multiple contacts in rapid succession or at the same time. We can use this property to design an interleaved biphasic pulse train stimulus which allows us to quickly measure multiple impedances. See Figure 5.8.

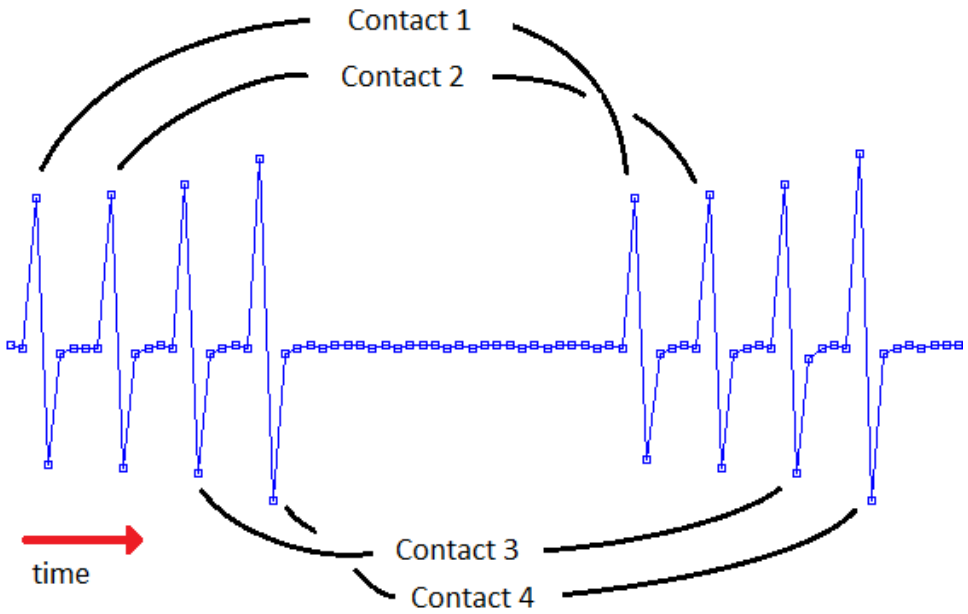

Figure 5.8: Interleaved pulse train. This specific example was made in BEDCS and the signal shown is the voltage measured on contact number 5 when the first 4 contacts are stimulated using interleaved biphasic pulse trains. Note that the voltage increases as we move closer to contact 5 (the physical distance between 4 and 5 is smaller than between 1 and 5, thus the voltage measured when we stimulate contact 4 is higher than when we stimulate contact 1).

When we present biphasic pulses in an interleaved fashion across multiple contacts, we can subsequently separate these pulses in the signal received on the recording contact. In the example shown in Figure 5.8, we know that every 1^{st}, 5^{th} , 9^{th} … peak belongs to the first stimulating contact, and every 2^{nd}, 6^{th} , 10^{th} … peak belongs to the second stimulating

contact, and so on. This method is more time efficient, as now multiple contacts can be measured in one stimulation cycle whereas before only a single contact was measured. This idea was not tested extensively during this project as the standard software provided by Advanced Bionics does not allow the user to design the stimuli on such a detailed level. This can however be done in BEDCS (a different type of software provided by Advanced Bionics, specifically for research purposes) and will be addressed briefly in chapter 6.

Using a single recording contact

A last option could be to reduce the number of recording contacts. Instead of using all 16 contacts for recording, we propose using just one contact (e.g. contact number 1) for recording. When we now stimulate all 16 contacts, we find 1 out of the 16 EFI curves as they were presented in Figure 3.1. As was stated in chapter 3, the peak value is unrealistically high due to the interface impedance. By fitting a curve through the remaining 15 contacts, we are able to estimate a more realistic impedance. See Figure 5.9.

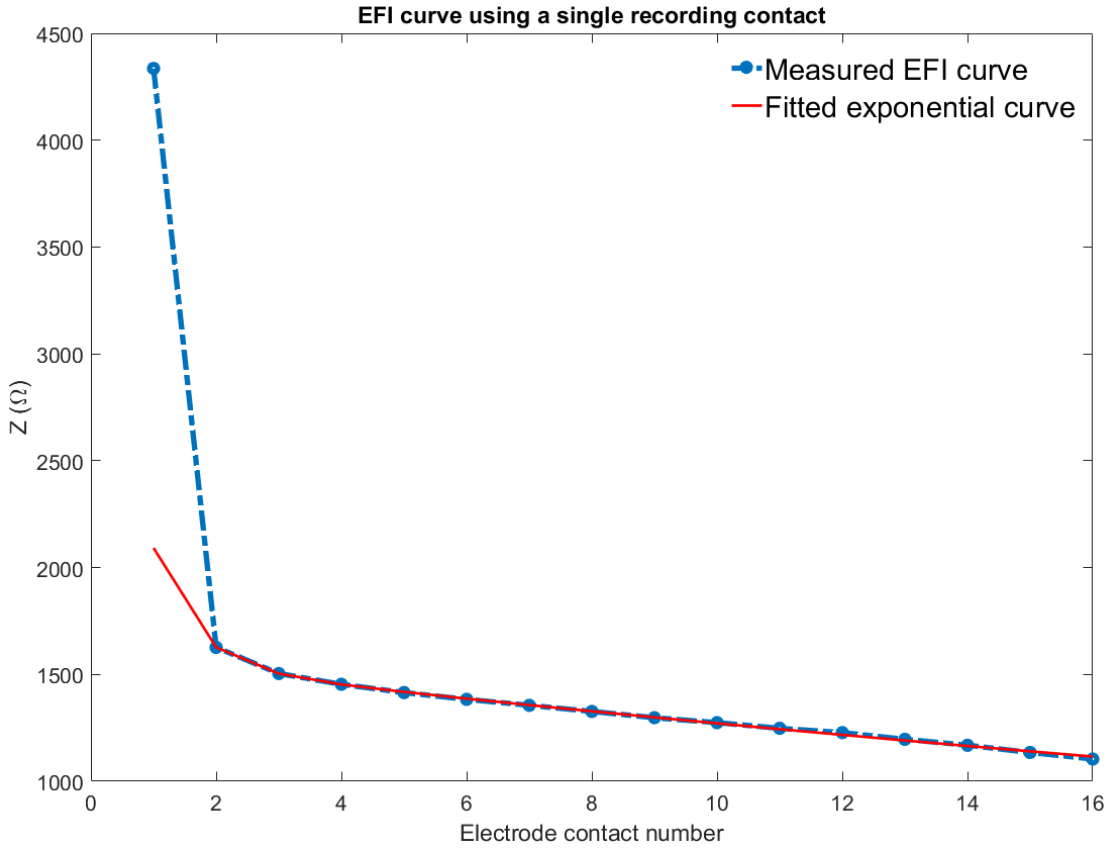

Figure 5.9: An EFI curve measured by recording on contact 1, and stimulating all 16 contacts. In blue the actual measurement is shown, including the large peak at contact number 1. In red the exponential curve fitted through contact 2 to 16 is shown.

Using the estimated value for contact 1, and the actual measured values for contact 2 to 16, we create a $1\ x\ 16$ row vector E. In a next step we set up a $16\ x\ 16$ dissimilarity matrix D by taking the absolute voltage differences between contacts: $D(i,j) = |E(i) - E(j)|$. From here on out, we can follow the steps as described in chapter 5 to complete the EFI-MDS analysis.

As a result the measurement time will be reduced by a factor of more than 16 (as only 1/16th of the "common" EFI matrix is measured, and the recording contact does not have to be switched).

The method described above was performed for all patients (post-hoc, on the existing data). Results are shown in Appendix D. The two distributions almost completely overlap, and it is not possible to distinguish fold-over from normal insertion. There are a couple of reasons for this. First off, the sample size of the fold-over group is still extremely small. Secondly, normal distributions were assumed, while the results suggest that the distributions might be logarithmic (however, when we assume logarithmic distributions, they still completely overlap). Lastly, the quality of the MDS solution might diminish because we are assuming equal contact impedance on all contacts, and equal flow of current in apical and basal direction. Common EFI measurements clearly show that this is not the case.

5.4 Discussion Method 1: 'EFI-MDS'

In this chapter we have elaborated upon the idea of analyzing EFI data through Multidimensional Scaling in order to detect electrode tip fold-over. The findings will be discussed briefly.

First off, we have seen that there are many types of MDS and that Metric Squared Stress MDS produces the solution that is closest to the CT-scan coordinates. Classical MDS performs slightly worse (with an MSE of ~ 1.22 versus an MSE of ~ 0.81 for Metric Squared Stress), but is much faster. Analysis of a EFI measurement using 16 electrode contacts takes $1.5\ ms$ when classical MDS is applied, and $\sim 55.7\ ms$ when Metric Squared Stress MDS is applied.
This means that Metric Squared Stress is the best option when we solely want to detect fold-over of the electrode tip. We propose that Metric Squared Stress MDS analysis of EFI data can potentially replace the common-practice post-operative CT scan which is performed to confirm the electrode's positioning.
However, when the goal is to monitor the electrode array tip in real-time, one might argue that Classical MDS is the better option as it is so much faster. Of course, this largely depends on how fast the EFI measurements can be performed. The post-operative EFI measurements that were used for this project took 2 minutes on average, and in this case the added time of the MDS analysis (be it $1.5\ ms$ or $55.7\ ms$) is negligible. If the EFI measurements can be sped up and real-time EFI-MDS becomes a viable option, then classical MDS comes in to play as a realistic option.

Secondly, in section 5.1.1 we have shown that it is possible to distinguish fold-overs from normal insertions by inspection of the MDS solution.
This can be done visually (which might be the preferred option for usage by surgeons in the operating theatre): normal insertions appear as smooth spiral curves and fold-overs appear as jagged bent-over curves where the fold-over point can be seen.
Ideally we want to find an objective measure that cannot be mistakenly interpreted. In section 5.2 a method to find such a measure was presented. For the limited data that is currently available, we were able to classify 100% of the insertions correctly. Keep in mind that the sample size for the fold-over group was only 2 and hence this number does not tell us much. Nonetheless, we predict that using this method with a sufficiently large sample size is an effective way of distinguishing fold-overs

from normal insertions. It is important to note that in this case we used the full $16\ x\ 16$ EFI matrix. When only the 4 most apical contacts were used ($4\ x\ 4$ matrix), both fold-overs were erroneously classified as normal insertions. If in future work it is decided to speed up the EFI measurements by reducing the number of contacts, the reliability of this objective measure is expected to decrease.

Lastly, a number of ideas were presented to increase the speed of EFI measurements. Unfortunately, it was not possible to test these ideas thoroughly during this project. This is due to the lack of EFI data from fold-over patients, which makes it difficult to verify the effectivity of the proposed methods.
There are 2 reasons why it was impractical to produce more data. One being that if we were to produce the data ourselves the EFI measurements would be done in a plastic model of the cochlea, submerged in saline solution. Measurements done in this way would not be comparable to the existing data (measured in real cochlea) due to the differences in resistivity between the cochlear walls and cochlear perilymph, and the plastic model and saline solution. We are limited to in vitro-experiments because inducing fold-overs in live patients is unethical. The second reason is that in order to produce fold-over data a cochlear electrode array would have to be folded on purpose, risking device failure. As cochlear implants are expensive (€16.405,- for a single device in the United Kingdom in 2007 [81]), this was not an option.
For future work, more (real patient) data should be gathered through cochlear implant manufacturers (Advanced Bionics, Cochlear, MED-EL) and hospitals.

In conclusion, we suspect that EFI-MDS is an effective method of detecting electrode tip fold-over. It is insightful for post-operative monitoring and in a future stadium it can possibly replace the need for a post-operative CT-scan. Furthermore EFI-MDS is possibly an effective method for intra-operative real-time monitoring, but this is yet to be confirmed. However, the foundation for future work has been laid.

Because we cannot further investigate this method efficiently without the proper data, we continue this project with a different idea proposal. This idea will be presented in chapter 6.
In the case of EFI-MDS, we essentially started out with the question “How can we detect fold-over using data gathered through telemetry?” and only in a second step focused on the question “How can we gather this data fast enough for real-time monitoring?”. We now turn these questions around. We first focus on finding data that can be gathered quickly through telemetry, and then focus on how to use this data to detect fold-over.

6. Method 2: Real-time Monitoring of Tip Impedance Values

In the preceding chapter we have discussed the possibilities and limitations of EFI-MDS. Now, we will discuss an alternative idea which takes into account the obstacles encountered in the EFI-MDS method. A major obstacle we encountered is that measuring an EFI is time consuming and makes real-time monitoring problematic. Here, we focus on finding a measure that could help us detect folding of the electrode array, but can also be recorded quickly so that it may be more viable for real-time monitoring.

As we have previously seen, a complete 16 by 16 EFI measurement takes long to perform but it is useful in detecting fold-over. Based on the method described in chapter 5, we present the following idea.

Instead of measuring the full intracochlear potential profile (as done in the 16x16 EFI), we will now measure just a small number of impedances. As fold-over occurs in the tip of the electrode, we will only focus on apical contacts and ignore the more basal contacts (see Figure 2.1). We will monitor the differences in measured impedances in real-time, as they tell us something about the distance between electrode contacts (electrical potential should decrease when we move further away from the current source in a conducting medium). See Figure 6.1.

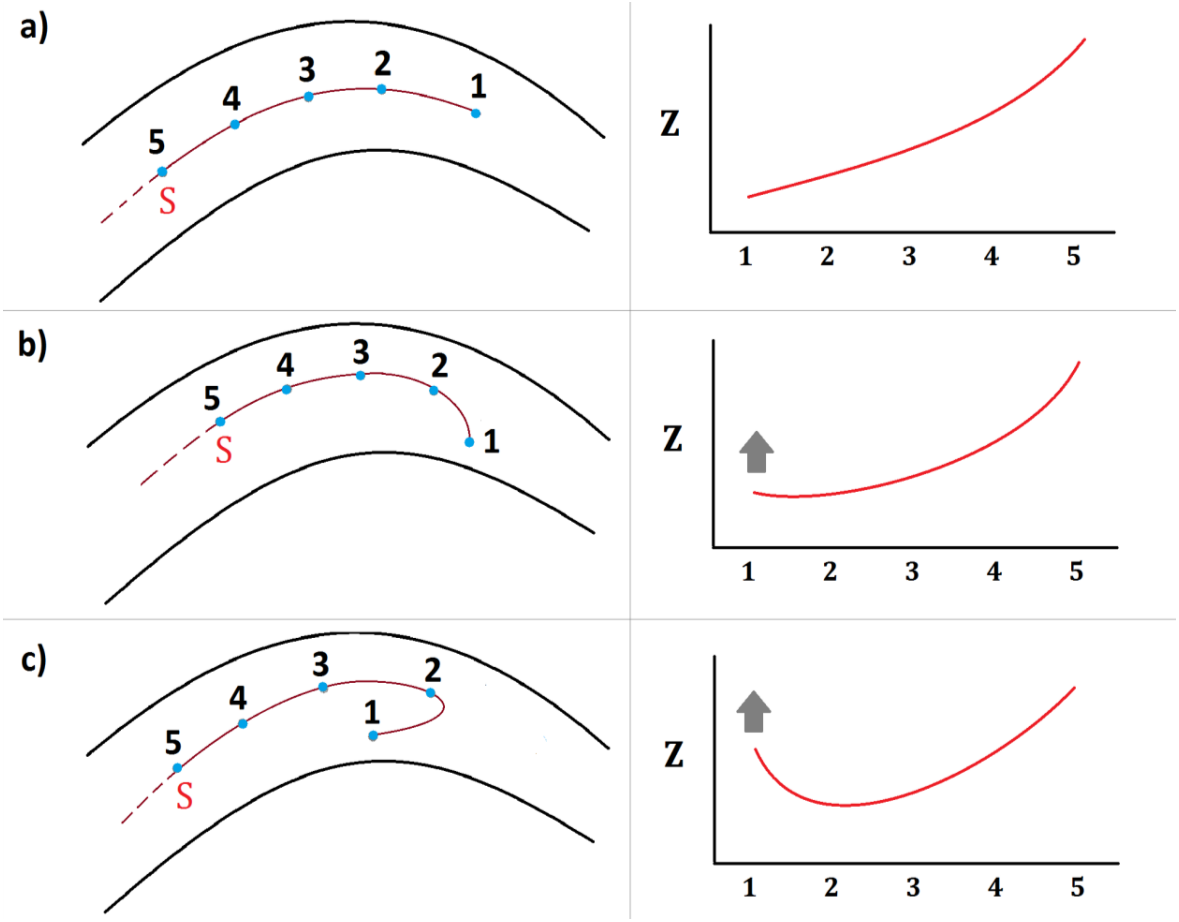

Figure 6.1: The stimulating contact is denoted with an 'S'. Note that in a normal situation, we expect to see a monotonic curve. When tip fold-over starts occurring the impedance in the apical contacts is expected to increase as they move closer to the stimulating contact

In section 5.3 a number of ideas were presented to speed up the EFI measurements. These are also applicable to speed up single impedance measurements and thus they will be applied here. We propose 2 options: measuring 2 impedances in a back-and-forth pattern, and measuring 4 impedances using an interleaved pulse train.

6.1 Stimulus Design

Both of the options mentioned above will be described and tested, and the results will be presented. Instead of EFIM we will be using BEDCS (also software provided by the manufacturer Advanced Bionics, but designed for research purposes allowing full customization of stimuli) to measure the intracochlear electrical potential.

A: Measuring two contacts in a back-and-forth pattern

Here, we will utilize 3 of the electrode contacts in the tip. The specific contacts can be chosen freely. One of the contacts is used as recording contact, and this contact is never switched (as mentioned before, this is time-consuming due to the design of the hardware). The remaining two contacts are stimulated in a back-and-forth fashion: the first contact is stimulated and the impedance is measured, subsequently this is repeated for the second contact, and back to the first, etc.

In section 5.1 we learned that the EFI stimulus types that lead to the best MDS results were “Sine 1” and “Pulse 2”, thus, we assume that these stimuli gave the most accurate impedance measurements. Ideally, we would have tested both a pulse and sine stimulus for this experiment, however, due to only having access to an old version of BEDCS and lacking a supervisor familiar with the software, we were limited to pulses. Luckily, we have seen that “Pulse 2” performed nearly as well as “Sine 1”, and thus we expect no problems. However, it would be worth repeating this experiment in the future using a sine stimulus. The stimulus we use here is based on “Pulse 2” and is a biphasic pulse with an amplitude of 59 µA, stimulus duration of 1000 µs (ideally we would have used a higher amplitude, e.g. the 120 µA used in “Pulse 2”, but this was not possible due to the outdated software and lack of expertise). We’ll call this ‘Stimulus A’. In a first step we measure a single EFI trace (1 recording contact, 16 stimulating contacts) using both this stimulus and using EFIM, and compare the results to make sure we are measuring correct values. See Figure 6.3.

As seen in the figure, the shape of the curve measured using this stimulus is similar to that of the curve measured in EFIM. It is slightly translated, and this might be explained by EFIM possibly using a different reference contact than BEDCS (causing an offset). However, this is not a problem for our application.

In the next step, we will use this stimulus to stimulate 2 contacts back-and-forth, while recording on a third in real time. The whole cycle (measuring, analyzing, and plotting) takes approximately 0.8 seconds, and every time a new impedance is measured, we calculate the difference between the last 2 measured values. By doing so we achieve a framerate of $\frac{1}{0.8} = 1.25$ Hz, which is low but acceptable considering the insertion is executed very slowly (see section 5.3). Keep in mind that the calculated difference is not the difference between the two impedances at the same point in time. One of the impedances is actually measured ~0.8 seconds earlier than the other. This is not ideal, but again, acceptable because the insertion is slow. In the second option that we will present later on, we solve this problem (at the cost of increased measurement time).

In Figure 6.2 we provide proof of concept of this method. We measure the impedances on an 'Advanced Bionics HiRes 90K Advantage MS' electrode in a stable situation, emerged in saline. The plot updates in real-time and shows the impedance difference between the two chosen stimulating contacts. Approximately at -10 seconds a finger is placed on the tip of the electrode array, inducing a change in impedances. Around -3 seconds the finger is removed and the plot returns to the stable situation. In section 6.2 we test this method by inserting an electrode array into a plastic model of the human cochlea.

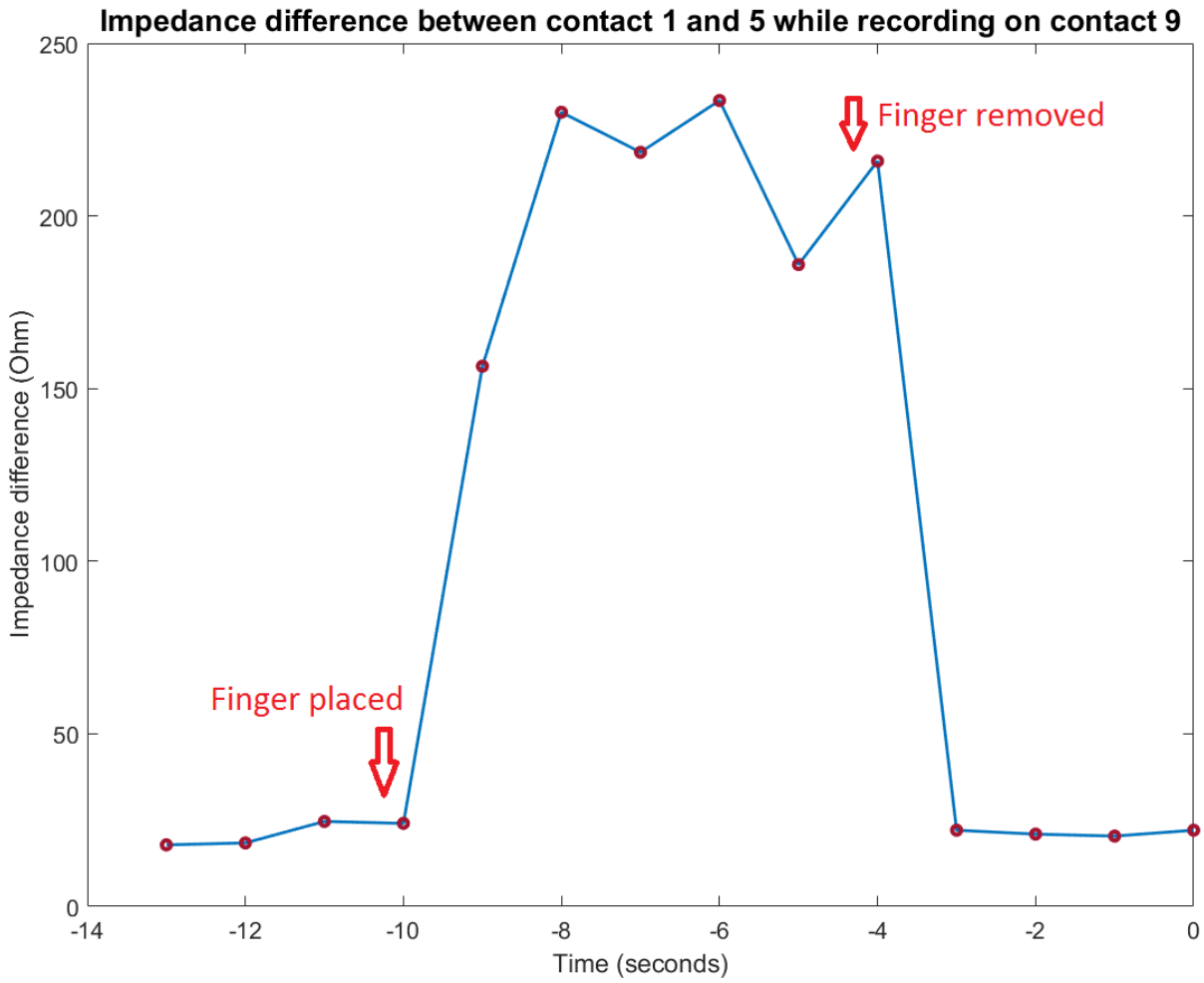

Figure 6.2: Real-time impedance difference trace measured using the back-and-forth method described above. The stimulating contacts are 1 and 3, and the recording contact is 5. At approximately -10 seconds, a finger is placed on the tip of the array, increasing the difference in measured impedances. Around -3 seconds, the finger is removed and the trace returns to the stable situation.

B: Measuring four contacts using an interleaved pulse train

Now, we will utilize 5 contacts: 4 stimulating contacts and 1 recording contact. Again, the specific contacts can be chosen freely and the recording contact is never switched. The 4 stimulating contacts are stimulated by interleaved pulse trains, as described in section 5.3. By doing so, we are able to measure multiple (4) impedances in a single "stimulus duration".

The advantage of this idea is that we measure 4 impedances instead of 1 in a similar time span. We utilize this by plotting 3 impedance differences (the difference between the most apical contact, and the remaining 3 contacts). The reasoning behind this is that looking at 3 impedances difference as

opposed to just 1 helps us deal with noise in the signal. When we are viewing just 1 impedance difference trace in real-time, it might be hard to distinguish a fold-over (i.e. impedance difference decreasing) from noise. When we view 3 traces, the chances that we mistakenly label noise as a fold-over decrease (when all 3 traces show a decrease in impedance difference, it is unlikely to be noise).

Using this method, one cycle takes ~0.9 seconds, which is slightly larger than in the method described above (framerate is $\sim 1\frac{1}{9}$ FPS). For the pulses we use the same stimulus parameters as earlier: an amplitude of 59 µA, and total stimulus duration of 1000 µs (the stimulus in Figure 5.8 is the exact stimulus that is used). We'll name this 'Stimulus B'.

Similar to before, we first measure a regular EFI trace in both EFIM and using this method to ensure we are measuring correct values. See Figure 6.3

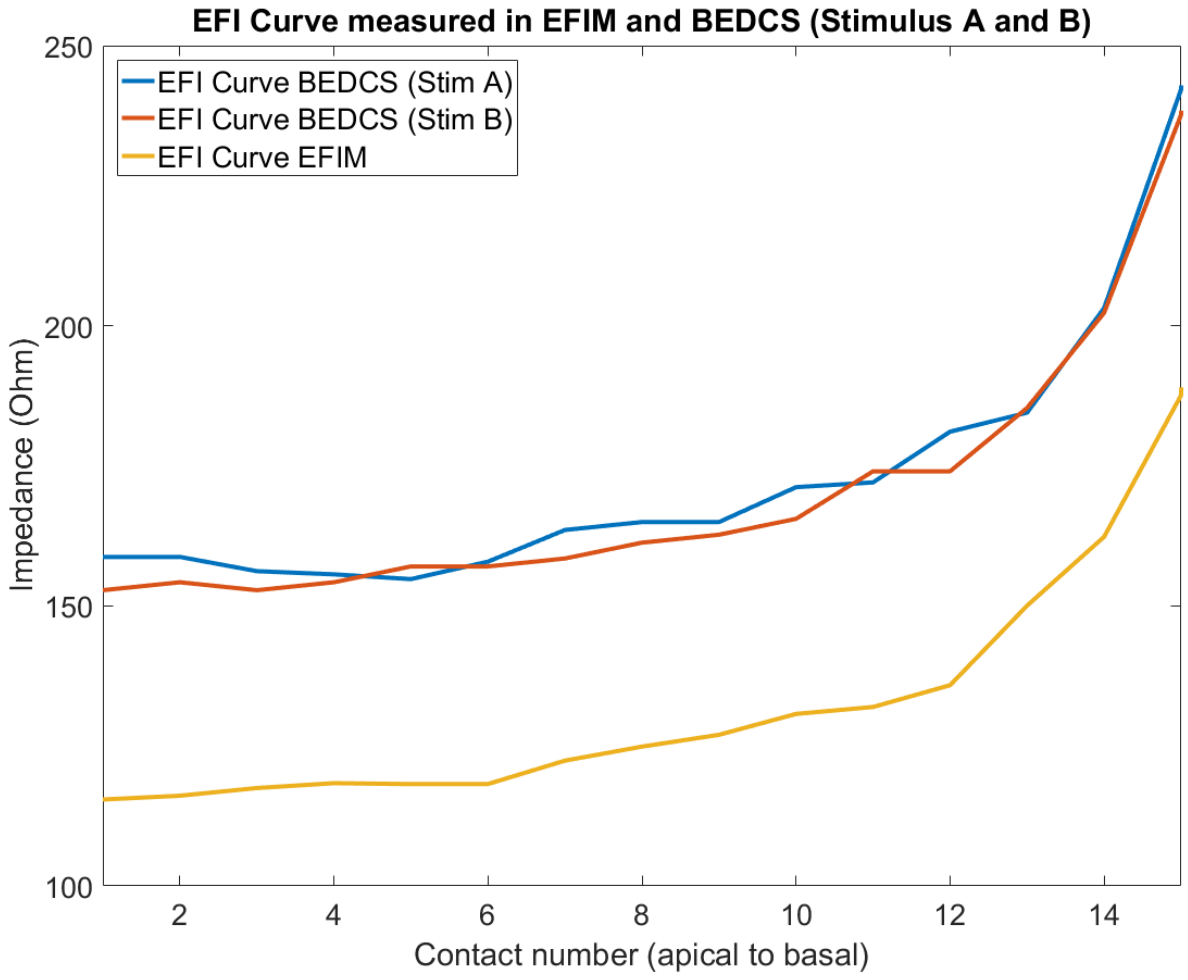

Figure 6.3: EFI curve measured in both EFIM and in BEDCS using stimulus A and B. The recording contact is number 16, which is left out of the plot for clarity. Contact 1 to 15 are stimulated. We see that Stimulus A and B provide similar results. The curve measured in EFIM has slightly lower impedance values. This could be explained by the fact that in EFIM the average of 10 cycles is taken, and in BEDCS we only measure 1 cycle. Another reason might be that EFIM uses a different reference contact than BEDCS, leading to an offset. Although the EFIM curve is translated in regard to the BEDCS curves, the shapes of all 3 curves are similar (and shaped as expected: a peak at the recording contact, and a decreasing impedance as we move away from the recording contact) and thus we will continue the experiment using these stimuli.

6.2 Human Cochlea Model: Testing and Results

We now test the methods presented in section 6.1. To do so, we use a plastic model of the human cochlea. This model was provided by Advanced Bionics and is made using a mold of real human cochlea. The model is fixed in a petri dish and submerged in saline, and placed under a microscope. Using a cochlear implant meant for animal testing, a number of insertions are performed in the cochlea model by an experienced surgeon from the LUMC otorhinolaryngology department (J. Frijns). Unfortunately, the number of repetitions that can be performed is limited. This is because there was only 1 insertion tool (a tool that is delivered with the CI product, meant to guide the insertion) available for this project, and these tools are designed to only be used once. It features a very thin stylet on which the electrode array is placed, and subsequently slid off of during the insertion into the cochlea. When using the same insertion tool multiple times, the stylet deforms and this renders the tool unusable. Having an experienced surgeon perform the experiment hopefully increases the number of repetitions we can perform (due to being familiar with the tool) and also ensures the array is implanted in a realistic manner, comparable to how it is done in the operating theatre. In Figure 6.4 the experiment set up is shown. We were able to perform 3 insertions: a normal insertion for both the back-and-forth method (stimulus A) and the interleaved pulse trains (stimulus B), and an induced fold-over using the back-and-forth method (stimulus A). After the third tests the stylet failed and we were not able to continue the experiment.

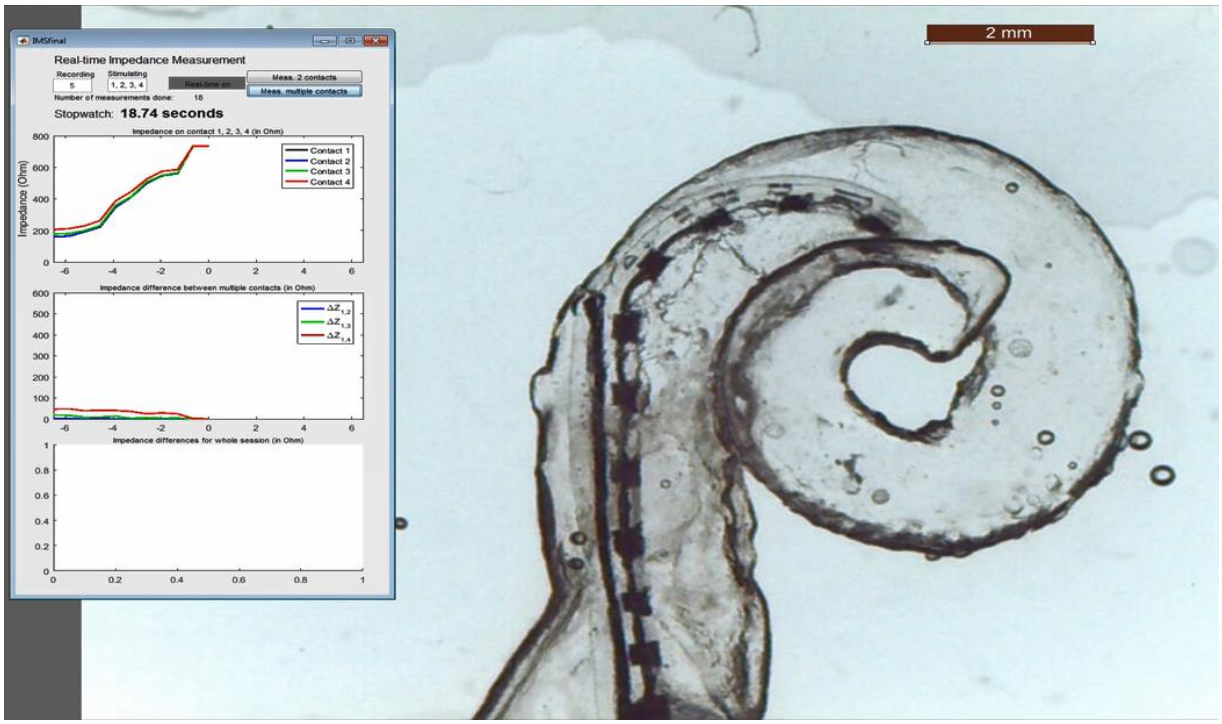

Figure 6.4: Experiment set up. On the right is the microscope image of the cochlea model (with a partially inserted electrode array). Note the stylet of the insertion tool (the straight vertical black line next to the electrode array). The array is pushed off of this stylet, into the cochlea. On the left is a MATLAB interface that shows the individual contact impedances of the 4 most apical contacts (the recording contact is number 5) in the top plot. The middle plot shows the impedance difference between contact 1-2, 1-3, and 1-4.

We start with the normal insertion using interleaved pulse train method. In Figure 6.5 the experiment results are shown.

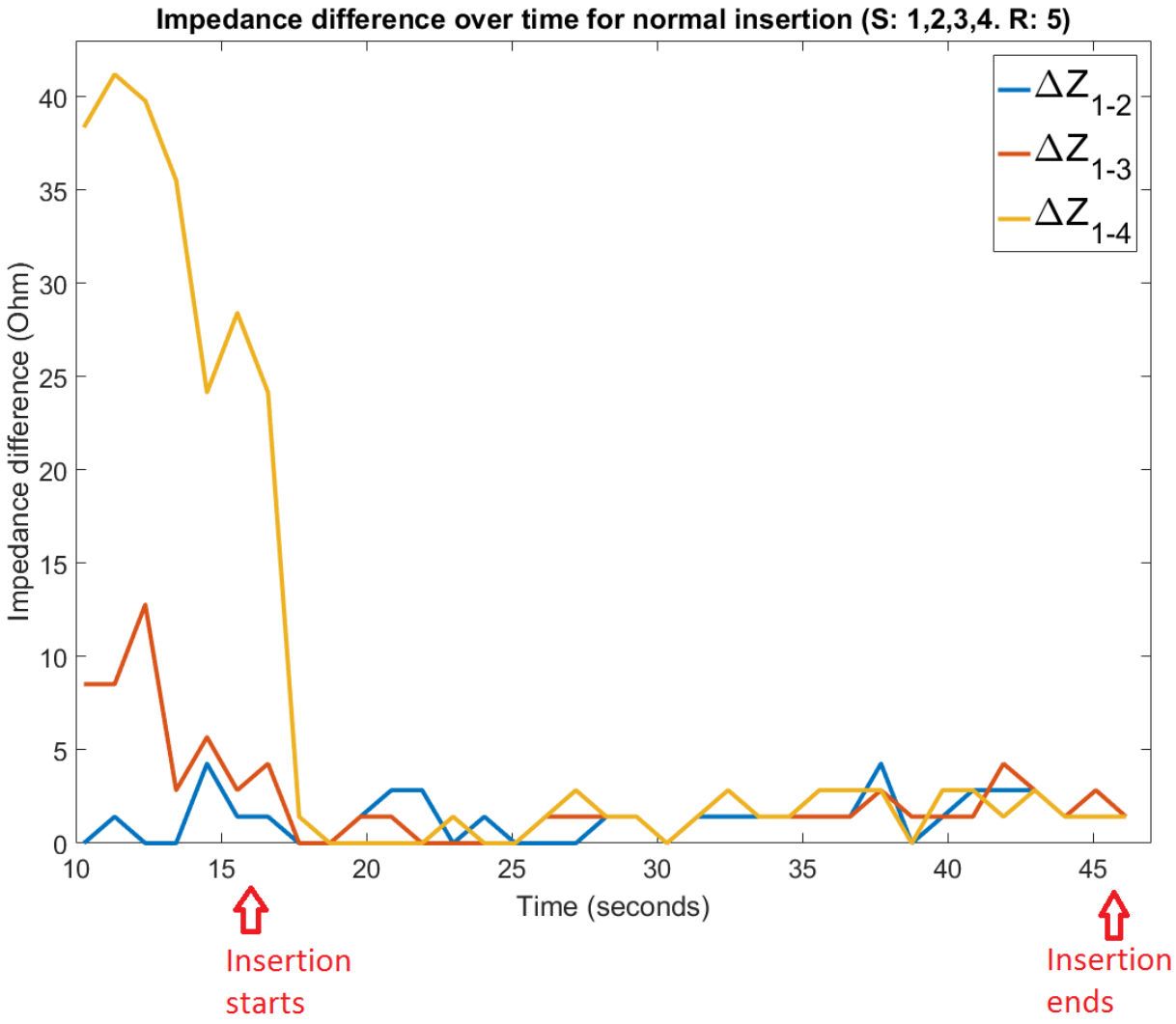

Figure 6.5: Results of insertion in cochlea model using 'Stimulus B' (interleaved pulse train). At 16 seconds the insertion starts and at 46 seconds the insertion ends. The insertion was performed by surgeon J. Frijns. The total insertion time is 30 seconds, and according to Frijns this is standard in the LUMC.

The large differences measured before the 16 second mark are explained by the array being moved around (outside of the cochlea model) and potentially being (partially) raised out of the saline. Note that still, as expected, the impedance difference between 1 and 4 at all times the largest, and between 1 and 2 is at all times the smallest. At 16 seconds the insertion starts and the impedance differences become very small. This is not surprising due to the contacts being extremely close to eachother (~1 mm). Because this is a normal insertion (and not a fold-over), we expect the impedance difference to remain approximately constant. This seems to be the case, however, the noise is extremely large compared to the signal. Note that at several points in time the impedance difference between contact 1 and 4 is smaller than the impedance difference between contact 1 and 2, while at no point in time contact 1 and 4 were physically closer together than contact 1 and 2. The noise is explained by the fact that we are dealing with a complex geometry and a very "unstable" procedure (contacts unpredictably touch the cochlear walls throughout the insertion). Furthermore

we are only measuring every 0.8 seconds and not averaging multiple cycles. In this current set-up we expect that it's not possible to distinguish a fold-over in the impedance difference traces.

We now move on to using the back-and-forth stimulation pattern (Stimulus A). The results are shown in Figure 6.6 (for both the normal insertion and the fold-over). For these two attempts, we set the gain in BEDCS to 1000 instead of 100 (which was used during the first attempt).

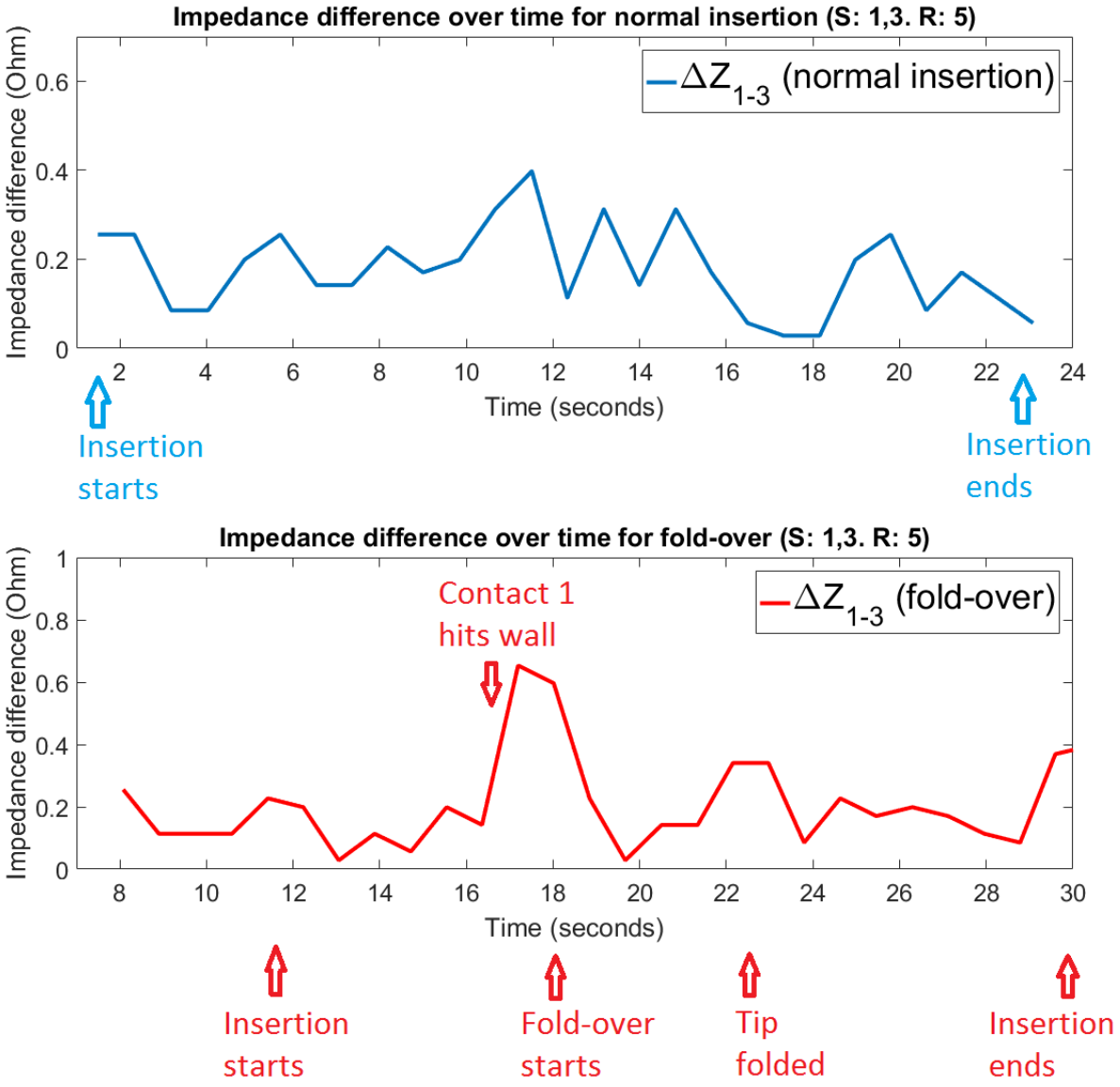

Figure 6.6: Results of insertion in cochlea model using 'Stimulus A' for both a normal insertion (blue) and a fold-over (red). Both insertions were performed by J. Frijns.

As seen in the figure, the noise is reduced compared to the first attempt, but compared to the signal it is still extremely large and the fold-over can definitely not be distinguished. For the normal insertion (top graph) we see that the signal remains approximately constant ($\pm 0.1\ \Omega$). This is expected as the intercontact distance remains (almost) constant throughout the entire insertion. For the fold-over (bottom graph) we see a similar small signal (whereas we expected a different outcome). A point of interest is around 16 seconds, where the first contact hits the inner cochlear wall and the fold-over starts forming. The small peak observed in the impedance difference might be

explained by the impedance on the first contact increasing as it is pressed again the insulating wall, while the second contact is still "floating" in the middle of the cochlear duct. At ~18 seconds the fold-over occurs and we would expect the impedance difference to drop. Unfortunately, the "stable" level observed before the first contact hit the cochlear wall was already close to zero, and we do not observe any further drop in impedance difference. In Figure 6.7 the microscope image is shown at 16 seconds and ~23 seconds into the insertion.

Figure 6.7: Microscope image of the fold-over at the moment the fold-over starts (~17-18 seconds) and where the fold-over is fully formed (~23 seconds). The small peak in impedance difference seen in Figure 6.6 may be explained by the first contact hitting the cochlear wall, as seen in the top image.

6.3 Discussion Method 2: 'Real-time monitoring of contact impedances'

In this chapter we have discussed the idea of monitoring contact impedances in real-time in order to detect electrode array tip fold-over. The findings are discussed here.

It is important to note that this idea has only been touched upon briefly in this project. We did not have the means to thoroughly research this method and thus no decisive conclusions can be made yet. There was only 1 insertion tool available which failed after 3 insertions. All work described in this section is merely a foundation for future work.

We have observed that noise is a problem in the current set-up. The measured noise is extremely large compared to the signal which makes it impossible to distinguish a fold-over from a normal insertion. Multiple factors play a role in this. First of all the anatomy of the cochlear duct is very complex (and varies for every patient): the duct is curved, tapered, and has physical irregularities along its full length. On top of that, the human cochlea features a thinner section of wall at approximately 270 degrees on the basal turn. This is where the facial nerve passes close to the cochlea, and the transversal resistance of the cochlear wall in this section was found to 5 to 10 times lower than in the remainder of the cochlea [46]. This fact was not taken into account in this project due to its complexity and does not apply to the plastic model of the cochlea that was used in this chapter, but it is expected to make real-time monitoring of the impedances more complex (the drop in transversal resistance may be interpreted as noise since it is hard to say when the electrode enters this particular section of the cochlea). Another reason for the large amount of noise is the fact that electrode contacts unpredictably hit the cochlear walls during the insertion which induces a spike of high impedance. Lastly, we are only measuring 1 cycle due to the fact we want to measure quickly. Averaging multiple cycles would result in a more stable impedance measurement.

We also need to be aware of the fact that the plastic model of the human cochlea is not an accurate representation of the real human cochlea. In the model, current can only flow out of the cochlea in the basal direction while in a real human cochlea a portion of the current will flow through the cochlear walls or exit the cochlea apically.

Another point of interest is the insertion duration. The insertions in these experiments were carried out by Prof. dr. ir. J.H.M. Frijns who has been performing cochlear implantation surgery in the LUMC for over 20 years. The insertions performed here averaged 24 seconds which is extremely fast according to literature [80]. In order to detect fold-over, slower insertions are preferred, especially as the current measurement speed is low (just over 1 measurement per second). It is important to realize that the "frame rate" required to successfully detect a fold-over before it completely forms is dependent on the surgeon's insertion speed.

Further experimentation is required to draw decisive conclusions on the effectivity of this method. When we compare this method to EFI-MDS, one might say that this method is more suitable for real-time intra-operative detection of electrode array fold-overs. The method described in this chapter uses fewer electrode contacts (previously we have seen that in EFI-MDS, we need a 16 x 16 EFI matrix to distinguish fold-overs from normal insertions) and thus is faster. However, the amount of noise (due to the reason presented earlier) and the low framerate are obstacles we could not overcome within the scope of this project. For future work, these issues should be the main points of focus.

References

[1] B. J. Gantz and T. C. W, "Combining acoustic and electrical hearing," *Laryngoscope,* vol. 113, pp. 1726-1730, 2003.

[2] F.-G. Zeng, "Trends in Cochlear Implants," *Trends In Amplification,* vol. 8, no. 1, 2004.

[3] A. Volta, "On the electricity excited by mere contact of conducting substances of different kinds," *Royal Soc Philos Trans,* vol. 90, pp. 403-431, 1800.

[4] A. M. Andreev, G. V. Gersuni and A. A. Volokhov, "On the electrical excitability of the human ear: On the effect of alternating currents on the affected auditory apparatus," *J Physiol USSR,* vol. 18, pp. 250-265, 1935.

[5] A. Djourno and E. C, "Auditory prosthesis by means of a distant electrical stimulation of the sensory nerve with the use of an indwelt coiling," *Presse Med,* vol. 65, p. 1417, 1957.

[6] A. Djourno, E. C and V. B, "Electric excitation of the cochlear nerve in man by induction at a distance with the aid of micro-coil included in the fixture," *C R Seances Biol Fil,* vol. 151, pp. 423-425, 1957.

[7] R. C. Bilger, "Electrical stimulation of the auditory nerve and auditory prostheses: A review of the literature," *Ann Otol Rhinol Laryngol Suppl,* vol. 86, pp. 11-20, 1977.

[8] R. C. Bilger and B. F. O, "Auditory prostheses in perspective," *Ann Otol Rhinol Laryngol Suppl,* vol. 86, pp. 92-140, 1977.

[9] A. A. Eshraghi, R. Nazarian, F. F. Telischi, S. M. Rajguru, E. Truy and C. Gupta, "The Cochlear Implant: Historical Aspects and Future Prospects," *The Anatomical Record,* vol. 295, pp. 1967-1980, 2012.

[10] "Cochlear Implants," National Institute on Deafness and Other Communication Disorders, 2016.

[11] I. Hochmair, "Cochlear Implants: Facts," MED-EL, September 2013. [Online]. Available: http://www.medel.com/cochlear-implants-facts/. [Accessed 7 May 2018].

[12] B. S. Wilson, "Engineering design of cochlear implant systems.," in *Auditory Prostheses: Cochlear Implants and Beyond*, New York, Springer-Verlag, 2004, pp. 14-52.

[13] D. S. Lee, L. J. S, S. H. Oh, S. K. Kim, J. W. Kim, J. K. Chung, M. C. Lee and K. C. S, "Cross-modal plasticity and cochlear implants," *Nature,* vol. 409, pp. 149-150, 2001.

[14] R. K. Shepherd and N. A. Hardie, "Deafness-induced changes in the auditory pathway: implications for cochlear implants," *Audiol Neurootol,* vol. 6, pp. 305-318, 2001.

[15] P. Gu, Y. Jiang, X. Gao, S. Huang, Y. Yuan, G. Wang, B. Li, X. Xi and P. Dai, "Effects of cochlear implant surgical technique on post-operative electrode impedance," *Acta Otalaryngol,* vol. 136, no. 7, pp. 677-681, 2016.

[16] B. S. Wilson and M. F. Dorman, "Cochlear Implants: A remarkable past and a brilliant future," *Hearing Research,* vol. 242, pp. 3-21, 2008.

[17] R. A. Tange, W. Grolman and A. Maat, "Intracochlear misdirected implantation of a cochlear implant," *Acta Otolaryngologica,* vol. 126, pp. 650-652, 2006.

[18] Y. L. M. Ying, J. W. Lin, J. S. Oghalai and R. A. Williamson, "Cochlear Implant Electrode Misplacement: Incidence, Evaluation, and Management," *Laryngoscope,* vol. 123, pp. 757-766, 2013.

[19] J. Hamzavi, W. D. Baumgartner, S. M. Pok, P. Franz and W. Gstoettner, "Variables affecting speech perception in postlingually deaf adults following cochlear implantation," *Acta Otolaryngol,* vol. 123, pp. 493-498, 2003.

[20] G. B. Wanna, J. H. Noble and M. L. Carlson, "Impact of electrode design and surgical approach on scalar location and cochlear implant outcomes," *Laryngoscope,* vol. 124, no. 6, pp. 1-7, 2014.

[21] C. C. Finley, T. A. Holden, L. K. Holden, B. R. Whiting, R. A. Chole, G. J. Neely, T. E. Hullar and M. W. Skinner, "Role of electrode placement as a contributor to variability in cochlear implant outcomes," *Otol Neurotol,* vol. 29, pp. 920-928, 2008.

[22] A. Aschendorff, J. Kromeier, T. Klenzner and R. Laszig, "Quality control after insertion of the nucleus contour and contour advance electrode in adults," *Ear Hear,* vol. 28, no. 2, pp. 75S-(S, 2007.

[23] M. W. Skinner, T. A. Holden and B. R. Whiting, "In vivo estimates of the position of advanced bionics electrode arrays in the human cochlea," *Ann Otol Rhinol Laryngol Suppl,* vol. 197, pp. 2-24, 2007.

[24] W. Grolman, A. Maat, Y. Verdam, B. Simis, N. Carelsen, N. Freling and R. A. Tange, "Spread of excitation measurements for the detection of electrode array foldovers: A prospective study comparing 3-dimensional rotational x-ray and intraoperative spread of excitation measurements," *Otol Neurotol,* vol. 30, pp. 27-33, 2009.

[25] M. G. Zuniga, A. Rivas, A. Hedley-Williams, R. H. Gifford, R. Dwyer, B. M. Dawant, L. W. Sunderhaus, K. L. Hovis, G. B. Wanna, J. H. Noble and R. F. Labadie, "Tip Fold-over in Cochlear Implantation: Case Series," *Otology & Neurology,* vol. 38, pp. 199-206, 2016.

[26] W. H. Slattery and W. M. Luxford, "Cochlear implantation in the congenital malformed cochlea.," *Laryngoscope,* vol. 105, pp. 1184-1187, 1995.

[27] L. J. Rotteveel, D. Proops and R. Ramsden, “Cochlear implantation in 53 patients with otosclerosis: demographics, computed tomographic scanning, surgery, and complications,” *Otol. Neurotol.,* vol. 25, pp. 943-952, 2004.

[28] D. W. Proops, R. L. Stoddart and I. Donaldson, “Medical, surgical and audiological complications of the first 100 adult cochlear implant pieces in Birmingham,” *J. Laryngol. Otol. Suppl.,* vol. 24, pp. 14-17, 1999.

[29] R. A. Hoffman and N. Cohen, “Complications of cochlear implant surgery,” *Ann. Otol. Rhinol. Laryngol. Suppl.,* vol. 166, pp. 420-422, 1995.

[30] A. A. Lassig, T. A. Zwolan and S. A. Elian, “Cochlear implant failures and revision,” *Otol Neurotol,* vol. 26, pp. 624-634, 2005.

[31] R. Tambyraja, M. Gutman and C. Megerian, “Cochlear implant complications: utility of federal database in systematic analysis,” *Arch. Otolaryngol. Head Neck Surg.,* vol. 131, pp. 245-250, 2005.

[32] T. Balkany, A. Hodges and O. Gomez-Marin, “Cochlear reimplantation,” *Laryngoscope,* vol. 109, pp. 351-355, 1999.

[33] L. H. M. Mens, “Advances in Cochlear Implant Telemetry: Evoked Neural Responses, Electrical Field Imaging, and Technical Integrity,” *Trends in Amplification,* vol. 11, no. 3, pp. 143-159, 2007.

[34] L. H. M. Mens, P. J. Boyle and J. J. Mulder, “The Clarion electrode positioner: approximation to the medial wall and current focussing,” *Audiol Neurotol,* vol. 8, pp. 166-175, 2003.

[35] F. J. Vanpoucke, P. P. B. Boermans and J. H. Frijns, “Assessing the Placement of a Cochlear Electrode Array by Multidimensional Scaling,” *IEEE Transactions on Biomedical Engineering,* vol. 59, no. 2, 2012.

[36] F. Vanpoucke, A. Zarowski and S. Peeters, “Identification of the impedance model of an implanted cochlear prosthesis from intracochlear potential measurements,” *IEEE Trans Biomed Eng,* vol. 51, pp. 2174-2183, 2004.

[37] A. A. Saoji and L. Litvak, “Use of phantom electrode technique to extend the range of pitches available through a cochlear implant,” *Ear Hear,* vol. 31, pp. 693-701, 2010.

[38] J. H. Frijns, R. K. Kalkman, F. J. Vanpoucke, J. Snel-Bongers and J. J. Briaire, “Simultaneous and non-simultaneous dual electrode stimulation in CI: Evidence for two neural response modalities,” *Acta Otolaryngol,* vol. 129, pp. 433-439, 2009.

[39] C. M. Zierhofer and R. Schatzer, “Simultaneous intracochlear stimulation based on channel interaction compensation: Analysis and first results,” *IEEE Trans Biomed Eng,* vol. 55, pp. 1907-1916, 2008.

[40] C. van der Honert and D. C. Kelsall, “Focused intracochlear electric stimulation with phased array channels,” *J amer Stat Assoc,* vol. 121, pp. 3703-3716, 2007.

[41] J. H. Frijns, D. M. Dekker and J. J. Briaire, “Neural excitation patterns induced by phased array stimulation in the implanted human cochlea,” *Acta Otolaryngol,* vol. 131, pp. 362-370, 2011.

[42] C. K. Berenstein, L. H. Mens, J. J. Mulder and F. J. Vanpoucke, “Current steering and current focusing in cochlear implants: Comparison on monopolar, tripolar and virtual channel electrode configuration,” *Ear Hear,* vol. 29, pp. 250-260, 2008.

[43] B. H. Bonham and L. M. Litvak, “Current focusing and steering: Modeling, physiology and psychophysics,” *Hear Res,* vol. 242, pp. 141-153, 2008.

[44] A. Kral, R. Hartmann, D. Mortazavi and R. Klinke, “Spatial resolution of cochlear implants: the electrical field and excitation of auditory afferents,” *Hear Res,* vol. 121, pp. 11-28, 1998.

[45] M. F. Suesserman and F. A. Spelman, “Lumped-parameter model for in vivo cochlear stimulation,” *IEEE Trans Biomed Eng,* vol. 40, pp. 237-245, 1993.

[46] F. Vanpoucke, A. Zarowski, J. Casselman, J. Frijns and S. Peeters, “The facial nerve canal: An important cochlear conduction path revealed by Clarion electrical field imaging,” *Otol Neurotol,* vol. 25, pp. 282-289, 2004.

[47] K. A. Gordon, B. C. Papsin and R. V. Harrison, “Programming cochlear implant stimulation levels in infants and children with a combination of objective measures,” *International Journal of Audiology,* vol. 43, pp. S28-S32, 2004.

[48] K. A. Gordon, B. C. Papsin and R. V. Harrison, “Toward a battery of behavioral and objective measures to achieve optimal cochlear implant stimulation levels in children,” *Ear and Hearing,* vol. 25, pp. 447-463, 2004.

[49] M. L. Hughes, “Fundamentals of Clinical ECAP Measures in Cochlear Implants: Part 1: Usie of the ECAP in Speech Processor Programming (2nd Ed.),” AudiologyOnline, 8 November 2010. [Online]. Available: https://www.audiologyonline.com/articles/fundamentals-clinical-ecap-measures-in-846. [Accessed 3 May 2018].

[50] J. Wolfe and H. Kasulis, “Relationships among objective measures and speech perception in adult users of the HiResolution Bionic Ear,” *Cochlear Implants International,* vol. 9, no. 2, pp. 70-81, 2008.

[51] M. Polak, A. Hodges and T. Balkany, “ECAP, ESR, and subjective levels for two different Nucleus 24 electrode arrays,” *Otology & Neurology,* vol. 26, pp. 639-645, 2005.

[52] J. Fayad and F. H. Linthicum, “Multichannel Cochlear Implants: relation of histopathology to performance,” *Laryngoscope,* vol. 116, pp. 1310-1320, 2006.

[53] B. Carelsen, W. Grolman, R. Tange, G. Streekstra, P. van Kemenade, R. Jansen, N. Freling, M. White, B. Maat and W. Fokkens, "Cochlear implant electrode array insertion monitoring with intra-operative 3D rotational X-ray," *Clinical Otolaryngology,* vol. 32, pp. 42-59, 2007.

[54] P. J. F. Groenen and I. Borg, "The Past, Present, and Future of Multidimensional Scaling," Economic Institute Report, 2013.

[55] M. C. Hout, M. H. Papesh and S. D. Goldinger, "Multidimensional Scaling," *Cognitive Science,* vol. 4, pp. 93-103, 2013.

[56] F.-G. Zeng, S. Rebscher, W. Harrison, X. Sun and H. Feng, "Cochlear Implants: System Design, Integration, and Evaluation," *Reviews in Biomedical Engineering,* vol. 1, pp. 115-142, 2008.

[57] F. J. Vanpoucke, P.-P. B. Boermans and J. H. Frijns, "Assessing the Placement of a Cochlear Electrode Array by Multidimensional Scaling," *IEEE Transactions on Biomedical Engineering,* vol. 59, no. 2, pp. 307-310, 2012.

[58] L. H. M. Mens, "Advances in Cochlear Implant Telemetry: Evoked Neural Responses, Electrical Field Imaging, and Technical Integrity," *Trends in Amplification,* vol. 11, no. 3, pp. 143-159, 2007.

[59] L. H. M. Mens, P. J. Boyle and J. J. Mulder, "The Clarion electrode positioner: approximation to the medial wall and current focussing," *Audiol Neurotol,* vol. 8, pp. 166-175, 2003.

[60] W. S. Togerson, "Multidimensional scaling of similarity," *Psychometrika,* vol. 30, pp. 379-393, 1965.

[61] F. Attneave, "Dimensions of similarity," *Am J Psychol,* vol. 63, pp. 516-556, 1950.

[62] R. N. Shepard, "The analysis of proximities: multidimensional scaling with an unknown distance function. Part I," *Pyschometrika,* vol. 27, pp. 125-140, 1962.

[63] R. N. Shepard, "The analysis of proximities: multidimensional scaling with an unkown distance function. Part II," *Psychometrika,* vol. 27, pp. 219-246, 1962.

[64] J. D. Carroll and P. E. Green, "Psychometric methods in marketing research: Part II, multidimensional scaling," *J Market Res,* vol. 34, pp. 193-204, 1997.

[65] N. C. Kenkel and L. Orlóci, "Applying metric and nonmetric multidimensional scaling to ecological studies: some new results," *Ecology,* vol. 67, pp. 919-928, 1986.

[66] G. B. Rabinowitz, "An introduction to nonmetric multidimensional scaling," *Am J Polit Science,* vol. 19, pp. 343-390, 1975.

[67] M. Hollins, R. Faldowski, S. Rao and F. Young, "Perceptual dimensions of tactile surface features: a multidimensional scaling analysis," *Percept Psychophys,* vol. 54, pp. 697-705, 1993.

[68] P. R. Amato, “Dimensions of the family environment as perceived by children: a multidimensional scaling analysis,” *J Marriage Fam,* vol. 52, pp. 613-620, 1990.

[69] S. L. Youngentob, B. A. Johnson, M. Leon, P. R. Sheehe and P. F. Kent, “Predicting odorant quality perceptions from multidimensional scaling of olfactory bulb glomerular activity patterns,” *Behav Neurosci,* vol. 120, pp. 1337-1345, 2006.

[70] J. A. Russel and M. Bullock, “Multidimensional scaling of emotional facial expressions: similarity from pre-schoolers to adults,” *J Pers Soc Psychol,* vol. 48, pp. 1290-1298, 1985.

[71] G. F. Ashby and P. N. A, “Toward a unified theory of similarity and recognition,” *Psychol Rev,* vol. 95, pp. 124-150, 1988.

[72] M. Hornberger, B. Bell, K. S. Graham and T. T. Rogers, “Are judgements of semantic relatedness systematically impaired in Alzheimer's disease?,” *Neuropsychologia,* vol. 47, pp. 3084-3094, 2009.

[73] L. Pedelty, C. L. S and S. K. Shevall, “Developmental changes in face processing: results from multidimensional scaling,” *J Exp Child Psychol,* vol. 39, pp. 421-436, 1985.

[74] A. Buja, D. F. Swayne, M. L. Littman, N. Dean, H. Hofmann and L. Chen, “Data Visualization with Multidimensional Scaling,” *Journal of Computational and Graphical Statistics,* vol. 17, pp. 444-472, 2008.

[75] W. S. Togerson, “Multidimensional Scaling: I. Theory and Method,” *Psychometrika,* vol. 17, no. 4, pp. 401-419, 1952.

[76] F. Wickelmaier, “An introduction to Multidimensional Scaling,” Denmark, 2003.

[77] I. Borg and P. Groenen, Modern Multidimensional Scaling: theory and applications (2nd ed.), New York: Springer-Verlag, 2005.

[78] J. B. Kruskal, “Nonmetric multidimensional scaling: a numerical method,” *Psychometrika,* vol. 29, pp. 115-129, 1964.

[79] J. B. Kruskal, “Multidimensional scaling by optimizing goodness of fit to a nonmetric hypothesis,” *Psychometrika,* vol. 29, pp. 1-27, 1964.

[80] G. P. Rajan, G. Kontorinis and J. Kuthubutheen, “The effects of insertion speed on inner ear function during cochlear implantation: a comparison study,” *Audiol Neurotol,* vol. 18, pp. 17-22, 2013.

[81] M. Bond, E. J and M. S, “Systematic reviews of the effectiveness and cost-effectiveness of multi-channel unilateral cochlear implants for adults,” *Clinical Otolaryngoloy,* vol. 35, no. 2, pp. 87-96, 2010.

[82] *Image on cover page:*
"Tip Fold-Over & Perimodiolar Cochlear Implant Electrodes: Research Update," MED-EL, 28 January 2019. [Online]. Available: https://blog.medel.pro/tip-fold-over-cochlear-implant-electrodes-research-update/. [Accessed 8 May 2019].

Appendix

Appendix A: CT-scans of electrode array fold-overs

Images are constructed by overlaying several CT-scan slices.
Electrode contact positions are indicated by green markers.

A.1

CT-scan of patient “A”. Patient suffers from tip fold-over, where only the first contacts are folded. Contact 1 and 3 are marked. Note that besides the fold-over issue, the insertion is very shallow. The insertion angle is roughly 180 degrees.

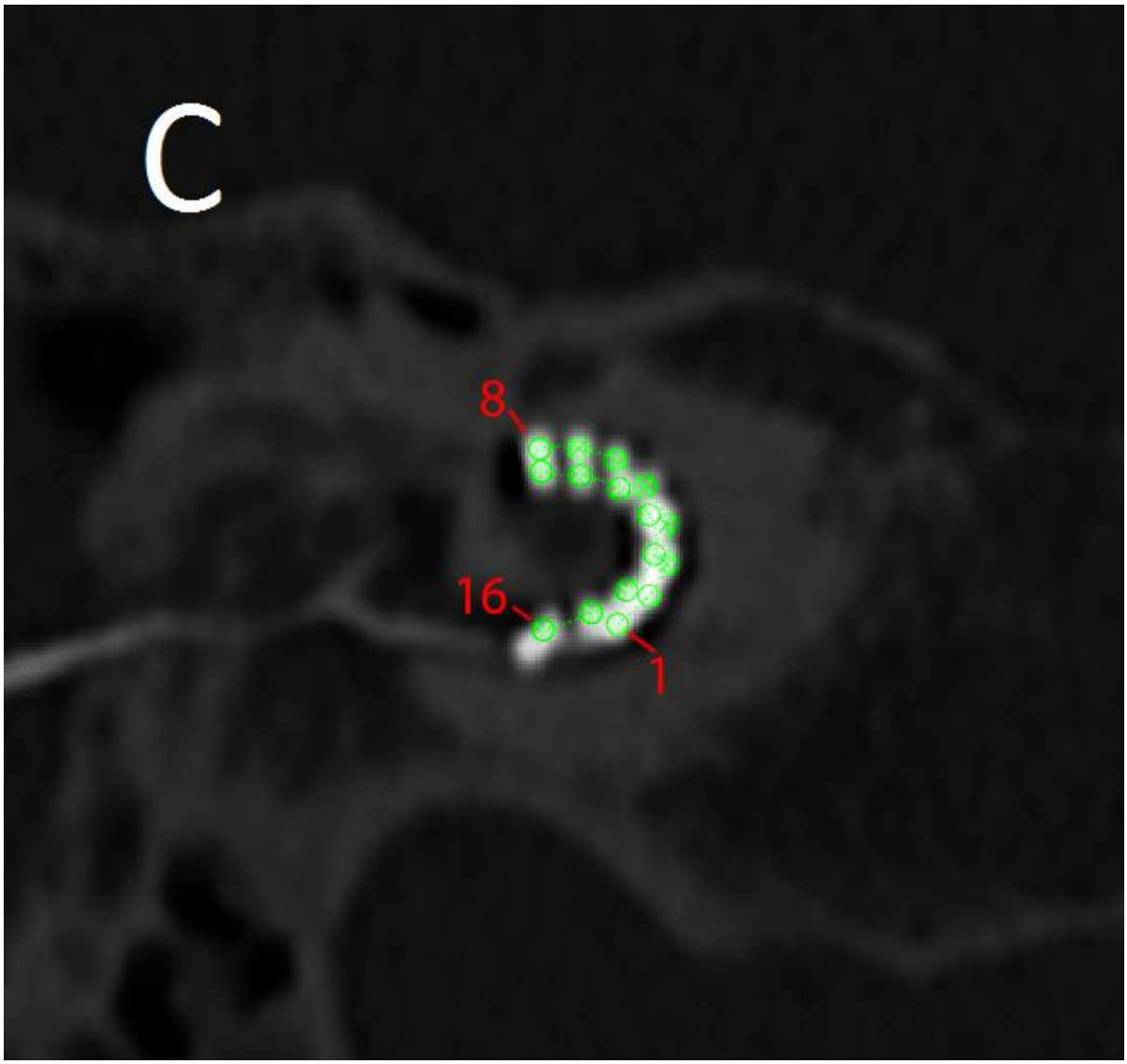

A.2

CT-scan of patient “B”. Patient suffers from tip fold-over, where only the first contacts are folded. Contact 1, 4, and 16 are marked. This insertion is less shallow than the insertion of patient A.

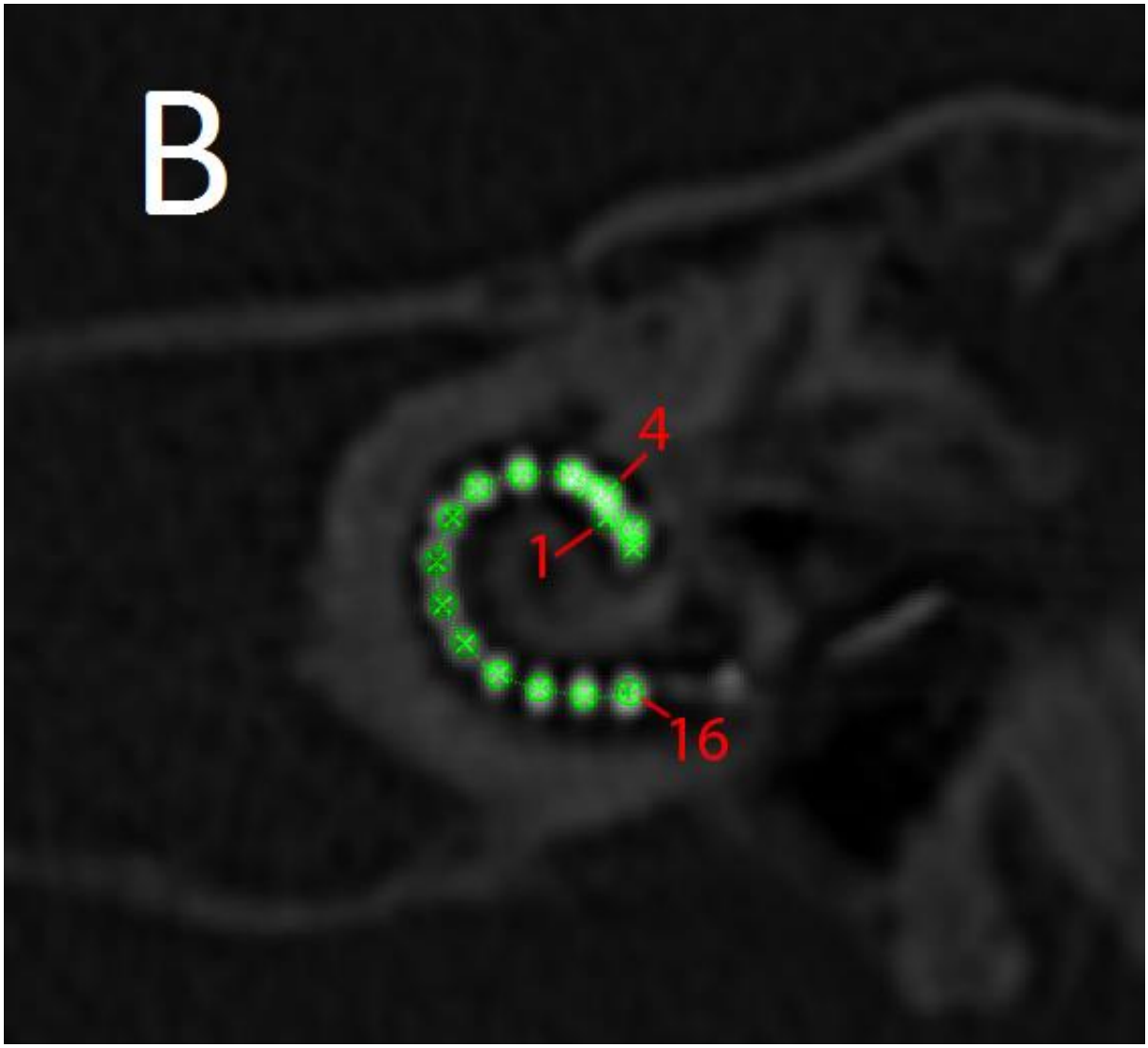

A.3

CT-scan of patient “B”. Patient suffers from complete electrode fold-over. The apical half of the electrode array is completely folded over and lined up with the basal half. Contacts 1, 8, and 16 are marked.

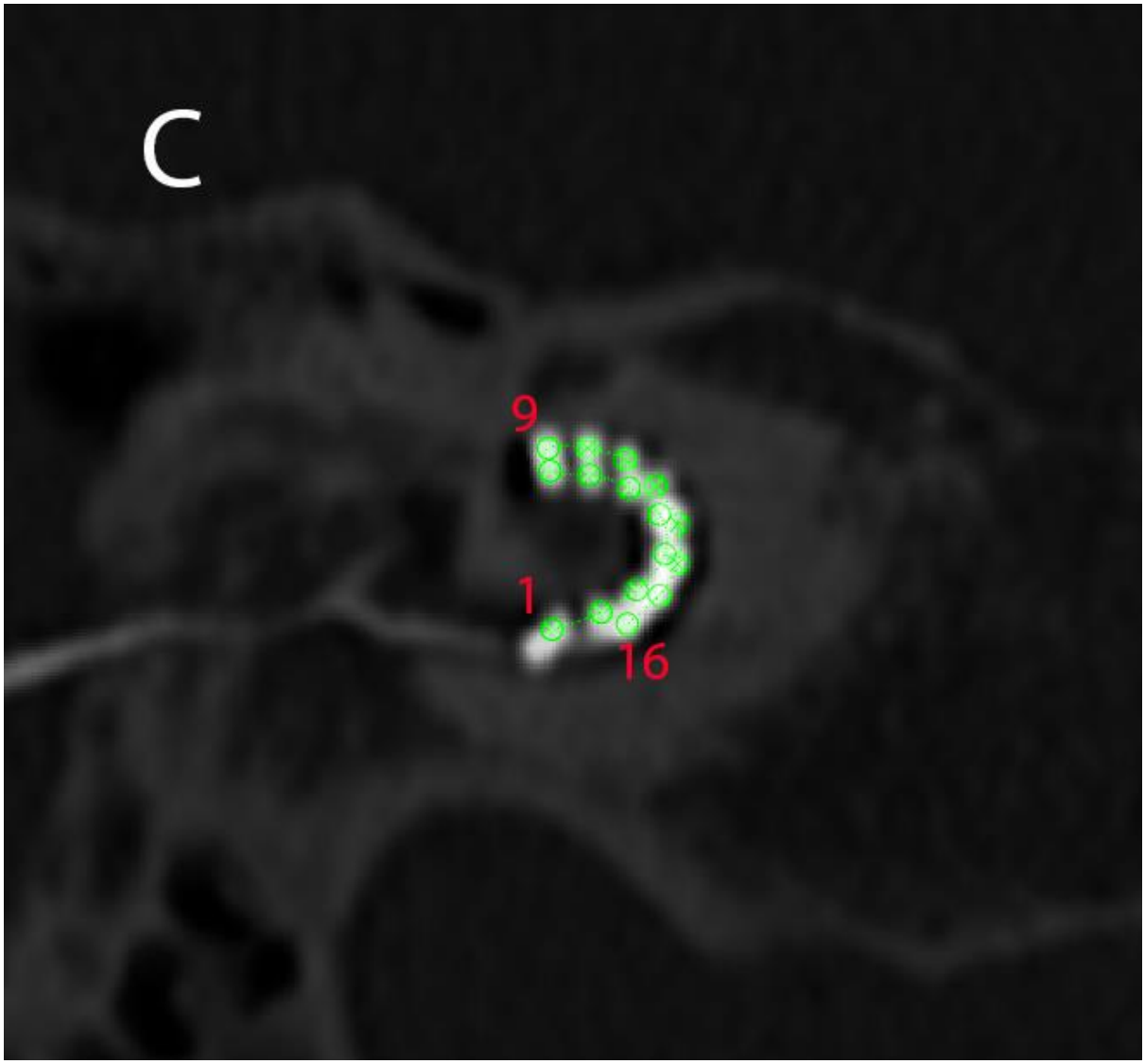

Appendix B: Minimum Probability of Error Test

In section 6.2 we perform a hypothesis test (Minimum probability of error test) to find a objective boundary value which helps us distinguish fold-overs from non fold-overs using the MDS analysis solution. In this appendix, the full hypothesis test is presented.

We perform MDS (metric squared stress) analysis on the EFI data gathered from a patient. From the MDS solution, the distance between contact 1 (most apical) and contact 3 is calculated. Let ***x*** be the the distance between these two contacts. We assume that **x** is normally distributed.

Minimum Probability of Error Test

The following hypotheses are presented:

$$H_0 = Measured\ value\ of\ \boldsymbol{x}\ does\ \boldsymbol{not}\ belong\ to\ a\ foldover$$

$$H_1 = Measured\ value\ of\ \boldsymbol{x}\ \boldsymbol{does}\ belong\ to\ a\ foldover$$

When (1) is true, we decide hypothesis H_1 is true (in other words, we are dealing with a fold-over). When (1) is not true, we decide hypothesis H_0 is true (in other words, we are dealing with a problem-free insertion).

$$\textbf{(2)}\quad \frac{p(x \mid H_1)}{p(x \mid H_0)} > \frac{p(H_0)}{p(H_1)}$$

Where:

$$p(x \mid H_0) = \frac{1}{\sqrt{2\pi\sigma_0^2}}\ e^{-\frac{1}{2\sigma_0^2}(x-\mu_0)^2}$$

And,

$$p(x \mid H_1) = \frac{1}{\sqrt{2\pi\sigma_1^2}}\ e^{-\frac{1}{2\sigma_1^2}(x-\mu_1)^2}$$

And $p(H_0)$ and $p(H_1)$ are the prior probabilities ($p(H_0) = \frac{264}{266}$ and $p(H_1) = \frac{2}{266}$).

Substituting the equations for $p(x \mid H_0)$ and $p(x \mid H_1)$ in **(1)**:

$$\frac{\frac{1}{\sqrt{2\pi\sigma_1^2}}\, e^{-\frac{1}{2\sigma_1^2}(x-\mu_1)^2}}{\frac{1}{\sqrt{2\pi\sigma_0^2}}\, e^{-\frac{1}{2\sigma_0^2}(x-\mu_0)^2}} = \frac{p(H_0)}{p(H_1)}$$

Which leads to:

$$\frac{\sigma_0}{\sigma_1} \cdot e^{-\frac{1}{2\sigma_1^2}(x-\mu_1)^2+\frac{1}{2\sigma_0^2}(x-\mu_0)^2} = \frac{p(H_0)}{p(H_1)}$$

Taking the natural logarithm on both sides and rewriting:

$$-\frac{1}{2\sigma_1^2}(x-\mu_1)^2 + \frac{1}{2\sigma_0^2}(x-\mu_0)^2 = \ln\left(\frac{p(H_0)}{p(H_1)} \cdot \frac{\sigma_1}{\sigma_0}\right)$$

Which leads to:

$$x^2(2\sigma_0^2 - 2\sigma_1^2) + x(4\mu_0\sigma_1^2 - 4\mu_1\sigma_0^2) + 4 \cdot \ln\left(\frac{p(H_0)\cdot\sigma_1}{p(H_1)\cdot\sigma_0}\right) + 2\sigma_0^2\mu_1^2 - 2\sigma_1^2\mu_0^2 = 0$$

Solving for **x** gives us:

$$x_{1,2} = \frac{-(4\mu_0\sigma_1^2 - 4\mu_1\sigma_0^2) \pm \sqrt{(4\mu_0\sigma_1^2 - 4\mu_1\sigma_0^2)^2 - 4\cdot(2\sigma_0^2 - 2\sigma_1^2)\cdot 4\cdot \ln\left(\frac{p(H_0)\cdot\sigma_1}{p(H_1)\cdot\sigma_0}\right) + 2\sigma_0^2\mu_1^2 - 2\sigma_1^2\mu_0^2}}{4\sigma_0^2 - 4\sigma_1^2}$$

These solutions for **x** indicate where the decision boundary between hypotheses H_0 and H_1 is (see section 5.2).

Appendix C: Distinguishing fold-over from normal insertion using 4 contacts

The distribution of distance between contact 1 and 3 in the Metric Squared Stress MDS solution, using only the most apical 4 contacts and the "Sine 1" EFI data. The distributions suggests that the data is actually a logarithmic distribution and not a normal distribution. The decision boundary was computed in the same way as described in section 5.2.

As seen in the figure, it is not possible to distinguish fold-overs from normal insertions. Reasons for this are:

1. The sample size for the fold-overs is extremely low (n = 2)
2. Normal distributions were assumed while the distributions might be logarithmic.
3. By using 4 contacts instead of 16, the quality of the MDS solution diminishes.

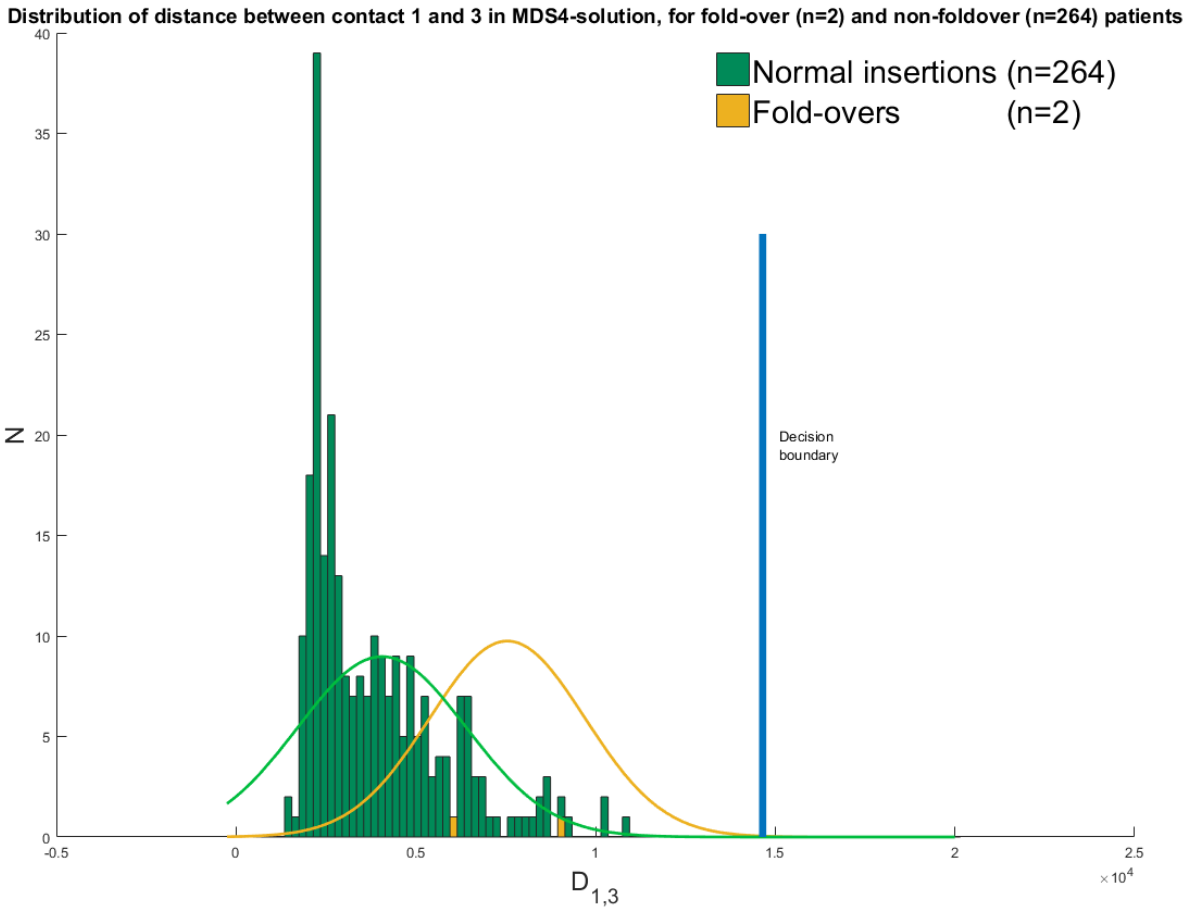

Appendix D: Distinguishing fold-over from normal insertion using 1 recording contact

The distribution of distance between contact 1 and 3 in the Metric Squared Stress MDS solution, using the "Sine 1" EFI data and only 1 recording contact. The method is described in section 5.3 (under the header 'Using a single recording contact'). Again, the distributions suggests that the data is actually a logarithmic distribution and not a normal distribution. The decision boundary was computed in the same way as described in section 5.2.

As seen in the figure, it is not possible to distinguish fold-overs from normal insertions. The two fitted probability density functions now almost completely overlap. Reasons for this are:

1. The sample size for the fold-overs is extremely low (n = 2)
2. Normal distributions were assumed while the distributions might be logarithmic.
3. By using 1 recording contact instead of 16, the quality of the MDS solution diminishes. By doing so, we are assuming equal contact impedance and equal flow of current in apical and basal direction of the cochlea. Common EFI measurements clearly show that this is not the case.